Genomic Diversity of Magnetotactic Bacteria from Underexplored Extreme Aquatic Habitats

Pranami Goswami

Supervisors: Prof. Wei Lin, Prof. Andrew P. Roberts, Assoc. Prof. David Heslop

A thesis submitted for the degree of Doctor of Philosophy

at the Australian National University

Research School of Earth Sciences
Australian National University

June 2025

Declaration

This thesis has been submitted as part of a dual Ph.D. program between the University of Chinese Academy of Sciences (UCAS) and the Australian National University (ANU). A copy has been submitted to UCAS in fulfilment of the requirements for the award of a Ph.D. degree. To the best of the author's knowledge, this thesis contains no material previously published or written by another person, except where proper acknowledgement is made.

Pranami Goswami

June 2025

Abstract

Magnetotactic bacteria (MTB) are metabolically versatile prokaryotes characterised by their ability to biomineralise intracellular magnetic nanocrystals within organelles called magnetosomes. These organelles assist MTB to align with geomagnetic field lines using magnetotaxis, thereby facilitating their navigation within chemically stratified aquatic environments. While the ecological and biogeochemical roles of MTB have been investigated extensively in freshwater and marine sediments, our understanding of their diversity, ecological function, and evolutionary significance in extreme and underexplored habitats remains limited. This doctoral research addresses these knowledge gaps by investigating MTB in two ecologically and geochemically distinct systems: acidic peatlands and oceanic oxygen minimum zones (OMZs). Using a multifaceted approach that integrates microbiological enrichment, microscopy, and genome-resolved metagenomics, the taxonomic novelty, metabolic diversity, and adaptive strategies of MTB in these environments have been investigated here.

In the first part of the thesis, MTB from the acidic Dajiuhu Peatland, located in the Shennongjia District of central China are investigated. This unique ecosystem, characterised by low pH (pH of 4.0 ± 0.2), high organic matter content, and pronounced redox stratification, provides a suitable niche for the discovery of a novel MTB strain, *Magnetominusculus dajiuhuensis* DJH-1^{Ts}. Morphological analyses using scanning and transmission electron microscopy reveal a coccobacilli shape and distinctive magnetosome chain organisation. Genomic analyses confirm the presence of a complete magnetosome gene cluster (MGC) comprising homologs of known magnetosome-associated genes such as *man1* through *man6*, as well as *mamA*, *mamB*, *mamE*, *mamI*, *mamK*, *mamM*, *mamO-Cter*, *mamP*, *mamQ-I*, *mamQ-II*, and the *mad* gene series (*mad2*, *mad10*, *mad23* to *mad26*, and *mad31*). Apart from this, metabolic pathways for denitrification, sulphate reduction, and anaerobic carbon fixation via the Wood–Ljungdahl pathway are also observed. These features collectively indicate the metabolic

versatility of the strain, allowing it to thrive under anaerobic conditions while contributing to critical biogeochemical processes. Fluorescence in situ hybridisation with a species-specific probe further confirm the taxonomic and morphological identity of this novel strain. The genome-based taxonomy places *M. dajiuhuensis* within a new genus, *Magnetominusculus*, under the phylum *Nitrospirota*, which expands the phylogenetic breadth of known MTB.

In the second part of the thesis, this investigation is extended to global oceanic OMZs, which are regions of suboxic to anoxic water columns where microbial communities exert strong control over nutrient dynamics. A total of 101 publicly available metagenomic datasets from OMZs were retrieved and processed. Using a combination of assembly, binning, and refinement tools, 30 MGC-containing bacterial metagenome-assembled genomes (MAGs) were recovered. These MAGs belong to diverse taxonomic lineages across 14 phylum-level classifications, including groups known to contain MTB as well as novel lineages previously not found to harbour MTB. Functional annotation reveals a variety of MGC architectures containing genes involved in nitrogen and sulphur metabolism. Kyoto Encyclopedia of Genes and Genomes (KEGG) pathway reconstructions and comparative genomic analyses suggest that these OMZ-derived potential MGC-containing bacteria maybe involved in denitrification, sulphate reduction, and carbon fixation under low-oxygen conditions, thereby playing a pivotal role in regulating oceanic redox processes. Computational pipelines were used for genome annotation, phylogenomics, and metabolic reconstruction. MGC screening was conducted using MagCluster, with annotations cross-verified via PSI-BLAST and visualised using clinker. Quality control and dereplication of MAGs were achieved using CheckM and dRep, respectively. Phylogenetic placement was inferred from single-copy marker genes using GTDB-Tk and ANI comparison was visualised using PairwiseANIViz. Functional annotations were derived from KofamKOALA and KEGGDecoder, providing insights into the completeness and diversity of metabolic pathways across taxa.

From a conceptual standpoint, the ecological plasticity and evolutionary significance of MTB are highlighted in this thesis, in underexplored extreme habitats. The discovery of MTB in peatlands adds to previous findings of MTB from the Dajiuhu Peatland, albeit with extensive and more thorough morphological and genomic characterisation; while the prevalence of MGC-containing bacteria (putative MTB) in OMZs underscores their capacity to adapt to low-oxygen marine environments. The utility of genome-resolved metagenomics in uncovering hidden microbial diversity and biogeochemical function in complex ecosystems is also underscored, which might otherwise go unnoticed.

This research extends the known ecological range and genomic repertoire of MTB. It introduces novel taxonomic representatives, elucidates metabolic strategies for life under extreme environmental pressures, and reinforces the role of MTB as crucial agents of redox-driven nutrient cycling. These findings not only augment our understanding of microbial ecology and evolution but also have implications for paleoenvironmental reconstruction, astrobiology, and biotechnological applications such as bioremediation and biomineralisation. Future work should aim to cultivate additional MTB from OMZs and other extreme environments, validate metabolic predictions through transcriptomics and proteomics, and explore the potential of MTB as biosignatures in Earth and planetary sciences.

Keywords: magnetotactic bacteria; acidic peatlands; oxygen minimum zones; *Nitrospirota*; biogeochemical cycling

Acknowledgements

I would like to express my deepest gratitude to my supervisors Professor Andrew P. Roberts and Assoc. Professor David Heslop at the Australian National University (ANU) and Professor Wei Lin at the Institute of Geology and Geophysics, Chinese Academy of Sciences (IGGCAS), for allowing me to pursue a dual-PhD program and for their invaluable guidance and encouragement throughout this journey. I convey my gratitude to my panel members at ANU, Professor Stewart Fallon and Professor Michael Ellwood, for their guidance and support during my candidature at ANU. Their unwavering support at every stage has been instrumental in shaping my academic path.

The COVID-19 pandemic significantly impacted my research timeline, causing a delay of nearly three years. However, I was able to use this time meaningfully in India, immersing myself in scientific literature and authoring a comprehensive review article that laid the foundation for much of my research. This period was especially challenging, and I thank my supervisors for their understanding and encouragement, which sustained my motivation through this difficult time.

As a dual-PhD candidate working across two institutions and countries, I had to travel internationally quite a few times. However, the continuous support of my supervisors ensured that the process remained smooth and manageable. I would like to extend special thanks to my fellow graduate student, Runjia Ji, who has played a foundational role in my research journey from the beginning. It is from her that I learned bioinformatic analysis, and her guidance over the past five years has been irreplaceable.

I also extend my sincere thanks to Dr. Liu Li and Dr. Wensi Zhang for their assistance with sample collection; to Asst. Professors Shen and Wan for generously reviewing my manuscripts whenever needed; and to Wang Zhe for offering her help with laboratory work without hesitation. I am equally thankful to the TEM and SEM facility engineers at IGGCAS, Lixin Gu and

Xu Tang, for their technical expertise in instrument handling and data acquisition. I thank relevant faculty and non-faculty members at the ANU for ensuring a smooth transition and stay during my time in Australia and helping me with administrative processes.

I want to acknowledge the support and understanding of my parents, parents-in-law, and sister, all of whom respected the value of higher education and encouraged me to pursue my academic goals. The loss of my mother-in-law during this period was a deeply personal hardship, and I remain grateful for the emotional strength my family provided during that time.

Most importantly, I am indebted to my husband, Shreyus, whose unwavering support made it possible for me to pursue this demanding academic endeavour. He carried the weight of family responsibilities on his shoulders with grace and optimism, allowing me the freedom to focus on my research. Lastly, I thank my beloved dog, Huw, whose joyful companionship brought immense comfort and motivation, particularly during the long and isolating pandemic years.

Contents

Chapter 1: Thesis Introduction

BACKGROUND AND SIGNIFICANCE

Microbial life in aquatic ecosystems is central to Earth's biogeochemical functioning. It drives the cycling of carbon, nitrogen, sulphur, and iron across oxic and anoxic interfaces. Within this microbial matrix, magnetotactic bacteria (MTB) occupy a particular ecological niche due to their capacity for intracellular biomineralisation and magnetic navigation. These prokaryotic organisms form membrane-bound crystals of magnetite (Fe_3O_4) and/or greigite (Fe_3S_4), named magnetosomes, which allow alignment with Earth's magnetic field to locate optimal redox zones in sediment and water columns (Uebe and Schüler, 2016; Bazylinski and Frankel, 2004). This behaviour, termed magnetotaxis, enables MTB to thrive at oxic–anoxic transition zones, where strong vertical gradients in oxygen, iron, and sulphur provide critical metabolic substrates (Bazylinski and Lefèvre, 2013; Lin et al., 2020).

Despite decades of discovery and cultivation of model strains such as *Magnetospirillum magneticum* AMB-1 (AMB-1) and *M. gryphiswaldense* MSR-1 (MSR-1) (Matsunaga et al., 1991; Schleifer et al., 1991), the broader ecological distribution, evolutionary diversity, and environmental roles of MTB remain underexplored, particularly in extreme environments characterised by fluctuating redox conditions. Two such environments—acidic peatlands and oceanic oxygen minimum zones (OMZs)—are emerging as critical biogeochemical interfaces under accelerating anthropogenic stress, yet they remain poorly sampled for MTB diversity and function (Goswami et al., 2022; Lin et al., 2020).

Understanding microbial ecology in peatlands is especially urgent because these ecosystems are globally significant carbon sinks and are increasingly vulnerable to warming and drying trends under climate

change (Gorham, 1991; Limpens et al., 2008). Microbial processes, including methane production, nitrogen transformations, and iron/sulphur cycling, mediate greenhouse gas fluxes in response to water table and temperature shifts (Bridgham et al., 2008; Turetsky et al., 2014). These fluxes have major implications for carbon-climate feedbacks (Wilson et al., 2016). Similarly, OMZs are expanding due to increased ocean stratification, warming, and nutrient loading, and have become hotspots of microbially mediated nitrogen loss and sulphur reduction (Stramma et al., 2008; Breitburg et al., 2018). Microbes in OMZs contribute to global nitrogen cycling via denitrification and anammox, and their activity modulates nitrous oxide emissions, linking local redox dynamics to atmospheric feedbacks (Lam and Kuypers, 2011; Ulloa et al., 2012).

Despite these global-scale consequences, MTB remain largely uncharacterised in OMZs and have only recently been isolated from acidic peatlands (Lin et al., 2020). This work is aimed at addressing that disparity, positioning MTB as a group with which to explore microbial adaptation, metabolic flexibility, and evolutionary diversification across these two redox-dynamic ecosystems.

Magnetotactic Bacteria as a Model System

MTB offer an exceptional system to study microbial behaviour, metabolism, and evolution in stratified aquatic environments. Their defining feature is the biomineralisation of magnetosomes, which is governed by magnetosome gene clusters (MGCs) that enable magnetotaxis. These MGCs include conserved genes such as *mam*, *mad*, *mms*, and *man*, which orchestrate the nucleation, shape control, and chain alignment of magnetic crystals (Lin et al., 2017a; Müller et al., 2020). This regulated organelle formation in a prokaryotic lineage makes MTB a rare model for studying bacterial compartmentalisation and organelle evolution.

While magnetosomes confer navigational advantages, they may also serve additional physiological roles: detoxification of reactive oxygen species, redox balancing, or iron storage under low-oxygen stress (Lin et al., 2017b; Strbak et al., 2019; Muñoz et al., 2020). These functions suggest that magnetosomes may have evolved in response to ancient environmental pressures that have been co-opted later for magnetotaxis.

MTB are taxonomically diverse and multi-phyletic, appearing across at least 16 bacterial phyla, including *Proteobacteria* (currently *Pseudomonadota*), *Nitrospirota*, *Desulfobacterota*, *Omnitrophota*, and *Planctomycetota* to name a few (Goswami et al., 2022; Uzun et al., 2020). This wide distribution reflects a complex evolutionary history involving vertical inheritance, lateral gene transfer, and ecological diversification. The discovery of magnetofossils (fossilised magnetosomes preserved in sediments) has also enabled paleoenvironmental reconstructions, suggesting that MTB were active as far back as 1.9–2.1 Ga (Kopp and Kirschvink, 2008). Thus, MTB serve not only as modern biogeochemical agents but also as windows into Earth's ancient microbial past.

Magnetotactic Bacteria from Extreme Aquatic Habitats

MTB have garnered increasing recognition not only for their widespread presence in stratified aquatic ecosystems but also for their impressive adaptability to extreme environmental conditions. These conditions encompass highly acidic, hypersaline, thermophilic, psychrophilic, and low-oxygen environments. This remarkable adaptability highlights their physiological and genomic plasticity and underscores their essential roles in biogeochemical cycling even under environmental stress. Among the most physiologically and genomically distinctive MTB are those within the phylum *Nitrospirota*, particularly members of the class *Thermodesulfovibrionia.* These bacteria thrive in iron- and sulphur-rich, anoxic habitats, characterised by their dense

magnetosome chains. Genomic analyses reveal that they possess pathways enabling them to exploit chemically dynamic redox interfaces effectively. A notable example is *Magnetominusculus dajiuhuensis* DJH-1^{Ts}, which was extracted magnetically from the acidic, waterlogged Dajiuhu Peatland in central China. This peatland has an average pH of 4.0± 0.2 (Zhang et al., 2024), which is a classic example of an extreme environment based on pH range (Gómez, 2011). Magnetic separation and characterisation of this novel species are discussed in detail in Chapter 4 of this thesis (Goswami et al., 2025). This novel species exhibits adaptations for anaerobic carbon fixation via the Wood–Ljungdahl pathway, demonstrating metabolic versatility that allows it to thrive in anaerobic environments with low pH. Its genome encodes an array of genes for denitrification, nitrogen fixation, and sulphur metabolism, which may enable it to couple magnetotaxis with nutrient acquisition in its niche habitat.

MTB have been observed in a variety of extreme and diverse habitats beyond their traditionally studied environments. For example, populations have been reported in hemipelagic sediments of the Eastern Pacific Ocean at depths of around 600 metres and in relatively cold waters (~8 °C), such as those in the Santa Barbara Basin (Stolz et al., 1986). In the eastern South Atlantic Ocean, live MTB cells have been found in both pelagic and hemipelagic zones, with a wide range of morphologies, including cocci, spirilla, vibroid, and rod-shaped cells (Petermann and Bleil, 1993). In equatorial marine regions like those near Singapore, tropical ecosystems have revealed high MTB diversity, suggesting their ecological significance in warm, shallow waters (Tan et al., 2021). A study of 16S rRNA gene sequences collected from seamounts in the Mariana Arc, between 238 m and 2023 m near Challenger Deep, uncovered 16 previously unidentified MTB groups (Liu et al., 2017).

In marine sediment from the Yellow Sea, groups affiliated with the phylum *Nitrospirae* were predominant among MTB communities

(Xu et al., 2018). In strongly alkaline settings, such as certain regions of California, three strains of *Desulfonatronum thiodismutans* were isolated from high-pH environments, with sulphate-reducing capabilities and possessing functional genes like *dsrAB* and *aprA*, which are essential for dissimilatory sulphate reduction (Lefèvre et al., 2011). Cold-adapted (psychrophilic) MTB have been found in Antarctic sediments and water samples from Admiralty Bay, King George Island, where environmental temperatures ranged from 0.1 to 0.8 °C (Abreu et al., 2016). Similarly, thermophilic MTB have been identified in Little Hot Creek Hot Springs, California, and Mono Lake, with some strains associated with *Nitrospirae* and Gammaproteobacteria lineages (Nash et al., 2008). Recent evidence from the Clarion–Clipperton Zone (East Pacific) has revealed the presence of deep-living MTB in hydrothermally oxygenated sediments, indicating their potential to inhabit inverse oxygen gradient zones formed by bottom-up fluid transport (Höfken et al., 2025).

Another thermophilic strain, *Candidatus* Thermomagnetovibrio paiutensis, was described from the geothermal fields at Great Boiling Springs, northern Nevada (Lefèvre et al., 2010). Additional MTB strains such as BW-2 and SS-5, which can biomineralise magnetite, were isolated from the hypersaline Salton Sea (Lefèvre et al., 2011). More recently, two Gammaproteobacteria MTB strains (FZSR-1 and FZSR-2) were recovered from salt ponds in Fuzhou Saltern, Bohai Bay, China (Liu et al., 2021). In acidic peatlands, Lin et al. (2020) observed active MTB cells with draft genomes linked to *Nitrospirae*, *Omnitrophica*, and Deltaproteobacteria.

Space exposure experiments using *Magnetospirillum gryphiswaldense* MSR-1 at 23 km altitude demonstrated survival of over 12% of the population, suggesting a degree of tolerance to desiccation, cold, ionizing radiation, and low-pressure conditions (Shen et al., 2023). Such resilience raises the possibility of MTB endurance in extraterrestrial environments. Beyond their roles in elemental cycling,

MTB influence sediment magnetic properties through magnetite and greigite biomineralisation, producing magnetofossils that serve as indicators of historical redox conditions and microbial activity. Their widespread distribution across polar regions, hydrothermal systems, saline basins, oxygen-depleted zones, and acid peatlands reflects their exceptional evolutionary adaptability. As environmental pressures from climate change intensify, a thorough understanding of MTB diversity, physiology, and ecosystem function is essential—not only for modelling their roles in present-day biogeochemical cycles but also for evaluating their utility as biosignatures in astrobiological exploration.

Knowledge Gaps in MTB Ecology

Despite recent advances, much current knowledge on MTB is derived from a narrow pool of cultivated strains and a limited range of habitats. Existing model organisms such as AMB-1, MSR-1, and *Desulfovibrio magneticus* RS-1 (Matsunaga et al., 1991; Sakaguchi et al., 2002) have provided invaluable insights but do not represent the full phylogenetic or metabolic diversity of MTB. Particularly underrepresented are the *Nitrospirota*-affiliated MTB, many of which form magnetosome chains with a large number of magnetosomes within each cell, and possess genomic features supporting sulphate reduction and carbon fixation (Jogler et al., 2010; Lin et al., 2014b). Strains such as *Candidatus* Magnetobacterium bavaricum and *Candidatus* Magnetobacterium casensis can form hundreds of magnetosomes per cell and store elemental sulphur intracellularly, traits suggesting significant ecological roles in redox cycling (Spring et al., 1993; Lin et al., 2014b). Yet, *Nitrospirota* MTB have not been cultivated in pure culture, and their population structure, genome content, and magnetosome architectures remain incompletely resolved. Similarly, the metabolic potential and distribution of MTB in OMZs remain unknown beyond a few indirect observations (Rhoads et al., 1991). There is also a lack of integrative studies that combine magnetic

separation, microscopy, genome-resolved metagenomics, and functional annotation across contrasting ecosystems.

OBJECTIVES AND SCOPE OF THE THESIS

The work presented in this thesis seeks to address critical gaps by using a dual-environment approach to investigate MTB communities from:

1. an acidic peatland system—the Dajiuhu Peatland in central China, and
2. oceanic OMZs—through genome-resolved re-analysis of publicly available metagenomes.

Once important preliminary introductory (Chapter 1), background (Chapter 2), and methodological issues (Chapter 3) are presented, new research on MTB from extreme environments is presented (Chapters 4 and 5). In Chapter 4, the magnetic separation and genomic characterisation of *Magnetominusculus dajiuhuensis* DJH-1^{Ts}, a newly identified member of the *Nitrospirota* phylum from Dajiuhu, China, are detailed. Its genome reveals novel configurations of magnetosome genes and metabolic modules supporting carbon fixation, nitrogen cycling, and sulphur respiration, demonstrating adaptations to anaerobic conditions (Goswami et al., 2025).

In Chapter 5, this inquiry is expanded to marine OMZs through a large-scale metagenomic survey of 101 datasets. From these, 30 MGC-containing bacterial MAGs are reconstructed and a further refined set of six high-confidence putative MTB MAGs are obtained. These six MAGs span four phyla, among which a novel lineage, *SM23-31*, is observed, which is not known to previously harbour MTB. These MAGs encode diverse MGCs and contain genes for denitrification, dissimilatory sulphur metabolism, and autotrophic CO_2 fixation, which suggests that MTB may contribute significantly to redox-sensitive element cycling in OMZs.

SIGNIFICANCE AND THESIS STRUCTURE

By characterising previously unknown MTB lineages in acidic and low-oxygen environments, this research expands both the taxonomic and functional boundaries of known MTB diversity. It introduces the first formally described acidophilic *Nitrospirota* MTB and contributes a suite of novel MTB genomes from OMZs. This dual-case approach links targeted isolation with metagenome analysis and provides a comprehensive view of MTB diversity, biogeography, and ecological function across two geochemically complex habitats. The findings hold relevance for modelling microbial feedbacks under climate change, particularly in carbon-rich wetlands and deoxygenating oceans (Stramma et al., 2008; Levin, 2018). The thesis is structured as follows:

- Chapter 1: introduction to the thesis structure and layout, briefly describing the bacterial group of interest, MTB.
- Chapter 2: a comprehensive review of MTB ecology, phylogeny, and function, which was published as a review article by Goswami et al. (2022).
- Chapter 3: discussion of methods used in this thesis.
- Chapter 4: details of the discovery and characterisation of *M. dajiuhuensis* DJH-1^{Ts}, a novel MTB species isolated from an acidic peatland, Dajiuhu, in Central China (Goswami et al., 2025).
- Chapter 5: a report of the metagenomic reconstruction of MGC-containing bacterial genomes (putative MTB) from marine OMZ datasets.
- Chapter 6: a synthesis of key findings and discussion of future research directions in the context of microbial adaptation, and climate feedbacks.

REFERENCES

Abreu, F., Martins, J. L. & Souza Silveira, T. “Candidatus magnetoglobus multicellularis”, a multicellular, magnetotactic prokaryote from a hypersaline environment. Int. J. Syst. Evol. Microbiol. 57, 1318–1322 (2007).

Abreu, F., Carolina, A., Araujo, V., Leão, P., Silva, K. T. & Carvalho, F. M. D. Culture independent characterisation of novel psychrophilic magnetotactic cocci from Antarctic marine sediments. Environ. Microbiol. 18, 4426–4441 (2016).

Bazylinski, D. A. & Frankel, R. B. Magnetosome formation in prokaryotes. Nat. Rev. Microbiol. 2, 217–230 (2004).

Bazylinski, D. A., Lefèvre, C. T. & Schüler, D. Magnetotactic Bacteria. In: Rosenberg, E., DeLong, E. F., Lory, S., Stackebrandt, E. & Thompson, F. (eds) The Prokaryotes: Prokaryotic Physiology and Biochemistry, 453–494 (Springer, 2013).

Breitburg, D. et al. Declining oxygen in the global ocean and coastal waters. Science 359, eaam7240 (2018).

Bridgham, S. D. et al. Rapid carbon response of peatlands to climate change. Ecology 89, 3041–3048 (2008).

Gómez, F. Extreme environment. In: Gargaud, M. et al. (eds) Encyclopedia of Astrobiology (Springer, 2011).

Gorham, E. Northern peatlands: Role in the carbon cycle and probable responses to climatic warming. Ecol. Appl. 1, 182–195 (1991).

Goswami, P. et al. Magnetotactic bacteria and magnetofossils: Ecology, evolution and environmental implications. npj Biofilms Microbiomes 8, 43 (2022).

Goswami, P. et al. Genomic and metabolic characterisation of a novel species Magnetominusculus dajiuhuensis DJH-1Ts sp. nov. from an acidic peatland. Syst. Appl. Microbiol. 48, 126605 (2025).

Höfken, A. F., von Dobeneck, T., Winklhofer, M., Kuhn, T. & Kasten, S. Life in a benthic mirror-world: Evidence for deep-living magnetotactic bacteria in hydrothermally bottom-up oxygenated Pacific ridge sediments. Geophys. Res. Lett. 52, e2024GL113606 (2025).

Jogler, C. et al. Cultivation-independent characterisation of 'Candidatus Magnetobacterium bavaricum' via ultrastructural, geochemical, ecological and metagenomic methods. Environ. Microbiol. 12, 2466–2478 (2010).

Kopp, R. E. & Kirschvink, J. L. The identification and biogeochemical interpretation of fossil magnetotactic bacteria. Earth-Sci. Rev. 86, 42–61 (2008).

Lam, P. & Kuypers, M. M. M. Microbial nitrogen cycling processes in oxygen minimum zones. Annu. Rev. Mar. Sci. 3, 317–345 (2011).

Lefèvre, C. T. et al. Nonmagnetotactic multicellular prokaryotes from low-saline, nonmarine aquatic environments and their unusual negative phototactic behavior. Appl. Environ. Microbiol. 76, 3220–3227 (2010).

Lefèvre, C. T. et al. Isolation of obligately alkaliphilic magnetotactic bacteria from extremely alkaline environments. Environ. Microbiol. 13, 2342–2350 (2011).

Limpens, J. et al. Peatlands and the carbon cycle: From local processes to global implications – a synthesis. Biogeosciences 5, 1475–1491 (2008).

Lin, W. et al. Genomic insights into the uncultured genus ‘Candidatus Magnetobacterium’ in the phylum Nitrospirae. ISME J. 8, 2463–2477 (2014).

Lin, W. et al. Origin of microbial biomineralisation and magnetotaxis during the Archean. Proc. Natl Acad. Sci. USA 114, 2171–2176 (2017).

Lin, W., Pan, Y. & Bazylinski, D. A. Diversity and ecology of and biomineralisation by magnetotactic bacteria. Environ. Microbiol. Rep. 9, 345–356 (2017).

Lin, W. et al. Expanding magnetic organelle biogenesis in the domain Bacteria. Microbiome 8, 152 (2020).

Liu, J. et al. Bacterial community structure and novel species of magnetotactic bacteria in sediments from a seamount in the Mariana volcanic arc. Sci. Rep. 7, 15343 (2017).

Liu, P. et al. Identification and characterisation of magnetotactic Gammaproteobacteria from a salt evaporation pool, Bohai Bay, China. Environ. Microbiol. https://doi.org/10.1111/1462-2920.15516 (2021).

Matsunaga, T., Sakaguchi, T. & Tadakoro, F. Magnetite formation by a magnetic bacterium capable of growing aerobically. Appl. Microbiol. Biotechnol. 35, 651–655 (1991).

Müller, F. D., Schüler, D. & Pfeiffer, D. A compass to boost navigation: Cell biology of bacterial magnetotaxis. J. Bacteriol. 202, e00368-20 (2020).

Muñoz, D. et al. Magnetosomes could be protective shields against metal stress in magnetotactic bacteria. Sci. Rep. 10, 11430 (2020).

Nash, C. Z. Mechanisms and evolution of magnetotactic bacteria. PhD thesis, California Institute of Technology (2008).

Petermann, H. & Bleil, U. Detection of live magnetotactic bacteria in South Atlantic deep-sea sediments. Earth Planet. Sci. Lett. 117, 223–228 (1993).

Rhoads, D. C. et al. The dysaerobic zone revisited: A magnetic facies? Geol. Soc. Lond. Spec. Publ. 58, 187–199 (1991).

Sakaguchi, T., Arakaki, A. & Matsunaga, T. Desulfovibrio magneticus sp. nov., a novel sulphate-reducing bacterium that produces intracellular single-domain-sized magnetite particles. Int. J. Syst. Evol. Microbiol. 52, 215–221 (2002).

Schleifer, K. H. et al. The Genus *Magnetospirillum* gen. nov. Description of *Magnetospirillum gryphiswaldense* sp. nov. and transfer of *Aquaspirillum magnetotacticum* to *Magnetospirillum magnetotacticum* comb. nov. Syst. Appl. Microbiol. 14, 379–385 (1991).

Shen, J. et al. Renaissance for magnetotactic bacteria in astrobiology. ISME J. 17, 1526–1534 (2023).

Spring, S., Amann, R., Ludwig, W., Schleifer, K.-H. & van Gemerden, H. Dominating role of an unusual magnetotactic bacterium in the microaerobic zone of a freshwater sediment. *Appl. Environ. Microbiol.* **59**, 2397–2403 (1993).

Stolz, J. F., Chang, S. B. R. & Kirschvink, J. L. Magnetotactic bacteria and single-domain magnetite in hemipelagic sediments. Nature 321, 849–851 (1986).

Stramma, L. et al. Expanding oxygen-minimum zones in the tropical oceans. Science 320, 655–658 (2008).

Strbak, O. & Dobrota, D. Archean iron-based metabolism analysis and the photoferrotrophy-driven hypothesis of microbial magnetotaxis origin. Geomicrobiol. J. 36, 278–290 (2019).

Tan, S. M., Ismail, M. H. & Cao, B. Biodiversity of magnetotactic bacteria in the tropical marine environment of Singapore revealed by metagenomic analysis. Environ. Res. 194, 110714 (2021).

Turetsky, M. R. et al. A synthesis of methane emissions from 71 northern, temperate, and subtropical wetlands. Glob. Change Biol. 20, 2183–2197 (2014).

Ulloa, O. et al. Microbial oceanography of anoxic oxygen minimum zones. Proc. Natl Acad. Sci. USA 109, 15996–16003 (2012).

Uzun, M. et al. Unravelling the diversity of magnetotactic bacteria through analysis of open genomic databases. Sci. Data 7, 252 (2020).

Wilson, R. M. et al. Stability of peatland carbon to rising temperatures. Nat. Commun. 7, 13723 (2016).

Xu, C. et al. Distribution and diversity of magnetotactic bacteria in sediments of the Yellow Sea continental shelf. J. Soils Sediments 18, 2634–2646 (2018).

Zhang, Y. M. et al. The stable carbon and hydrogen isotopic composition of microbial fatty acids traces microbial metabolism in soils and peats. Geochim. Cosmochim. Acta 365, 85–100 (2024).

Chapter 2: Literature Review

SUMMARY OF CHAPTER

A detailed review of magnetotactic bacteria (MTB) and magnetofossils is presented in this chapter, focusing on their ecological significance, evolutionary origins, and environmental roles across diverse aquatic systems. It brings together decades of research on MTB, from their initial discovery and morphological diversity to recent advances in omics, magnetic characterisation, and separation techniques. The review further outlines the phylogenetic breadth of MTB across 16 phyla, discusses their roles in elemental cycling and potential for bioremediation, and evaluates the paleoenvironmental importance of magnetofossils as proxies for ancient microbial life and redox conditions. A special emphasis is placed on the relevance of MTB to stratified environments, including OMZs, and the emerging recognition of their widespread presence and functional versatility in such systems. This review article was published in *npj Biofilms and Microbiomes*, and it forms the conceptual backbone of this thesis by defining the broader ecological and evolutionary context into which my experimental work fits.

The following chapter appears as published in: Goswami, P., He, K., Li, J., Pan, Y., Roberts, A. P., & Lin, W. (2022). Magnetotactic bacteria and magnetofossils: Ecology, evolution and environmental implications. *npj Biofilms and Microbiomes*, 8:43; https://doi.org/10.1038/s41522-022-00304-0

Magnetotactic bacteria and magnetofossils: ecology, evolution and environmental implications

Pranami Goswami[1,2,3,4], Kuang He[1,2,5], Jinhua Li[1,2], Yongxin Pan[1,2,3], Andrew P. Roberts[4*] and Wei Lin[1,2*]

[1]Key Laboratory of Earth and Planetary Physics, Institute of Geology and Geophysics, Chinese Academy of Sciences, Beijing 100029, China.

[2]France-China Joint Laboratory for Evolution and Development of Magnetotactic Multicellular Organisms, Chinese Academy of Sciences, Beijing 100029, China.

[3]College of Earth and Planetary Sciences, University of Chinese Academy of Sciences, Beijing 100049, China.

[4]Research School of Earth Sciences, Australian National University, ACT, Canberra 2601, Australia.

[5]Frontiers Science Center for Deep Ocean Multispheres and Earth System, Key Laboratory of Submarine Geosciences and Prospecting Techniques, MoE and College of Marine Geosciences, Ocean University of China, Qingdao 266100, China.

*Emails: weilin@mail.iggcas.ac.cn (W.L.) and andrew.roberts@anu.edu.au (A.P.R.)

ABSTRACT

Magnetotactic bacteria (MTB) are a group of phylogenetically diverse and morphologically varied microorganisms with a magnetoresponsive capability called magnetotaxis or microbial magnetoreception. MTB are a distinctive constituent of the microbiome of aquatic ecosystems because they use Earth's magnetic field to align themselves in a north or south facing direction and efficiently navigate to their favoured microenvironments. They have been identified worldwide from diverse aquatic and waterlogged microbiomes, including freshwater, saline, brackish and marine ecosystems and some extreme environments. MTB play important roles in the biogeochemical cycling of iron, sulphur, phosphorus, carbon and nitrogen in nature and have been recognised from *in vitro* cultures to sequester heavy metals like selenium, cadmium and tellurium, which makes them prospective candidate organisms for aquatic pollution bioremediation. The role of MTB in environmental systems is not limited to their lifespan; after death, fossil magnetosomal magnetic nanoparticles (known as magnetofossils) are a promising proxy for recording paleoenvironmental change and geomagnetic field history. Here, we summarize the ecology, evolution and environmental function of MTB and paleoenvironmental implications of magnetofossils in light of recent discoveries.

Keywords: magnetotactic bacteria; magnetotaxis; magnetofossils; bioremediation; heavy metals

INTRODUCTION

The terms biomineralisation and magnetoreception are invariably associated with magnetotactic bacteria (MTB). Magnetoreception involves use of Earth's magnetic field for motility and navigation and biomineralisation is a capability by which organisms produce minerals[1,2]. MTB are so far the only known group of prokaryotes with the ability to perform both biomineralisation and magnetoreception[3]. MTB have been proposed to represent some of the most ancient organisms capable of biomineralisation[4]. This group of bacteria was discovered in 1963 by Salvatore Bellini[5], and was rediscovered independently in 1974 by Richard Blakemore[6]. The latter study also identified magnetosomal magnetic particles for the first time, which were referred to as "iron-rich particles". MTB form magnetite (Fe_3O_4) and/or greigite (Fe_3S_4) crystals, generally in bead-like chains[7] (Figure 1). Magnetotaxis is one of their primary modes of motility[7]. Many organisms can use the geomagnetic field for navigation. Birds, fish, and certain migratory animals among others top this list, while desert ants, newts, spiny lobsters, snails, bogong moths and certain other invertebrates have been recently found to possess a magnetic sense of some sort[8,9,10,11]. Some mammals, too, can respond to Earth's magnetic field. Laboratory experiments indicate that wood mice and mole rats make use of magnetic field lines while siting nests; certain cattle and deer use the field for body orientation while grazing; and dogs appear to orient toward north or south when they excrete[12,13,14]. Magnetic orientation is associated with many organisms, and understanding its origin is a subject of extensive research.

Magnetoreception represents a spectrum of capabilities of which magnetotaxis is a sub-set. While magnetoreception is mostly associated with higher organisms that use a magnetic sense for mobility, magnetotaxis is associated with microorganisms. It is related to previously discovered methods of taxis such as chemotaxis and aerotaxis, which are common modes of transportation and translocation by bacteria and

archaea[15,16]. However, unlike chemotaxis or aerotaxis, which are multi-directional, magnetotaxis mostly involves upward/downward movement in search of optimal microenvironments near chemical gradients in water/sediment, aligning passively along Earth's magnetic field[17]. It is thought that magnetotaxis along with chemotaxis/aerotaxis provides an additional benefit to MTB by permitting a one-dimensional search along the oxic-anoxic interface (OAI) in aquatic environments to enable MTB to find optimal oxygen concentrations to carry out necessary physiological functions[18]. MTB ecology, diversity and evolution have been reviewed previously (e.g.,[19,20,21]); however, recent developments of omics, cultivation and magnetic measurements have expanded our understanding of MTB and magnetofossils. Multiple studies have pointed out that magnetotaxis is monophyletic in origin; that is, it originated from a single common ancestor[22,23,24]. This would make it a primordial physiological phenomenon and (probably) the earliest case of magnetoreception and systematic biomineralisation on Earth[25,4]. Following this discovery, diverse multi-disciplinary studies have sought to answer several significant questions. Are MTB widespread across the domain *Bacteria*? How did magnetotaxis originate and evolve? Do MTB have a significant role in biogeochemical element cycling? These questions are of multidisciplinary interest to microbiologists, geologists, physicists and chemists. In this paper, we review progress to date in addressing these questions. We discuss the phylogenetic diversity of MTB and their potential role in the biogeochemical cycling of elements, and compare the metabolic pathways of all sixteen phylum-level MTB lineages identified so far. Moreover, we discuss expanding oxygen minimum zones (OMZs) in the oceans; diverse MTB likely live in OMZs and their environmental role in such settings has been under-studied.

MTB Diversity and Ecology

MTB occur in multiple lineages of the bacterial tree of life, although with a patchy distribution. They include cocci, vibrio, rod, spirilla and

multicellular morphotypes[26,27,19,20]. Until 2012, both cultured and uncultured MTB could be grouped mostly into the Proteobacteria phylum (including the Alphaproteobacteria, Gammaproteobacteria and Deltaproteobacteria classes) and a few in the *Nitrospirae* phylum[27] (Figure 2a). In 2012, a novel uncultivated ovoid MTB (designated SKK-01) from Lake Chiemsee, Germany, was discovered and characterised to belong to the candidate phylum *Omnitrophica* (also known as candidate division OP3)[28] (Fig 2b). In 2015 and 2017, two additional bacterial phyla, the candidate phylum *Latescibacteria*[29] and the phylum *Planctomycetes*[21], respectively, were identified to contain MTB based on the presence of magnetosome gene clusters (MGCs, a group of genes responsible for magnetosome biomineralisation and magnetotaxis) in their genomes (Figure 2c). More recently, advances in metagenomic approaches, large-scale field studies and public database mining studies have expanded the total number of MTB-containing phylum-level lineages from five to sixteen[30,31,24], which greatly increases the taxonomic and genomic diversity of MTB across the domain *Bacteria* (Figure 2d). These findings highlight a much higher diversity of MTB lineages in the domain *Bacteria* than previously anticipated. On the basis of MGC types in MTB genomes, putative Fe_3O_4-producing MTB have been identified in all MTB lineages so far except for the *Latescibacteria* phylum, while putative Fe_3S_4-producing MTB exist in at least five bacterial phyla[31]. MTB affiliated with the *Nitrospirae* phylum are biogeochemically important because many members of this group produce several hundred magnetosomal magnetite crystals per cell rather than the normal 10-50 crystals in most MTB[26,32]. Characteristic examples are the *Candidatus* Magnetobacterium bavaricum, which was discovered by Petersen et al.[33] and was subsequently phylogenetically defined by Spring et al.[26] as magnetotactic rods that form elongated, bullet-shaped and kinked crystals arranged in a parallel chain-like fashion that appear as rope-like strands or bundles. Hanzlik et al.[34,35] studied the chain architecture of *Ca.* Magnetobacterium bavaricum in detail.

Apart from producing magnetite within magnetosomes, cells of *Ca.* Magnetobacterium bavaricum also harbour sulphur globules, solely comprising cyclo-octasulphur (S8), which gives them a probable role in both iron and sulphur cycling in nature[31,36]. The second example is *Ca.* Magnetobacterium casensis, which is smaller than *Ca.* Magnetobacterium bavaricum and produces around 200–500 magnetosomal Fe_3O_4 particles per cell[37,38,39]. Recent 16S rRNA-based and metagenomic surveys suggest that magnetotactic *Nitrospirae* are more diverse and more widely distributed than previously thought[40,31], which emphasizes their environmental importance in various ecosystems.

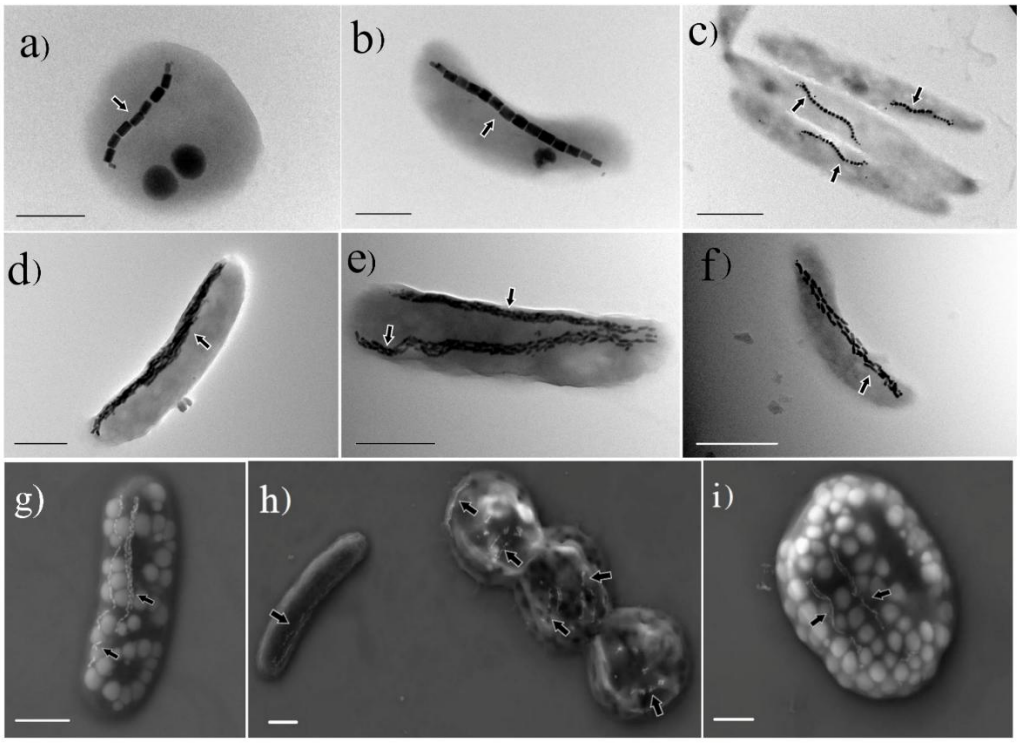

Figure 1: Transmission electron microscope (a-f) and scanning electron microscope (g-i) images of various MTB. Black arrows indicate magnetosome chains. Scale bars: (a-b) = 0.5 µm, c = 1 µm, d = 0.1 µm, (e-i) = 1 µm

Apart from single-celled bacteria, multicellular magnetic prokaryotes (MMPs) are flagella-aided motile organisms that also produce magnetic nanocrystals, as first reported by Farina et al.[41]. Despite their multicellular organisation, MMPs have coherent magnetosome-chain polarity across their cells[41]. Many studies have now been carried out involving especially the spherical MMP morphotype (sMMP)[42,43,44,45,46,47,48]. A second morphotype, ellipsoidal MMP (eMMP), has been found in the Mediterranean Sea and Pacific Ocean[49,50,51,52,53,54,55,56,57]. MMPs are affiliated within the *Deltaproteobacteria* and MTB from this group produce Fe_3O_4 and/or Fe_3S_4 nanoparticles[23,31]. Studies of MMPs also provide insights into the origin and evolution of bacterial multicellularity, which is one of the most prevalent evolutionary innovations in the bacterial world[58].

MTB have been identified from diverse biomes with highly variable, including extreme, environments. For instance, MTB flourish in shallow hemipelagic sediments (at ~600 m depths) at 8 °C, in Santa Barbara Basin, Eastern Pacific Ocean[59]. Petermann and Bleil[60] discovered live MTB from pelagic and hemipelagic sediments in the eastern South Atlantic Ocean. They observed assorted cocci, spirilla, vibrioids and even rod-shaped MTB morphologies in pelagic environments on the African continental margin and on Walvis Ridge at ~3,000 m and ~1,000 m water depths, respectively. More recently, MTB have been observed from tropical marine environments in Singapore, which adds to equatorial MTB biodiversity[61]. A recent phylogenetic analysis of 16S rRNA gene sequences of microbial communities from a seamount in the Mariana volcanic arc (238–2,023 m) near Challenger Deep, tropical western Pacific Ocean, revealed 16 novel MTB populations[62]. Abundant MTB have also been observed in seafloor sediments of the Yellow Sea with *Nitrospirae* being the dominant group[63]. In more extreme environments, Lefèvre et al.[64] isolated three MTB strains of Desulfonatronum thiodismutans from hyper-alkaliphilic habitats in California, USA, that are obligate alkaliphiles (with optimal growth at pH 9.0–9.5) and sulphate reducers. Essential genes (i.e., dissimilatory sulphite

reductase (*dsrAB*) and adenosine-5′-phosphate reductase (*aprA*)) were identified that verify that the novel strains are sulphate reducers. Psychrophilic MTB have been characterised from water and sediment samples from Admiralty Bay, King George Island, Antarctica, where average water temperatures during sampling ranged between 0.1 and 0.8 °C[65]. Nash et al.[66] characterised a thermophilic MTB variety belonging to *Nitrospirae* from Little Hot Creek Hot Springs, California, and another *Gammaproteobacteria* MTB from the hyper-alkaline and hyper-saline Mono Lake. Lefèvre et al.[67] discovered a thermophilic MTB that they named *Candidatus* Thermomagnetovibrio paiutensis from mud and water samples in hot springs of the Great Boiling Springs geothermal field in Gerlach, northern Nevada. Two rod-shaped *Gammaproteobacteria* MTB strains, BW-2 and SS-5, from the hyper-saline Salton Sea were the first isolated MTB from the *Gammaproteobacteria* class that biomineralise magnetite[68]. Further *Gammaproteobacteria* MTB strains FZSR-1 and FZSR-2 were identified recently from a salt evaporation pool in Fuzhou saltern, Bohai Bay, China[69]. Lin et al.[31] also discovered living MTB cells in a relatively acidic peatland soil with draft genomes dominantly comprising magnetotactic *Nitrospirae*, *Omnitrophica* and *Deltaproteobacteria*.

Origin and Evolution of MTB

Ancient atmospheric molecular O_2 in the Archean, 2.4 billion years ago (Ga), was less than 0.001% of the atmosphere today[70] and Fe(II) concentrations probably ranged between 0.03 and 0.5 mM[71,72] (modern oceanic iron concentrations range between 0.05 and 2.0 nM[73]). Archean ocean sulphate concentrations were also less than 1/100 of present levels, with concentrations lower than 200 μM[74,75] and N_2 was a bulk gas with similar levels to today[76]. Oxygen concentrations in the atmosphere and surface ocean first rose at ~2.4 Ga in the Great Oxygenation Event (GOE)[77] with a second increase in the Neoproterozoic Oxygenation Event[78] (NOE), which established a more modern ocean redox profile. The GOE is

generally thought to have facilitated the emergence of eukaryotes[79] while Betts et al.[80] argue that the NOE was associated with emergence of large and complex multicellular organisms. Thus, the GOE and NOE were fundamental pacemakers for evolution of life on Earth, although the beginning of microbial life must have been much earlier than the GOE. There is evidence of microbial life originating sometime during the early Archean at ~3.5-3.8 Ga[79,81]. The presence of biogenic carbon has been uncovered in detrital zircon grains from Jack Hills, Western Australia[82]; if verified by further studies, the beginning of microbial life can be traced to ~4.1 Ga in the late Hadean Eon. Further evidence is required to corroborate this early age, which potentially transforms the way scientists view paleo-environments on Earth.

Fossilised magnetosomal magnetic particles (referred to as magnetofossils) can be preserved in sediments or rocks. Magnetofossil records trace an evolutionary history of MTB to the Cretaceous and with less certainty to the Paleoproterozoic at around ~1.9 Ga[83,84,85], which suggests that MTB should have an early origin. Furthermore, phylogenetic and molecular clock analyses suggest an Archean origin for genetic functionality of magnetosome biomineralisation (which is needed to perform magnetotaxis); specifically, emergence of MGCs is estimated to date to the Archean Eon (~3.38–3.21 Ga)[25] or even earlier[24,31]. It is important to remember that atmospheric oxygen was most likely sparse in the Archean so that an anoxic environment prevailed[86,87,88,89]. In addition to magnetotaxis, magnetosomal particles have been proposed to act as iron storage and sequestration organelles, or as gravity detection units or 'geobatteries' that provided energy from elemental oxidation-reduction cycling[90]. It has recently been proposed that the initial role of magnetosomal magnetic particles was to mitigate intracellular reactive oxygen species (ROS) toxicity and that, eventually, they were co-opted for magnetotaxis in early Earth environments[4]. A photoferrotrophy-driven origin of magnetotaxis has also been proposed; that is, magnetosome

formation was a by-product of Archean iron cycling and magnetotaxis evolved as a result of environmental pressure of co-evolved cyanobacteria and metabolically-accumulated magnetite[91]. Magnetosomes have also been proposed to provide a protective shield in a metal-stressed environment[92]. To ascertain the evolutionary history of MTB, integration of microbiology, evolutionary biology, geobiology, biogeochemistry and geochronology is required.

Recent development of metagenomics and single-cell genomics allows direct reconstruction of MTB genomes from environmental samples without cultivation. Comparison of these novel genomes with those from cultivated MTB strains provides insights into the evolution of magnetotaxis. Magnetosome protein phylogeny largely mirrors that of organisms at or above the class or phylum level, which suggests that vertical inheritance followed by multiple independent MGC losses mainly drove bacterial evolution of magnetotaxis at higher taxonomic levels[23,25,31]. Subsequent evolutionary trajectories of magnetotaxis at lower taxonomic ranks appear to be much more complicated and multiple evolutionary processes including horizontal gene transfers, gene duplications and/or gene losses may have been involved[93,94,95]. Metagenomic sequences with similarity to known magnetosome genes have been found in the microbiomes of some animals and even humans, which might suggest that MTB sensed by their hosts may produce symbiotic magnetoreception in these organisms[96,97,98]. It has also been suggested recently that the ability to biologically control magnetite precipitation might have been a fundamental feature of eukaryotic biology that was likely present in the last common ancestor of some archaea and extant eukaryotes[99].

Magnetic Characterisation and Quantification of MTB and Magnetofossils

Magnetofossils are distributed widely in freshwater and marine sediments[83]. Recently, their presence has also been reported in

ferromanganese (Fe-Mn) crusts and abyssal manganese nodules[100,101,102,103]. Several methods exist for identifying magnetofossils. The most direct way is to observe them under a transmission electron microscope (TEM). Kirschvink and Chang[104] first observed magnetofossils under a TEM from deep-sea sediments of the Southwest Atlantic, Equatorial Pacific, and South Atlantic Oceans. Petersen et al.[105] found additional magnetofossil morphotypes from South Atlantic marine sediments, with bullet-, prismatic- and octahedral shapes that they considered to be the predominant natural remanent magnetisation (NRM) carrier in sediments with ages from Quaternary to Eocene. Magnetosomal magnetite crystals usually have a [111] elongation direction, while Li et al.[106] found that bullet-shaped biogenic magnetite grows in a two-stage process with the second stage involving elongation in the [100] direction. Kopp and Kirschvink[83] proposed a series of criteria to identify magnetofossils. For instance, biogenic magnetosomal magnetite crystals have a narrow size distribution and distinctive morphologies with blunt crystal edges, high chemical purity, crystallographic perfection and chain arrangement.

Magnetic techniques provide complementary approaches that are commonly used to initially identify magnetofossils before direct TEM observation. These methods include low-temperature remanence measurements, first-order reversal curve (FORC) diagrams, and ferromagnetic resonance (FMR) spectroscopy. Moskowitz et al.[107] suggested that low-temperature isothermal remanent magnetisation (IRM) measurements can be used to distinguish magnetite magnetosome chains. They defined δ as $\delta = (IRM_{80K}\text{-}IRM_{150K})/IRM_{80K}$ and the δ ratio = δ_{FC}/δ_{ZFC}, where δ_{FC} and δ_{ZFC} are the difference between field cooled (FC) and zero field cooled (ZFC) IRM curves at 150 K and 80 K, respectively. Moskowitz et al.[107] concluded that biogenic magnetite chains are present when the δ ratio > 2. However, when magnetosome chains are oxidized, the δ ratio becomes less diagnostic. The test suggested by Chang et al.[108],

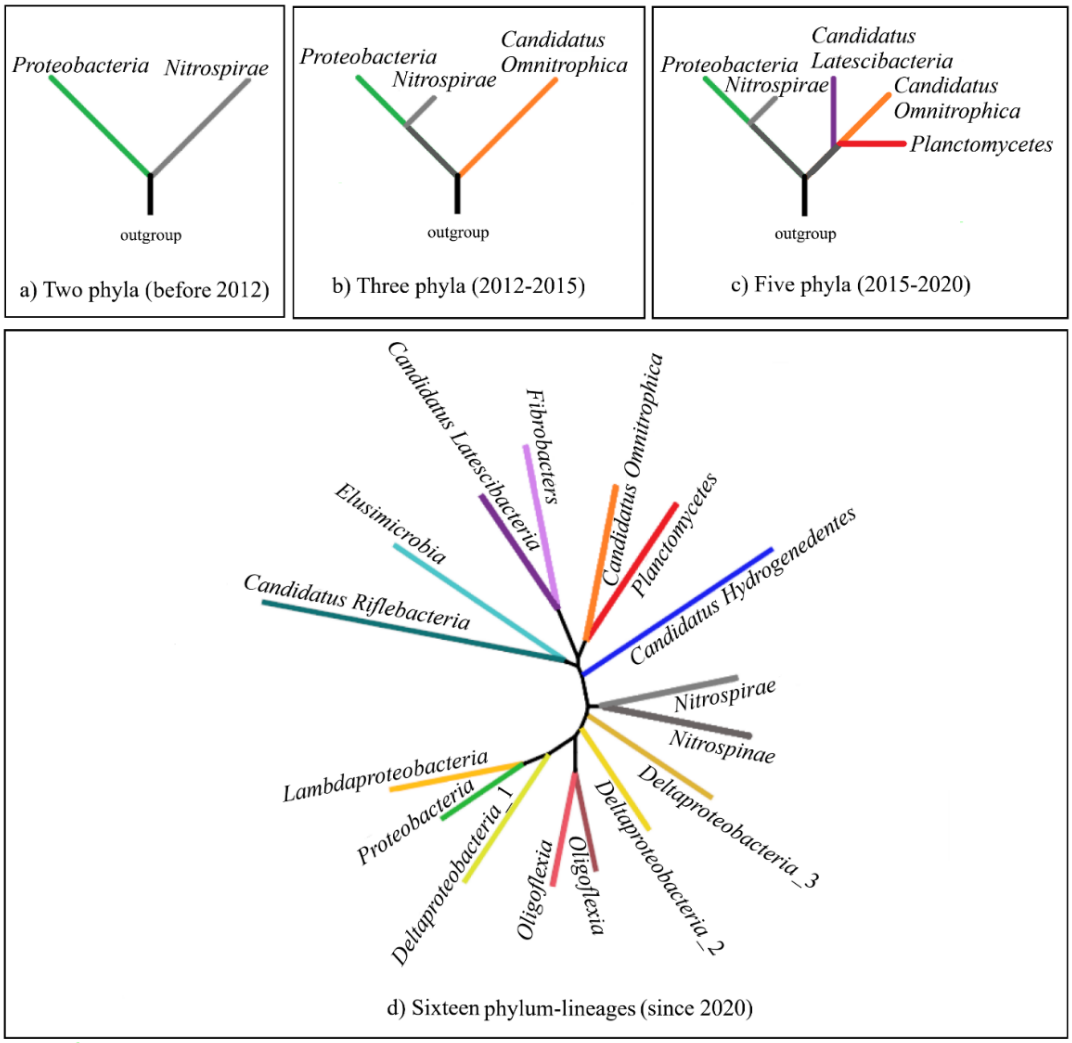

Figure 2: Schematic representation of the gradual expansion of the phylogenetic tree of MTB in the *Bacteria* domain. a) Before 2012, only two phyla (*Proteobacteria* and *Nitrospirae*) were identified to contain MTB. b) Between 2012 and 2015, an additional branch for the *Candidatus* Omnitrophica phylum was added[28]. c) Subsequently, two bacterial phyla (*Candidatus* Latescibacteria[29] and Planctomycetes[21]) were added to the MTB tree of life based on the presence of magnetosome gene clusters in their genomes. d) The latest addition to the MTB tree has expanded its branches to a total of sixteen bacterial phylum-level lineages[31,30]. All taxonomic groupings are based on the NCBI taxonomy (https://www.ncbi.nlm.nih.gov/taxonomy).

based on low temperature cycling of a saturation IRM imparted at room temperature, is more robust for oxidized magnetosomes. Chang et al.[109] reported that a double Verwey transition temperature signal can also be used to identify magnetofossils and suggested that ~100 K and ~120 K are the Verwey transition temperatures of biogenic and detrital magnetite, respectively, although it has also been suggested that the two Verwey transitions could result from other factors[110].

FORC diagrams are normally interpreted in terms of the magnetic coercivity distribution and magnetostatic interactions among single domain magnetic particles[111,112,113]. When interactions among uniaxial single domain particles are negligible or weak, FORC diagrams will have a central ridge along the horizontal B_c axis, with a small vertical distribution along the vertical B_u axis. Although magnetic particles in magnetosome chains have strong interactions among them, the entire chain will act as a single needle with uniaxial magnetisation that does not interact with other chains[114]. Therefore, MTB samples produce a central ridge in FORC diagrams[115,116,117,118,119]. However, when magnetofossil chains are broken, magnetic particles clump together so that interactions become strong; a central ridge usually persists and FORC distributions spread vertically in the B_u direction[120]. Inorganic magnetite with weak interactions also produce a central ridge FORC signature. Thus, if a FORC central ridge is observed, further TEM observations are needed to demonstrate the presence of magnetofossils.

FMR spectroscopy is sensitive to the magnetic anisotropy of the chain configuration[121]. The magnetic anisotropy of MTB arises mainly from dipolar interactions among adjacent magnetic particles in a chain, which behaves like an elongated single domain particle[114]; therefore, FMR is used to indicate the presence of magnetosome chains[122,123]. The main FMR parameters are as follows: the effective *g*-factor (g_{eff}), asymmetry ratio (A) and empirical parameter (α), where $g_{\mathrm{eff}} = h\nu/\beta B_{\mathrm{eff}}$, h is Planck's constant, ν is the microwave frequency, β is the Bohr magneton and B_{eff} is

the maximum absorption field, $A = \Delta B_{high}/\Delta B_{low}$, where $\Delta B_{high} = B_{high} - B_{eff}$, and $\Delta B_{low} = B_{eff} - B_{low}$. The full width at half maximum is defined as $\Delta B_{FWHM} = B_{high} + B_{low}$ (Figure 3e). Weiss et al.[122] proposed that a magnetosome chain will have $A < 1$ and $g_{eff} < 2.12$. Kopp et al.[123] proposed an empirical parameter, defined as $\alpha = 0.17A + 9.8 \times 10^{-4}\Delta B_{FWHM}$/mT, and concluded that $A < 1$ and $g_{eff} < 2.12$ are insufficient to ensure the presence of magnetofossils. However, all of their measured MTB had $\alpha < 0.25$, and magnetofossil-bearing samples have $\alpha = 0.25$-0.30. When α is larger, magnetofossil contents are lower. Kodama et al.[124] suggested that detrital and extracellularly produced authigenic magnetite (D + Ex) dominate sediments with $\alpha > 0.40$, while magnetofossil-rich sediments have $\alpha < 0.35$ and $A < 1$. However, inorganic elongated single domain particles in a volcanic tuff also have $0.3 < \alpha < 0.35$ and $A < 1$[125]. Kind et al.[126] investigated magnetic components in Holocene Lake sediments by combining anhysteretic remanent magnetisation (ARM), IRM, FORC diagrams and FMR spectra and suggested a combination of FORC and FMR measurements to detect magnetofossils in natural environments. Blattmann et al.[127] applied quantitative FMR to analyse magnetofossil variations in Lake Constance, which records sediment-water interface redox changes. FMR spectroscopy is also used widely to detect magnetofossils in pre-Quaternary marine sediments[116,128].

To better understand the magnetic properties of magnetofossils, micromagnetic modelling has been applied to build a link between magnetofossil size distributions and magnetic properties. Muxworthy and Williams[129] found that the largest reported interacting magnetosomal magnetite particles still have single-domain behaviour based on micromagnetic simulations. Chang et al.[130] used micromagnetic models to build a link between magnetic properties and magnetofossil size distributions from Ocean Drilling Program (ODP) Site 1263 during the Paleocene-Eocene thermal maximum (PETM). Moreover, micromagnetic modelling demonstrates that magnetosome chain structures play a more important role in controlling magnetic particle coercivity than

morphology[130]. Different MTB species have different chain structures and magnetic particle numbers. Therefore, magnetofossil diversity probably affects the magnetic properties of bulk samples, especially when magnetofossils are the main NRM carrier. Berndt et al.[131] modelled magnetosome chain morphologies (including crystal size, elongation, chain length, and intra-chain spacing) and found that inter-chain spacing can control the magnetism of magnetosomal magnetic particles such as coercivity, coercivity of remanence and saturation magnetisation.

Heslop et al.[132] calculated the vector difference sum (VDS) of components in NRM demagnetisation curves to quantify magnetofossil contents from sediments offshore of northwestern Australia. In addition, IRM unmixing and principal component analyses applied to FORCs (FORC-PCA) are used to quantify magnetic components in sediments. Two categories of methods are used to unmix IRM acquisition curves. One is single sample IRM-unmixing, which includes fitting of log-normal, skewed generalized Gaussian, and Burr-XII distribution models[133,134,135]. Egli[136] concluded that the dispersion parameter of biogenic magnetite is < 0.2, while values for detrital magnetite particles are between 0.3 and 0.4. Chang et al.[130] analysed magnetic components from PETM sediments using a cumulative log-Gaussian function and decomposed IRM acquisition curves into three components, including biogenic soft and hard magnetite, and a soft detrital component. They suggested that magnetofossil components contribute 76% of the total remanent magnetisation during the PETM onset. A further IRM unmixing approach is endmember-based IRM unmixing, with non-negative matrix factoring[137]. Usui et al.[138] reconstructed the biogenic proportion of particles using this approach and obtained a two biogenic magnetite endmember solution by combining χ_{ARM}/IRM ratios (a magnetic mineral grain size proxy) and FORC diagrams. They concluded that the two biogenic magnetite endmembers represent isotropic and bullet-shaped magnetofossils.

Lascu et al.[139] and Harrison et al.[140] demonstrated that FORC-PCA can help to determine biogenic and detrital magnetite abundances. FORC diagrams enable characterisation of magnetic minerals with different domain states and interaction fields. Channell et al.[141] applied this method to trace variations of three magnetic endmembers (EMs) in the Rockall Trough (NE Atlantic), including a magnetofossil EM. Roberts et al.[142] used FORC-PCA to detect magnetic property variations during early diagenetic reduction, including loss of a magnetofossil component due to dissolution and to estimate the proportions of different minerals in different diagenetic systems. Yamazaki et al.[143] applied FORC-PCA to two cores from the western North Pacific Ocean and the South Pacific Ocean and identified two non-interacting single domain EMs, which represent biogenic soft and biogenic hard components, respectively[144]. Qian et al.[145] used FORC-PCA analysis of eastern Mediterranean sediments to demonstrate that elevated magnetofossil abundances occur at oxidation fronts above organic-rich intervals. FORC-PCA is becoming increasingly common for quantifying sedimentary magnetofossil contents in sediments[146,147,148]. Combining magnetic measurements and TEM or scanning electron microscope (SEM) observations can provide information to identify, characterise and quantify magnetofossils in natural samples (Figure 3).

Paleoenvironmental and Paleomagnetic Implications of Magnetofossils

Varying proportions of different magnetofossil morphotypes can reflect the paleoredox level of sediments[100,101,103,149,150,151]. Abundant bullet-shaped magnetofossils have been detected in reducing environments with higher total organic carbon (TOC), while octahedral magnetofossils appear to dominate relatively oxic environments. However, Lean and McCave[152] found that more elongated magnetofossils occur in low-TOC horizons. Therefore, the paleoenvironmental implications of magnetofossil morphologies need further investigation, especially the relationship between magnetofossil abundance and sediment nutrient content.

Moreover, if magnetofossils undergo diagenetic modification, the relationship between their abundance and paleoenvironment will change[153]. For example, moderate TOC availability promotes mild diagenetic iron reduction that reduces sedimentary iron so that it becomes bioavailable to MTB[116]. However, high TOC produces sulphidic diagenetic environments in which magnetite magnetofossils dissolve[154]. Equant magnetofossils dissolve more easily than bullet-shaped forms[155], and bullet-shaped magnetofossils are more easily dissolved than hexagonal prisms and octahedral forms[153]. Magnetofossils are ideal ancient magnetic field recorders. In environments where magnetofossils are preserved, Ouyang et al.[156] and Chen et al.[157] demonstrated that that they have a higher magnetic recording efficiency than detrital magnetite, while Li et al.[158] found that biogenic magnetite can be less efficiently magnetised than detrital magnetite. Debate also remains about whether magnetofossils record a biogeochemical remanent magnetisation (BGRM). Tarduno et al.[159] suggested that magnetofossils that survive burial below the Fe-redox boundary can produce delayed BGRM acquisition. Roberts et al.[116] noted that paleomagnetic signals carried by magnetofossils must be acquired at shallow depths based on comparison between two nearby records. Tests for offsets between paleomagnetic signals carried by detrital and biogenic magnetite indicate no depth lag, so evidence is still lacking for the BGRM mechanism[156,157]. Yamazaki et al.[160] found that elongated magnetofossils inhabit lower parts of a redox zonation, while isotropic forms occupy shallower levels.

Although there are few reports of greigite magnetofossils, it has been suggested that they can be reliable paleomagnetic recorders[161]. Pósfai et al.[162] proposed that greigite in Miocene sedimentary rocks is similar to biogenic crystals produced by MMP and Chang et al.[163] concluded that greigite magnetofossils are potentially widespread in ancient sediments. The favoured MTB habitat depth relates to their ability to contribute to a BGRM; future detailed studies of the vertical distribution of MTB

populations within the water column or sediments are required to constrain the habitat range of MTB.

Ecosystem Functions of MTB

MTB are distributed globally in aquatic ecosystems[21]. They can comprise up to ~30% of the microbiome in some habitats[26] and their biomineralising capability is assumed to be important for biogeochemical cycling of iron in sediments[90]. Recent discovery of an Archean origin for MTB further suggests that they may have contributed to iron cycling throughout Earth history. With reports of the ability of MTB to fix nitrogen[164,165], sequester carbon[166], and to incorporate elements like sulphur, phosphorus, selenium, calcium, etc., into biominerals (Figure 4)[39,166,32,64,28,57,167,168,169,170,171,95], evidence is growing to indicate that MTB play important roles in global biogeochemical cycling. Here we compare the major KEGG pathways of representative MTB genomes across all known sixteen bacterial phylum-level lineages, which suggest that MTB have phylogenetically diverse metabolic features (Figure 5). What is not yet clear is the extent to which they impact the total cycling budget of each element.

To better understand iron biomineralisation, the processes and products of biomineralisation, the relevant genetics and magnetotaxis need to be analysed. The ability to navigate by magnetotaxis depends on whether magnetosomal magnetite particles are fully developed[19]. Magnetotaxis is best achieved with fully developed crystals (~30–150 nm)[59,172,7] rather than with immature crystals (~30 nm or smaller). Cornejo et al.[172] studied the biomineralisation mechanism for mature octahedral crystal formation inside magnetosome membranes in *Magnetospirillum magneticum* strain AMB-1 (AMB-1), whereas Li et al.[173] studied the mechanism for mature bullet-shaped crystal formation in *Deltaproteobacterial* strain WYHR-1. These and further studies could

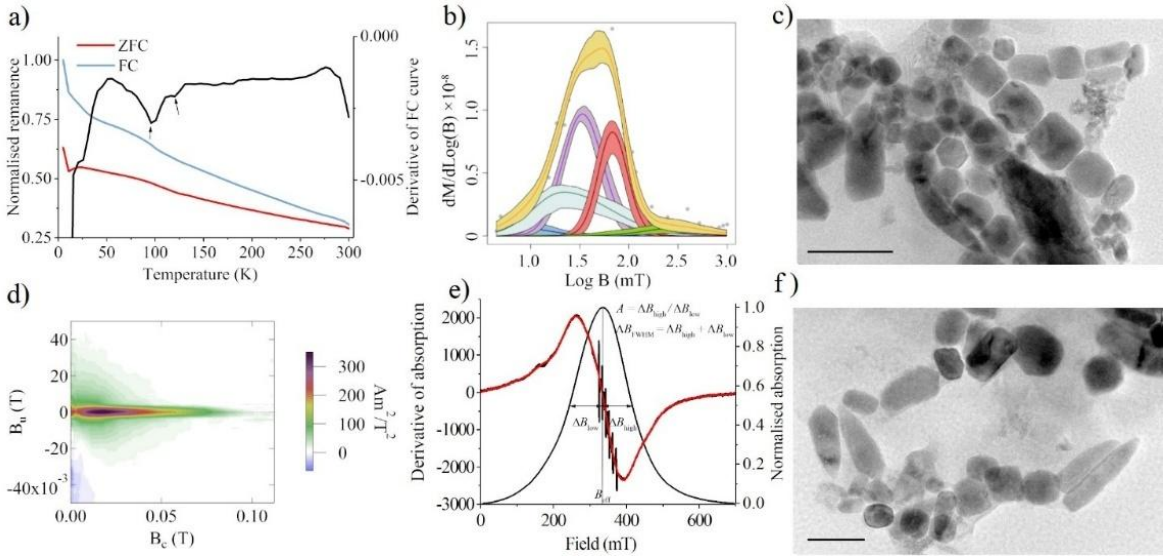

Figure 3: Methods for identifying magnetofossils in samples from core MD01-2444 at 26.74 m depth. a) Low-temperature magnetic measurements (blue and red curves: normalized zero field cooled (ZFC) and field cooled (FC) curves, respectively; black curve: normalized first derivative of the FC curve; peaks with arrows (~100 K and ~115 K) are indicative of biogenic and detrital magnetite, respectively). b) Coercivity distribution from IRM acquisition curve unmixing (grey dots: IRM acquisition data; orange curve: spline fit based on measured data; purple and red curves: biogenic soft and biogenic hard components, respectively; shaded areas for each curve are 95% confidence intervals). c) and f) TEM images of magnetic extracts from the same sample. Scale bars: c = 200 nm, f = 100 nm. The main magnetofossil morphotypes are prisms, octahedra and bullets. d) FORC diagram with a central ridge signature that is indicative of non-interacting single domain magnetic particles. e) Ferromagnetic resonance (FMR) and FMR absorption spectra (black curve: measured FMR spectrum; red curve: fitted FMR spectrum; black humped curve: normalized FMR absorption spectrum). Definition of commonly used magnetofossil-indicative parameters are shown in e.[123]

help to better understand crystal biomineralisation in various MTB strains. Magnetic particle growth is important because assemblages of mature magnetosomal magnetite particles in chain-like structures produce an intracellular magnetic dipole that interacts with Earth's magnetic field to assist MTB cells in magnetic navigation[174,114,175,176]. Therefore, research on the growth stage of magnetosomal crystals in different MTB populations would help to better understand underlying magnetotaxis mechanisms.

Bioavailable iron is scarce in many environments today, which may limit MTB population growth[113]. In particular, iron is scarce in high-nitrate low-chlorophyll (HNLC) oceans. Addition of iron from, for example, eolian dust or volcanic ash inputs, can fertilise surface ocean primary productivity, which increases the chlorophyll content in iron-limited biomes[177,178,179]. Solubilisation of iron from such inputs plays a key role in carbon and nitrogen fixation into biomass, which makes iron bioavailability responsible for primary production in these ecosystems[180,181,182,183]. Export of carbon from the surface ocean to the seafloor can also stimulate mild diagenetic release of iron in the uppermost sediment to release a limitation on MTB productivity in pelagic environments and allows MTB populations to grow[116]. Considering the global MTB distribution in aquatic ecosystems, it has been suggested that MTB communities play significant roles in present-day global iron cycling[20,184].

Apart from MTB, magnetic inclusions have been reported within the purple-sulphur bacterial genera, *Rhodopseudomonas* and *Ectothiorhodospira*[185]. These inclusions have no prismatic crystal structure and they lack a lipid-membrane to enclose magnetosomes. Unlike the microaerophilic model strains, AMB-1 and *Magnetospirillum gryphiswaldense* strain MSR-1 (MSR-1), recent analysis of an anaerobic sulphate-reducer, *Desulfuvibrio magneticus* strain RS-1 (RS-1), is gaining popularity as a model MTB organism[186,187]. This species constructs sub-cellular electron-dense Fe-rich granules (sometimes including phosphorus

and oxygen) that are encased by a lipid-like membrane. These "ferrosome" (iron body) granules are independent and separate entities from magnetosomes and are proposed to play a vital role in storing iron under anaerobic respiration during extreme iron starvation conditions[188]. This aligns with the findings of Amor et al. that magnetite in AMB-1 only represents about ~25–30% of the total iron mass in a bacterial cell[189]. Broader iron storage remains to be explored in relation to other MTB species to explore their probably crucial role in global iron cycling.

Apart from the well-studied Fe_3O_4 and Fe_3S_4 biomineralisation products within MTB, diverse other inclusions contain elemental sulphur, polyphosphate, calcium, etc. Sulphur-rich inclusions have been identified in *Magnetovibrio* strains MV-1 and MV-2 of the *Alphaproteobacteria* class and in many *Nitrospirae* MTB[7,32,190,28,191,57]. It was initially proposed that some MTB, like *Nitrospirae* MTB, are capable of adapting to chemical gradients near the OAI by adjusting their metabolic strategies - either by moving downward to accumulate reduced sulphur species or upward to oxidise stored sulphur with oxygen[192]. This redox-controlled response is supported by analysis of the vertical distribution of *Ca.* Magnetobacterium bavaricum in sediments[32] and by genomic characterisation of *Ca.* Magnetobacterium casensis[38]. *Ca.* Magnetobacterium casensis and *Ca.* Magnetobacterium bavaricum are proposed to conduct sulphur oxidation with nitrate and/or oxygen as electron acceptors in the upper micro-oxic layer and to perform sulphate reduction in the anoxic lower layer, suggesting a complex metabolic strategy of *Nitrospirae* MTB and electron shuttling depending on redox conditions[38,193,39].

Bazylinski and Blakemore[164] revealed that *Magnetospirillum magnetotacticum* strain MS-1 (MS-1) fixes nitrogen at rates equivalent to those of *Azospirillum lipoferum* when cultured microaerobically under nitrogen limiting conditions, where *Azospirillum* species were among the earliest known potential nitrogen fixers for cereal plants[194]. Apart from

MS-1, two *Magnetospirillum* strains, including MSR-1 and AMB-1, when proliferated in nitrogen limiting, semi-solid media can also fix nitrogen via nitrogenase[164]. MSR-1 contains indispensable nitrogenase structural genes required for nitrogen fixation in the presence of the DRAT-DRAG nitrogenase post-translational regulatory system[165] (Figure 5).

Carbon sequestration is a key consideration when analysing pollution mitigation potency of a plant or microorganism, both in terrestrial and aquatic habitats. Microorganisms and other autotrophs drive the carbon cycle because they are at the forefront of carbon cycle feedback mechanisms and their primary production is critical in carbon cycling[195]. Marine phytoplankton have a well-known role in CO_2 sequestration[196]; chemolithoautotrophs do the same under dark conditions in deeper, less-oxic/anoxic parts of ocean water or sediment redox gradients[197]. If not obligate, most MTB are facultative chemolithoautotrophs, which might suggest an underlying role in CO_2 fixation[19]. Most terrestrial plants and microorganisms contain genes that encode a key metabolic pathway known as the Calvin-Benson-Bassham pathway (CBB) that allows the plant/microbe to sequester bioavailable carbon from the environment. Ribulose-1,5-bisphosphate carboxylase/oxygenase (RuBisCO) is an abundant protein that catalyses the CO_2 fixation reaction[198]. The *cbbM* gene that encodes form II RuBisCO was identified in magnetotactic chemolithoautotrophs like *Magnetovibrio* strains MV-1 and MV-2 and *Magnetospirillum* strain MS-1; these species are proposed to be important in carbon cycling and primary productivity[166]. *Gammaproteobacteria* MTB strains BW-2 and SS-5 from the hyper-saline Salton Sea have a partial RuBisCO gene sequence and potentially use the CBB pathway for autotrophy[68]. MTB from the *Etaproteobacteria* (*Magnetococcus marinus* strain MC-1) use the reverse tricarboxylic acid (rTCA) cycle for autotrophy[199], while magnetotactic *Nitrospirae* are proposed to fix CO_2 via the reductive acetyl-CoA (Wood-Ljungdahl or WL) and/or reductive tricarboxylic acid (rTCA) pathways[38,193,200] (Figure 5).

Uncultured MTB cells from the Seine River, France, contain vesicles rich in barium and calcium oxide[171] and MTB from Lake Pavin, France, biomineralise $CaCO_3$ in addition to magnetosomal magnetite[201]. Instances of phosphorous sequestration by *Magnetococcaceae* alongside magnetite chains have also been demonstrated in ferruginous Lake Pavin[168] and in the anoxic Black Sea[169]. Schulz-Vogt et al.[169] suggested that magnetotactic cocci act as a shuttle (using magnetotaxis) to transport phosphorous from the upper to the lower stratum of the suboxic zone, which prevents eutrophication resulting from excess phosphorus accumulation in the upper stratum.

Elements can also deposit on MTB cell surfaces, which is important in analysing the role of MTB in heavy-metal bioremediation and magnetic separation of metal-loaded MTB cells from aquatic bodies. For example, Arakaki and colleagues[202] observed electron-dense Cd^{2+} deposits enveloping RS-1 cell surfaces under TEM when cells were cultured in growth media containing 1.3 ppm Cd^{2+}. Mono-dispersed crystalline inclusions have 20–40 nm sizes and were easily distinguished from magnetic particles in TEM images[202]. A novel *Alphaproteobacterium* MTB species grown in a cobalt supplemented medium has efficient biosorption competence with 89% cobalt removed by magnetic separation of the biomass[203]. Tellurite (O_3Te^{2-}) uptake by MTB followed by biomineralisation of discrete tellurium crystals alongside and separate from magnetite crystals was observed by Tanaka et al.[204]. These authors then demonstrated that when a growth medium is supplemented with selenite (SeO_3^{2-}), elemental selenium nanoparticles with no definitive form gradually built up and some precipitated within cells, in conjunction with and autonomous from magnetite particles[170]. Quantitative analysis revealed that MTB accumulate selenium at a higher rate per cell than other non-iron element accumulations. For example, Se accumulated by MTB is higher than O_3Te^{2-} uptake and Cd adsorbed by factors of 2.4 and 174, respectively[170]. Elemental adsorption on cell surfaces is not specific to

MTB, but they can contribute to metal pollutant removal via magnetic separation. Heavy metal recovery from diodes and resistors of waste printed circuit boards using MTB is a latest discovery in terms of MTB applications in bioremediation[205].

Although such high metal concentrations are usually not encountered in natural environments, analysis of samples from polluted water bodies will help to identify the usefulness of MTB for bioremediation, e.g., MTB morphotypes have been observed in hydrocarbon contaminated microcosms from the Gulf of Fos, France, and hypothesised to be involved in degrading hydrocarbons or other aromatic compounds[206]. It remains to be shown if MTB extracted from such microcosms can be grown in defined induction experiments using aromatic substrates under anaerobic conditions. MTB could, therefore, be potent model organisms for bioremediating contaminated water bodies and surface sediment. As new MTB genomes are obtained by metagenomics and single-cell genomics of environmental samples, identification and characterisation of key proteins involved in these metabolic pathways will provide an important way to understand the ecological functions of MTB.

MTB as a Potential Important Constituent of OMZ Microbiomes

Oxygen minimum zones (OMZs) are oxygen delimiting/nutrient rich sections of an oceanic gradient[207]. Waters above and below the OMZ have higher oxygen concentrations compared to the OMZ interval. OMZs are global sinks for reactive nitrogen because they have the highest microbial activity that conserves available oxygen and produces N_2 and N_2O as respiration by-products[208] and have been termed "microbial reactors" with global significance[209]. OMZs have expanded gradually over the past 50 years due to ocean warming, which reduces oxygen solubility[210,211,212].

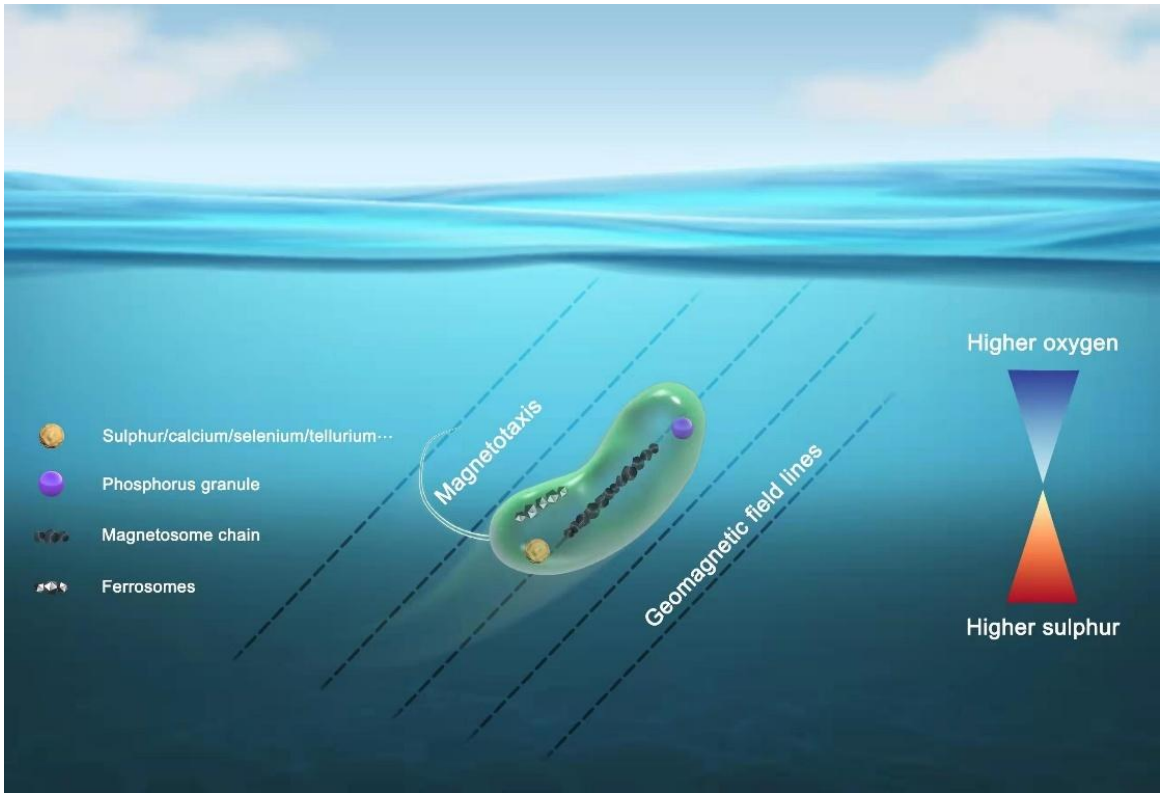

Figure 4: Magnetotaxis, combined with chemotaxis and aerotaxis, allows MTB to efficiently locate and maintain an optimal position for survival and growth in habitats with vertical redox concentration gradients in water columns and sediments around an oxic-anoxic interface (OAI). MTB are widely distributed in aquatic environments from marine to freshwater ecosystems and are thought to play important roles in the cycling of various elements (e.g., Fe, C, N, S, P and some heavy metals like tellurium and selenium).

Microbiological analyses of oceanic OMZs reveal that the most abundant phyla are *Proteobacteria*, *Bacteroidetes*, *Actinobacteria*, *Planctomycetes* and *Marinimicrobia* (previously known as Marine Group A)[213]. A characteristic feature of the OMZ microbiome is its predominant role in the biogeochemical cycling of marine nitrogen[214,215], sulphur[216,217,218,219] and carbon[215]. Rhoads et al.[220] showed that MTB can occur within an OMZ at oxygen levels as low as < 4 mg L^{-1}. The range of dissolved oxygen

contents in an OMZ appears to be optimal for MTB to thrive (0.1–0.5 mg L^{-1}). It has been hypothesised that marine dysaerobic zones (with 0.1–0.5 mL L^{-1} dissolved oxygen concentrations) have a biogenic magnetite inventory based on TEM results in which fine-grained (80–100 nm) subrounded cubic magnetite predominates[220]. High nitrate concentrations in OMZs suggest that these oxygen-limiting microenvironments should harbour greater denitrifying MTB populations[220]. Symbiotic occurrences have been proven by studying the "cryptic" sulphur cycle in OMZs around the world[221]. OMZ biogeochemistry is important in the greater oceanic system with implications even outside the oceans. For example, consortia of ectosymbiotic, sulphate-reducing, chemolithoautotrophic *Deltaproteobacteria* and Excavata protists have been reported[222]. Sulphur-reducing bacteria with magnetosomes have also been observed in microbial mats on carbonate concretions from the Black Sea alongside other archaea that aid methane oxidation[223]. Sulphur-reducing gammaproteobacterial MTB even occur as extracellular symbionts on marine bivalves[224]. OAIs and OMZs are ecological niches in which MTB thrive within chemical gradients; tweaking the chemistry of such environments will likely affect much of the microbial community. The increasing importance of OMZs in the modern ocean could imply that global MTB populations will increase over time with accelerating ocean warming and that they could help to limit deterioration of ocean ecosystem health.

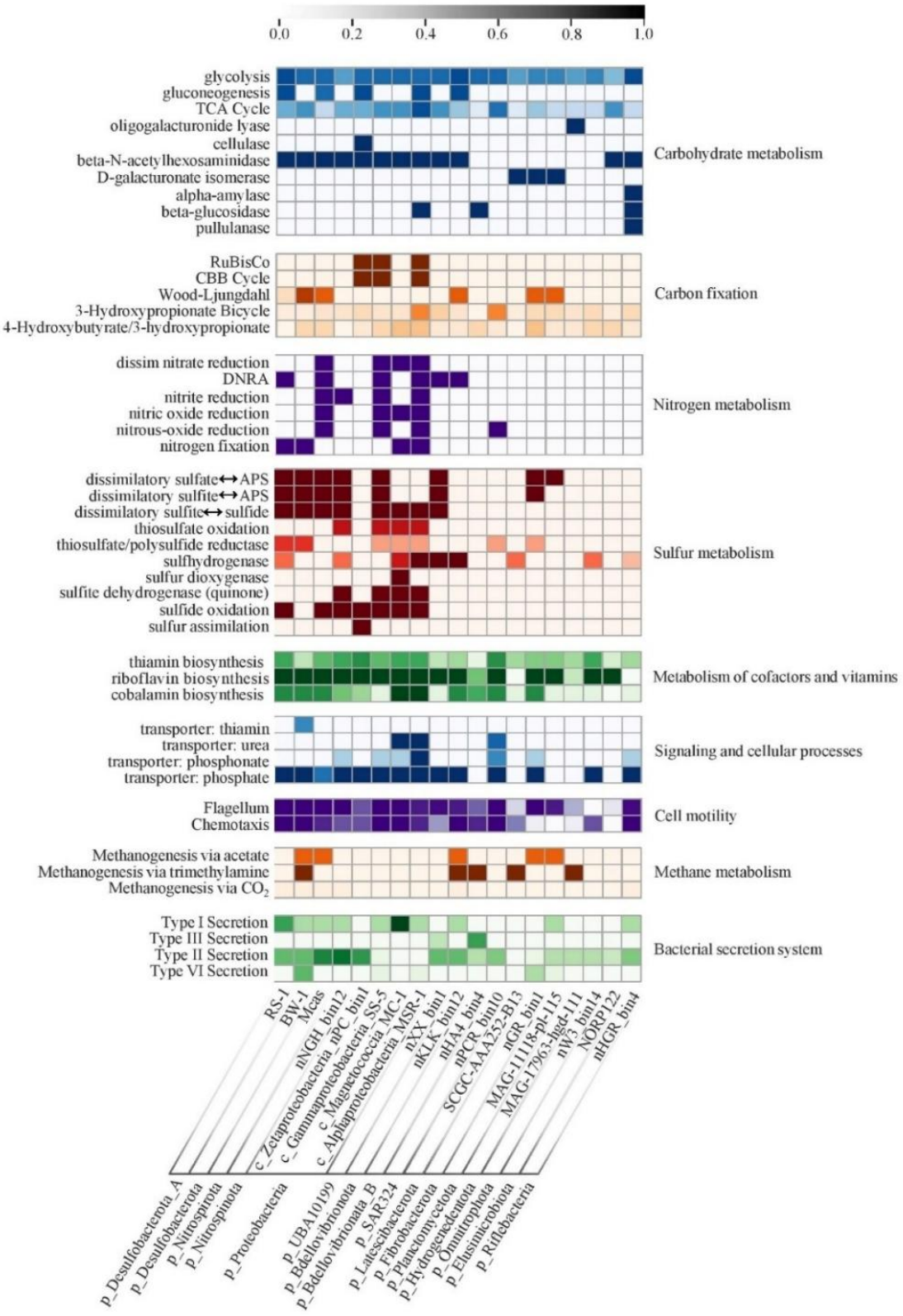

Figure 5: Metabolic pathways of representative MTB genomes across 16 bacterial phylum-level lineages. The colour gradient represents the

completeness of major metabolic pathways inferred from the presence or absence of genes. Dark represents a complete or nearly complete pathway, and white represents a pathway that is absent or mainly incomplete. Note that most available MTB genomes are draft or incomplete, so we cannot rule out that the absence or incompleteness of metabolic pathways maybe due to the fragmented nature of draft genomes. All taxonomic groupings are based on the GTDB taxonomy (Release 89, https://gtdb.ecogenomic.org).

OUTLOOK

MTB are distributed widely in aquatic ecosystems globally. Understanding of the phylogenetic taxonomy and metabolic flexibility of MTB has expanded greatly over the past decade, which suggests an unexpected natural diversity of these microorganisms. Continued discovery of novel MTB lineages from different environments highlight our limited knowledge of their diversity and ecology. Continuing cultivation-dependent and -independent MTB analyses will be crucial to understand their diversity and taxonomy more fully. We anticipate great progress in defining the phylogenetic diversity and evolutionary origin of MTB in the coming years. MTB incorporate elements from their surroundings to produce several biomineral types, with magnetic iron-bearing minerals being the primary biomineralisation product. In addition to iron biomineralisation, MTB can fix nitrogen, oxidize/reduce sulphur and sequester carbon and phosphorus from the environment. These findings suggest that MTB play important roles in biogeochemical elemental cycling through time, although their contributions are yet to be evaluated quantitatively. Moreover, MTB in marine OMZs/OAIs may play a role in ocean biogeochemical cycling and, in turn, in trimming eutrophication. If this is demonstrated by further work, MTB could be a natural eutrophication repressor that could become important with ongoing

global warming. Additionally, MTB can be used in pollution bioremediation by accumulating heavy metals on their surfaces by adsorption (e.g., Cd) and intracellularly (e.g., O_3Te^{2-} and Se). The magnetism of MTB ensures that metal-loaded MTB cells can be separated magnetically from contaminated waters. Magnetofossils are important in paleoenvironmental, paleoclimatic and paleomagnetic interpretations of sediments and sedimentary rocks. Further research is needed to understand the environmental adaptability of MTB and limiting factors that affect magnetofossil preservation to develop robust magnetofossil proxies for past environmental changes.

ACKNOWLEDGEMENTS

We thank Runjia Ji and Jia Liu for preparing Figure 1 and Runjia Ji for her help with Figures 4 and 5. This work was supported by the CAS-TWAS President's Fellowship (Series No 2019-054), National Natural Science Foundation of China (NSFC) Grants 41822704 and 41621004, the Key Research Program of the Chinese Academy of Sciences (ZDBS-SSW-TLC001), the Key Research Program of the Institute of Geology and Geophysics, Chinese Academy of Sciences (IGGCAS-202102), the Youth Innovation Promotion Association of the Chinese Academy of Sciences and Australian Research Council grant DP140104544.

AUTHOR CONTRIBUTIONS

W.L., A.P.R. and P.G. conceived the review. All authors contributed to the writing and editing.

COMPETING INTERESTS

The authors declare no competing financial or non-financial interests.

DATA AVAILABILITY

All NCBI accession numbers of MTB genomes used in Figure 5 are as follows-

HG794546.1 Magnetospirillum gryphiswaldense MSR-1;

CP000471.1 Magnetococcus marinus MC-1;

CP032508.2 Gamma proteobacterium SS-5;

JADFZC010000123.1 Oligoflexales bacterium isolate nHA4_bin4;

JADFZW010000010.1 Oligoflexia bacterium isolate nKLK_bin12;

AP010904.1 Desulfovibrio magneticus RS-1;

FWEV01000001.1 Candidatus Desulfamplus magnetomortis BW-1 PRJEB14757;

NVTF01000001.1 Elusimicrobia bacterium isolate NORP122;

JADFYW010000100.1 Fibrobacteria bacterium isolate nGR_bin1;

DUZM01000001.1 Candidatus Hydrogenedentes bacterium isolate MAG_17963_hgd_111 Ga0180437_10002127;

ASWY01000001.1 Latescibacteria bacterium SCGC AAA252-B13;

JADGAO010000100.1 Nitrospinae bacterium isolate nNGH_bin12;

JMFO00000000 Candidatus Magnetobacterium casensis;

JADGBR010000010.1 Candidatus Omnitrophica bacterium isolate nW3_bin14;

DUZJ01000001.1 Planctomycetes bacterium isolate MAG_11118_pl_115;

JADGAS010000010.1 Zetaproteobacteria bacterium isolate nPC_bin1;

JADFZL010000010.1 Candidatus Riflebacteria bacterium isolate nHGR_bin4;

JADGAT010000100.1 SAR324 cluster bacterium isolate nPCR_bin10;

JADGCS010000100.1 Deltaproteobacteria bacterium isolate nXX_bin1

The original data for Figure 3 can be found in https://doi.org/10.6084/m9.figshare.17122277.v1

CODE AVAILABILITY

MagCluster (https://github.com/RunJiaJi/magcluster), code: magcluster prokka 19mtb_genomes;
KofamKOALA server (https://www.genome.jp/tools/kofamkoala/) (DOI: https://doi.org/10.1093/bioinformatics/btz859);
KEGG-Decoder (https://github.com/bjtully/BioData/tree/master/KEGGDecoder) (DOI: https://doi.org/10.1038/s41396-018-0091-3), code: KEGG-decoder --input 19mtb.txt --output out.list --vizoption static -m myorder.txt

Figure 3b was produced using by Max UnMix (http://shinyapps.its.carleton.edu/max-unmix/) and Figure 3d was drawn using FORCinel v3.06 (https://wserv4.esc.cam.ac.uk/nanopaleomag/?page_id=51).

REFERENCES

1. Kirschvink, J. L., Jones, D. S. & MacFadden, B. J. Magnetite biomineralisation and magnetoreception in organisms. (Springer US, 1985). doi:10.1007/978-1-4613-0313-8_16.
2. Frankel, R. B. & Blakemore, R. P. Iron Biominerals. (Springer US, 1991). doi:10.1007/978-1-4615-3810-3.
3. Uebe, R. & Schüler, D. Magnetosome biogenesis in magnetotactic bacteria. Nat. Rev. Microbiol. 14, 621–637 (2016).
4. Lin, W., Kirschvink, J. L., Paterson, G. A., Bazylinski, D. A. & Pan, Y. On the origin of microbial magnetoreception. Natl. Sci. Rev. 7, 472–479 (2020).
5. Bellini, S. On a unique behavior of freshwater bacteria. Chin. J. Oceanol. Limnol. 27, 3–5 (2009).
6. Blakemore, R. P. Magnetotactic bacteria. Science 190, 377–379 (1975).
7. Bazylinski, D. A. & Frankel, R. B. Magnetosome formation in prokaryotes. Nat. Rev. Microbiol. 2, 217–230 (2004).

8. Boles, L. C. & Lohmann, K. J. True navigation and magnetic maps in spiny lobsters. Nature 421, 60–63 (2003).
9. Nordmann, G. C., Hochstoeger, T. & Keays, D. A. Unsolved mysteries: Magnetoreception—a sense without a receptor. PLoS Biol. 15, e2003234 (2017).
10. Wajnberg, E. et al. Magnetoreception in eusocial insects: An update. J. R. Soc. Interface 7, 207–225 (2010).
11. Dreyer, D. et al. The Earth's magnetic field and visual landmarks steer migratory flight behavior in the nocturnal Australian Bogong moth. Curr. Biol. 28, 2160–2166 (2018).
12. Malkemper, E. P. et al. Magnetoreception in the wood mouse (Apodemus sylvaticus): Influence of weak frequency-modulated radio frequency fields. Sci. Rep. 5, 9917 (2015).
13. Begall, S., Malkemper, E. P., Červený, J., Němec, P. & Burda, H. Magnetic alignment in mammals and other animals. Mamm. Biol. 78, 10–20 (2013).
14. Hart, V. et al. Dogs are sensitive to small variations of the Earth's magnetic field. Front. Zool. 10, 80 (2013).
15. Engelmann, T. W. Neue methode zur untersuchung der sauerstoffausscheidung pflanzlicher und thierischer organismen. Pflüger, Arch. Gesammte Physiol. Menschen Thiere 25, 285–292 (1881).
16. Adler, J. Chemotaxis in bacteria. Science 153, 708–716 (1966).
17. Vali, H. & Kirschvink, J. L. Observations of magnetosome organisation, surface structure, and iron biomineralisation of undescribed magnetic bacteria: Evolutionary speculations. in Iron Biominerals 97–115 (Springer US, 1991).
18. Mao, X., Egli, R., Petersen, N., Hanzlik, M. & Liu, X. Magneto-chemotaxis in sediment: First insights. PLoS One 9, e102810 (2014).
19. Lefèvre, C. T. & Bazylinski, D. A. Ecology, diversity, and evolution of magnetotactic bacteria. Microbiol. Mol. Biol. Rev. 77, 497–526 (2013).

20. Lin, W., Bazylinski, D. A., Xiao, T., Wu, L. F. & Pan, Y. Life with compass: Diversity and biogeography of magnetotactic bacteria. Environ. Microbiol. 16, 2646–2658 (2014).
21. Lin, W., Pan, Y. & Bazylinski, D. A. Diversity and ecology of and biomineralisation by magnetotactic bacteria. Environ. Microbiol. Rep. 9, 345–356 (2017).
22. Abreu, F. et al. Common ancestry of iron oxide- and iron-sulphide-based biomineralisation in magnetotactic bacteria. ISME J. 5, 1634–1640 (2011).
23. Lefèvre, C. T. et al. Monophyletic origin of magnetotaxis and the first magnetosomes. Environ. Microbiol. 15, 2267–2274 (2013).
24. Lin, W. et al. Genomic expansion of magnetotactic bacteria reveals an early common origin of magnetotaxis with lineage-specific evolution. ISME J. 12, 1508–1519 (2018).
25. Lin, W. et al. Origin of microbial biomineralisation and magnetotaxis during the Archean. Proc. Natl. Acad. Sci. U. S. A. 114, 2171–2176 (2017).
26. Spring, S. et al. Dominating role of an unusual magnetotactic bacterium in the microaerobic zone of a freshwater sediment. Appl. Environ. Microbiol. 59, 2397–2403 (1993).
27. Amann, R., Peplies, J. & Schüler, D. Diversity and taxonomy of magnetotactic bacteria. in Magnetoreception and Magnetosomes in Bacteria 25–36 (Springer, 2006).
28. Kolinko, S. et al. Single-cell analysis reveals a novel uncultivated magnetotactic bacterium within the candidate division OP3. Environ. Microbiol. 14, 1709–1721 (2012).
29. Lin, W. & Pan, Y. A putative greigite-type magnetosome gene cluster from the candidate phylum Latescibacteria. Environ. Microbiol. Rep. 7, 237–242 (2015).
30. Uzun, M., Alekseeva, L., Krutkina, M., Koziaeva, V. & Grouzdev, D. Unravelling the diversity of magnetotactic bacteria through analysis of open genomic databases. Sci. Data 7, 252 (2020).

31. Lin, W. et al. Expanding magnetic organelle biogenesis in the domain Bacteria. Microbiome 8, 1–28 (2020).
32. Jogler, C. et al. Cultivation-independent characterisation of 'Candidatus Magnetobacterium bavaricum' via ultrastructural, geochemical, ecological and metagenomic methods. Environ. Microbiol. 12, 2466–2478 (2010).
33. Vali, H., Forster, O., Amarantidis, G. & Petersen, N. Magnetotactic bacteria and their magnetofossils in sediments. Earth Planet. Sci. Lett. 86, 389–400 (1987).
34. Hanzlik, M., Winklhofer, M. & Petersen, N. Spatial arrangement of chains of magnetosomes in magnetotactic bacteria. Earth Planet. Sci. Lett. 145, 125–134 (1996).
35. Hanzlik, M., Winklhofer, M. & Petersen, N. Pulsed-field-remanence measurements on individual magnetotactic bacteria. J. Magn. Magn. Mater. 248, 258–267 (2002).
36. Eder, S. H. K., Gigler, A. M., Hanzlik, M. & Winklhofer, M. Sub-micrometer-scale mapping of magnetite crystals and sulphur globules in magnetotactic bacteria using confocal Raman micro-spectrometry. PLoS One 9, 1–12 (2014).
37. Lin, W., Li, J., Schüler, D., Jogler, C. & Pan, Y. Diversity analysis of magnetotactic bacteria in Lake Miyun, northern China, by restriction fragment length polymorphism. Syst. Appl. Microbiol. 32, 342–350 (2009).
38. Lin, W. et al. Genomic insights into the uncultured genus 'Candidatus Magnetobacterium' in the phylum Nitrospirae. ISME J. 8, 2463–2477 (2014).
39. Li, J., Liu, P., Wang, J., Roberts, A. P. & Pan, Y. Magnetotaxis as an adaptation to enable bacterial shuttling of microbial sulphur and sulphur cycling across aquatic oxic-anoxic interfaces. J. Geophys. Res. Biogeosci. 125, e2020JG006012 (2020).

40. Qian, X. et al. Identification of novel species of marine magnetotactic bacteria affiliated with Nitrospirae phylum. Environ. Microbiol. Rep. 11, 330–337 (2019).
41. Farina, M., Lins de Barros, H. G. P., Esquivel, D. M. S. & Danon, J. Ultrastructure of a magnetotactic microorganism. Biol. Cell 48, 85–88 (1983).
42. Winklhofer, M., Abraçado, L. G., Davila, A. F., Keim, C. N. & Lins De Barros, H. G. P. Magnetic optimization in a multicellular magnetotactic organism. Biophys. J. 92, 661–670 (2007).
43. Keim, C. N. et al. Multicellular life cycle of magnetotactic prokaryotes. FEMS Microbiol. Lett. 240, 203–208 (2004).
44. Abreu, F. et al. 'Candidatus Magnetoglobus multicellularis', a multicellular, magnetotactic prokaryote from a hypersaline environment. Int. J. Syst. Evol. Microbiol. 57, 1318–1322 (2007).
45. Lins, U., Keim, C., Evans, F., Farina, M. & Buseck, P. Magnetite (Fe3O4) and greigite (Fe3S4) crystals in multicellular magnetotactic prokaryotes. Geomicrobiol. J. 24, 43–50 (2007).
46. Wenter, R., Wanner, G., Schüler, D. & Overmann, J. Ultrastructure, tactic behaviour and potential for sulphate reduction of a novel multicellular magnetotactic prokaryote from North Sea sediments. Environ. Microbiol. 11, 1493–1505 (2009).
47. Zhou, K. et al. Adaptation of spherical multicellular magnetotactic prokaryotes to the geochemically variable habitat of an intertidal zone. Environ. Microbiol. 15, 1595–1605 (2013).
48. Zhang, R. et al. Characterisation and phylogenetic identification of a species of spherical multicellular magnetotactic prokaryotes that produces both magnetite and greigite crystals. Res. Microbiol. 165, 481–489 (2014).
49. Lefèvre, C. et al. Characterisation of Mediterranean magnetotactic bacteria. J. Ocean Univ. China 6, 355–359 (2007).
50. Zhou, K. et al. A novel genus of multicellular magnetotactic prokaryotes from the Yellow Sea. Environ. Microbiol. 14, 405–413 (2012).

51. Du, H. et al. Temporal distributions and environmental adaptations of two types of multicellular magnetotactic prokaryote in the sediments of Lake Yuehu, China. Environ. Microbiol. Rep. 7, 538–546 (2015).
52. Chen, Y. R. et al. A novel species of ellipsoidal multicellular magnetotactic prokaryotes from Lake Yuehu in China. Environ. Microbiol. 17, 637–647 (2015).
53. Chen, Y. R. et al. Novel species and expanded distribution of ellipsoidal multicellular magnetotactic prokaryotes. Environ. Microbiol. Rep. 8, 218–226 (2016).
54. Dong, Y. et al. The detection of magnetotactic bacteria in deep sea sediments from the east Pacific Manganese Nodule Province. Environ. Microbiol. Rep. 8, 239–249 (2016).
55. Leao, P. et al. Ultrastructure of ellipsoidal magnetotactic multicellular prokaryotes depicts their complex assemblage and cellular polarity in the context of magnetotaxis. Environ. Microbiol. 19, 2151–2163 (2017).
56. Teng, Z. et al. Diversity and characterisation of multicellular magnetotactic prokaryotes from coral reef habitats of the Paracel Islands, South China Sea. Front. Microbiol. 9, 2135 (2018).
57. Qian, X. X. et al. Juxtaposed membranes underpin cellular adhesion and display unilateral cell division of multicellular magnetotactic prokaryotes. Environ. Microbiol. 22, 1481–1494 (2020).
58. Lyons, N. A. & Kolter, R. On the evolution of bacterial multicellularity. Curr. Opin. Microbiol. 24, 21–28 (2015).
59. Stolz, J. F., Chang, S. B. R. & Kirschvink, J. L. Magnetotactic bacteria and single-domain magnetite in hemipelagic sediments. Nature 321, 849–851 (1986).
60. Petermann, H. & Bleil, U. Detection of live magnetotactic bacteria in South Atlantic deep-sea sediments. Earth Planet. Sci. Lett. 117, 223–228 (1993).
61. Tan, S. M., Ismail, M. H. & Cao, B. Biodiversity of magnetotactic bacteria in the tropical marine environment of Singapore revealed by metagenomic analysis. Environ. Res. 194, 110714 (2021).

62. Liu, J. et al. Bacterial community structure and novel species of magnetotactic bacteria in sediments from a seamount in the Mariana volcanic arc. Sci. Rep. 7, 1–11 (2017).
63. Xu, C., Zhang, W., Pan, H., Du, H. & Xiao, T. Distribution and diversity of magnetotactic bacteria in sediments of the Yellow Sea continental shelf. J. Soils Sediments 18, 2634–2646 (2018).
64. Lefèvre, C. T., Frankel, R. B., Posfai, M., Prozorov, T. & Bazylinski, D. A. Isolation of obligately alkaliphilic magnetotactic bacteria from extremely alkaline environments. Environ. Microbiol. 13, 2342–2350 (2011).
65. Abreu, F. et al. Culture-independent characterisation of a novel magnetotactic member affiliated to the Beta class of the Proteobacteria phylum from an acidic lagoon. Environ. Microbiol. 20, 2615–2624 (2018).
66. Nash, C. Z. Mechanisms and evolution of magnetotactic bacteria. (California Institute of Technology, 2008).
67. Lefèvre, C. T. et al. Moderately thermophilic magnetotactic bacteria from hot springs in Nevada. Appl. Environ. Microbiol. 76, 3740–3743 (2010).
68. Lefèvre, C. T. et al. Novel magnetite-producing magnetotactic bacteria belonging to the Gammaproteobacteria. ISME J. 6, 440–450 (2012).
69. Liu, P. et al. Identification and characterisation of magnetotactic Gammaproteobacteria from a salt evaporation pool, Bohai Bay, China. Environ. Microbiol. http://doi.org/10.1111/1462-2920.15516 (2021).
70. Lyons, T. W., Reinhard, C. T. & Planavsky, N. J. The rise of oxygen in Earth's early ocean and atmosphere. Nature 506, 307–315 (2014).
71. Holland, H. D. The oceans: A possible source of iron in iron-formations. Econ. Geol. 68, 1169–1172 (1973).
72. Konhauser, K. O. et al. Iron formations: A global record of Neoarchaean to Palaeoproterozoic environmental history. Earth-Sci. Rev. 172, 140–177 (2017).

73. de Baar, H. J. W. & de Jong, J. T. M. Distributions, sources and sinks of iron in seawater. in The Biogeochemistry of Iron in Seawater 123–253 (John Wiley & Sons Ltd., 2001).

74. Walker, J. C. G. & Brimblecombe, P. Iron and sulphur in the pre-biologic ocean. Precambrian Res. 28, 205–222 (1985).

75. Habicht, K. S., Gade, M., Thamdrup, B., Berg, P. & Canfield, D. E. Calibration of sulphate levels in the Archean ocean. Science 298, 2372–2374 (2002).

76. Catling, D. C. & Zahnle, K. J. The Archean atmosphere. Sci. Adv. 6, eaax1420 (2020).

77. Holland, H. D. The chemical evolution of the atmosphere and oceans. Geol. Mag. 122, 404–405 (1985).

78. Canfield, D. E., Poulton, S. W. & Narbonne, G. M. Late-Neoproterozoic deep-ocean oxygenation and the rise of animal life. Science 315, 92–95 (2007).

79. Knoll, A. H. & Nowak, M. A. The timetable of evolution. Sci. Adv. 3, e1603076 (2017).

80. Betts, H. C. et al. Integrated genomic and fossil evidence illuminates life's early evolution and eukaryote origin. Nat. Ecol. Evol. 2, 1556–1562 (2018).

81. Nutman, A. P., Bennett, V. C., Friend, C. R. L., van Kranendonk, M. J. & Chivas, A. R. Rapid emergence of life shown by discovery of 3,700-million-year-old microbial structures. Nature 537, 535–538 (2016).

82. Bell, E. A., Boehnke, P., Harrison, T. M. & Mao, W. L. Potentially biogenic carbon preserved in a 4.1 billion-year-old zircon. Proc. Natl. Acad. Sci. U. S. A. 112, 14518–14521 (2015).

83. Kopp, R. E. & Kirschvink, J. L. The identification and biogeochemical interpretation of fossil magnetotactic bacteria. Earth-Sci. Rev. 86, 42–61 (2008).

84. Hounslow, M. W. & Maher, B. A. Quantitative extraction and analysis of carriers of magnetisation in sediments. Geophys. J. Int. 124, 57–74 (1996).

85. Montgomery, P., Hailwood, E. A., Gale, A. S. & Burnett, J. A. The magnetostratigraphy of Coniacian late Campanian chalk sequences in southern England. Earth Planet. Sci. Lett. 156, 209–224 (1998).
86. Blankenship, R. E. Early evolution of photosynthesis. Plant Physiol. 154, 434–438 (2010).
87. Williams, B. P., Aubry, S. & Hibberd, J. M. Molecular evolution of genes recruited into C 4 photosynthesis. Trends Plant Sci. 17, 213–220 (2012).
88. Ilbert, M. & Bonnefoy, V. Insight into the evolution of the iron oxidation pathways. Biochim. Biophys. Acta Bioenerg. 1827, 161–175 (2013).
89. Camacho, A., Walter, X. A., Picazo, A. & Zopfi, J. Photoferrotrophy: Remains of an ancient photosynthesis in modern environments. Front. Microbiol. 8, 323 (2017).
90. Simmons, S. L. & Edwards, K. J. Geobiology of magnetotactic bacteria. in Magnetoreception and Magnetosomes in Bacteria 77–102 (Springer, 2006).
91. Strbak, O. & Dobrota, D. Archean iron-based metabolism analysis and the photoferrotrophy-driven hypothesis of microbial magnetotaxis origin. Geomicrobiol. J. 36, 278–290 (2019).
92. Muñoz, D. et al. Magnetosomes could be protective shields against metal stress in magnetotactic bacteria. Sci. Rep. 10, 11430 (2020).
93. Monteil, C. L. et al. Genomic study of a novel magnetotactic Alphaproteobacteria uncovers the multiple ancestry of magnetotaxis. Environ. Microbiol. 20, 4415–4430 (2018).
94. Du, H. et al. Magnetosome gene duplication as an important driver in the evolution of magnetotaxis in the Alphaproteobacteria. mSystems 4, e00315–e00319 (2019).
95. Monteil, C. L. et al. Repeated horizontal gene transfers triggered parallel evolution of magnetotaxis in two evolutionary divergent lineages of magnetotactic bacteria. ISME J. 14, 1783–1794 (2020).

96. Natan, E., Fitak, R. R., Werber, Y. & Vortman, Y. Symbiotic magnetic sensing: Raising evidence and beyond. Philos. Trans. R. Soc. Lond. B 375, (2020).

97. Natan, E. & Vortman, Y. The symbiotic magnetic-sensing hypothesis: Do magnetotactic bacteria underlie the magnetic sensing capability of animals? Mov. Ecol. 5, 22 (2017).

98. Simon, R. A. et al. Magnetotactic bacteria from the human gut microbiome associated with orientation and navigation regions of the brain. J. Oceanol. Limnol. 39, 2044–2052 (2021).

99. Bellinger, M. R. et al. Conservation of magnetite biomineralisation genes in all domains of life and implications for magnetic sensing. Proc. Natl. Acad. Sci. USA 119, (2022).

100. Yuan, W., Zhou, H., Yang, Z., Hein, J. R. & Yang, Q. Magnetite magnetofossils record biogeochemical remanent magnetisation in hydrogenetic ferromanganese crusts. Geology 48, 298–302 (2020).

101. Jiang, X. D. et al. Characterisation and quantification of magnetofossils within abyssal manganese nodules from the Western Pacific Ocean and implications for nodule formation. Geochem. Geophys. Geosyst. 21, e2019GC008811 (2020).

102. Hassan, M. bin et al. Presence of biogenic magnetite in ferromanganese nodules. Environ. Microbiol. Rep. 12, 288–295 (2020).

103. Oda, H., Nakasato, Y. & Usui, A. Characterisation of marine ferromanganese crust from the Pacific using residues of selective chemical leaching: Identification of fossil magnetotactic bacteria with FE-SEM and rock magnetic methods. Earth, Planets Space 70, 1–10 (2018).

104. Kirschvink, J. L. & Chang, S. B. R. Ultrafine-grained magnetite in deep-sea sediments - Possible bacterial magnetofossils. Geology 12, 559–562 (1984).

105. Petersen, N., von Dobeneck, T. & Vali, H. Fossil bacterial magnetite in deep-sea sediments from the South-Atlantic Ocean. Nature 320, 611–615 (1986).

106. Li, J. et al. Biomineralisation, crystallography and magnetic properties of bullet-shaped magnetite magnetosomes in giant rod magnetotactic bacteria. Earth Planet. Sci. Lett. 293, 368–376 (2010).

107. Moskowitz, B. M., Frankel, R. B. & Bazylinski, D. A. Rock magnetic criteria for the detection of biogenic magnetite. Earth and Planetary Science Letters 120, 283–300 (1993).

108. Chang, L. et al. Low-temperature magnetic properties of pelagic carbonates: Oxidation of biogenic magnetite and identification of magnetosome chains. J. Geophys. Res. Solid Earth 118, 6049–6065 (2013).

109. Chang, L., Heslop, D., Roberts, A. P., Rey, D. & Mohamed, K. J. Discrimination of biogenic and detrital magnetite through a double Verwey transition temperature. J. Geophys. Res. Solid Earth 121, 3–14 (2016).

110. Jackson, M. J. & Moskowitz, B. On the distribution of Verwey transition temperatures in natural magnetites. Geophys. J. Int. 224, 1314–1325 (2021).

111. Pike, C. R., Roberts, A. P. & Verosub, K. L. Characterizing interactions in fine magnetic particle systems using first order reversal curves. J. Appl. Phys. 85, 6660–6667 (1999).

112. Roberts, A. P., Pike, C. R. & Verosub, K. L. First-order reversal curve diagrams: A new tool for characterizing the magnetic properties of natural samples. J. Geophys. Res. Solid Earth 105, 28461–28475 (2000).

113. Roberts, A. P., Heslop, D., Zhao, X. & Pike, C. R. Understanding fine magnetic particle systems through use of first-order reversal curve diagrams. Rev. Geophys. 52, 557–602 (2014).

114. Dunin-Borkowski, R. E. et al. Magnetic microstructure of magnetotactic bacteria by electron holography. Science 282, 1868–1870 (1998).

115. Pan, Y. X. et al. Rock magnetic properties of uncultured magnetotactic bacteria. Earth Planet. Sci. Lett. 237, 311–325 (2005).

116. Roberts, A. P. et al. Magnetotactic bacterial abundance in pelagic marine environments is limited by organic carbon flux and availability of dissolved iron. Earth Planet. Sci. Lett. 310, 441–452 (2011).

117. Chen, A. P., Egli, R. & Moskowitz, B. M. First-order reversal curve (FORC) diagrams of natural and cultured biogenic magnetic particles. J. Geophys. Res. Solid Earth 112, B08S90 (2007).

118. Egli, R., Chen, A. P., Winklhofer, M., Kodama, K. P. & Horng, C.-S. Detection of noninteracting single domain particles using first-order reversal curve diagrams. Geochem. Geophys. Geosyst. 11, Q01Z11 (2010).

119. Li, J., Wu, W., Liu, Q. & Pan, Y. Magnetic anisotropy, magnetostatic interactions and identification of magnetofossils. Geochem. Geophys. Geosyst. 13, Q10Z51 (2012).

120. Amor, M. et al. Key signatures of magnetofossils elucidated by mutant magnetotactic bacteria and micromagnetic calculations. J. Geophys. Res. Solid Earth 127, e2021JB023239 (2022).

121. Charilaou, M., Winklhofer, M. & Gehring, A. U. Simulation of ferromagnetic resonance spectra of linear chains of magnetite nanocrystals. J. Appl. Phys. 109, 093903 (2011).

122. Weiss, B. P. et al. Ferromagnetic resonance and low-temperature magnetic tests for biogenic magnetite. Earth Planet. Sci. Lett. 224, 73–89 (2004).

123. Kopp, R. E. et al. Ferromagnetic resonance spectroscopy for assessment of magnetic anisotropy and magnetostatic interactions: A case study of mutant magnetotactic bacteria. J. Geophys. Res. Solid Earth 111, B12S25 (2006).

124. Kodama, K. P., Moeller, R. E., Bazylinski, D. A., Kopp, R. E. & Chen, A. P. The mineral magnetic record of magnetofossils in recent lake sediments of Lake Ely, PA. Glob. Planet. Change 110, 350–363 (2013).

125. Chang, L. et al. Magnetic detection and characterisation of biogenic magnetic minerals: A comparison of ferromagnetic resonance and first-

order reversal curve diagrams. J. Geophys. Res. Solid Earth 119, 6136–6158 (2014).

126. Kind, J., Gehring, A. U., Winklhofer, M. & Hirt, A. M. Combined use of magnetometry and spectroscopy for identifying magnetofossils in sediments. Geochem. Geophys. Geosyst. 12, Q08008 (2011).

127. Blattmann, T. M. et al. Ferromagnetic resonance of magnetite biominerals traces redox changes. Earth Planet. Sci. Lett. 545, 116400 (2020).

128. Larrasoaña, J. C. et al. Magnetotactic bacterial response to Antarctic dust supply during the Palaeocene-Eocene thermal maximum. Earth Planet. Sci. Lett. 333, 122–133 (2012).

129. Muxworthy, A. R. & Williams, W. Critical single-domain/multidomain grain sizes in noninteracting and interacting elongated magnetite particles: Implications for magnetosomes. J. Geophys. Res. Solid Earth 111, B12S12 (2006).

130. Chang, L. et al. Coupled microbial bloom and oxygenation decline recorded by magnetofossils during the Palaeocene–Eocene Thermal Maximum. Nat. Commun. 9, 4007 (2018).

131. Berndt, T. A., Chang, L. & Pei, Z. Mind the gap: Towards a biogenic magnetite palaeoenvironmental proxy through an extensive finite-element micromagnetic simulation. Earth Planet. Sci. Lett. 532, 116010 (2020).

132. Heslop, D. et al. Quantifying magnetite magnetofossil contributions to sedimentary magnetisations. Earth Planet. Sci. Lett. 382, 58–65 (2013).

133. Kruiver, P. P., Dekkers, M. J. & Heslop, D. Quantification of magnetic coercivity components by the analysis of acquisition curves of isothermal remanent magnetisation. Earth Planet. Sci. Lett. 189, 269–276 (2001).

134. Egli, R. Analysis of the field dependence of remanent magnetisation curves. J. Geophys. Res. Solid Earth 108, 2081 (2003).

135. Zhao, X., Fujii, M., Suganuma, Y., Zhao, X. & Jiang, Z. Applying the Burr type XII distribution to decompose remanent magnetisation curves. J. Geophys. Res. Solid Earth 123, 8298–8311 (2018).

136. Egli, R. Characterisation of individual rock magnetic components by analysis of remanence curves. 2. Fundamental properties of coercivity distributions. Phys. Chem. Earth 29, 851–867 (2004).

137. Heslop, D. & Dillon, M. Unmixing magnetic remanence curves without a priori knowledge. Geophys. J. Int. 170, 556–566 (2007).

138. Usui, Y., Yamazaki, T. & Saitoh, M. Changing abundance of magnetofossil morphologies in pelagic red clay around Minamitorishima, Western North Pacific. Geochem. Geophys. Geosyst. 18, 4558–4572 (2017).

139. Lascu, I. et al. Magnetic unmixing of first-order reversal curve diagrams using principal component analysis. Geochem. Geophys. Geosyst. 16, 2900–2915 (2015).

140. Harrison, R. J. et al. An improved algorithm for unmixing first-order reversal curve diagrams using principal component analysis. Geochem. Geophys. Geosyst. 19, 1595–1610 (2018).

141. Channell, J. E. T. et al. Magnetic record of deglaciation using FORC-PCA, sortable-silt grain size, and magnetic excursion at 26 ka, from the Rockall Trough (NE Atlantic). Geochem. Geophys. Geosyst. 17, 1823–1841 (2016).

142. Roberts, A. P. et al. Signatures of reductive magnetic mineral diagenesis from unmixing of first-order reversal curves. J. Geophys. Res. Solid Earth 123, 4500–4522 (2018).

143. Yamazaki, T., Fu, W., Shimono, T. & Usui, Y. Unmixing biogenic and terrigenous magnetic mineral components in red clay of the Pacific Ocean using principal component analyses of first-order reversal curve diagrams and paleoenvironmental implications. Earth, Planets Space 72, 120 (2020).

144. Egli, R. Characterisation of individual rock magnetic components by analysis of remanence curves, 1. Unmixing natural sediments. Stud. Geophys. Geod. 48, 391–446 (2004).

145. Qian, Y. et al. Assessment and integration of bulk and component-specific methods for identifying mineral magnetic assemblages in environmental magnetism. J. Geophys. Res. Solid Earth 125, 1–19 (2020).
146. Inoue, K., Yamazaki, T. & Usui, Y. Influence of magnetofossils on paleointensity estimations inferred from principal component analyses of first-order reversal curve diagrams for sediments from the Western Equatorial Pacific. Geochem. Geophys. Geosyst. 22, 1–15 (2021).
147. Wagner, C. L. et al. Diversification of iron-biomineralising organisms during the Paleocene-Eocene thermal maximum: Evidence from quantitative unmixing of magnetic signatures of conventional and giant magnetofossils. Paleoceanogr. Paleoclimatol. 36, 1–25 (2021).
148. Zhang, Q. et al. Magnetotactic bacterial activity in the North Pacific Ocean and its relationship to Asian dust inputs and primary productivity since 8.0 Ma. Geophys. Res. Lett. 48, 1–11 (2021).
149. Hesse, P. P. Evidence for bacterial palaeoecological origin of mineral magnetic cycles in oxic and sub-oxic Tasman Sea sediments. Mar. Geol. 117, 1–17 (1994).
150. Yamazaki, T. & Kawahata, H. Organic carbon flux controls the morphology of magnetofossils in marine sediments. Geology 26, 1064–1066 (1998).
151. He, K. & Pan, Y. Magnetofossil abundance and diversity as paleoenvironmental proxies: A case study from Southwest Iberian margin sediments. Geophys. Res. Lett. 47, e2020GL087165 (2020).
152. Lean, C. M. B. & McCave, I. N. Glacial to interglacial mineral magnetic and palaeoceanographic changes at Chatham Rise, SW Pacific Ocean. Earth Planet. Sci. Lett. 163, 247–260 (1998).
153. Yamazaki, T. Reductive dissolution of biogenic magnetite. Earth, Planets Space 72, 150 (2020).
154. Mathias, G. L. et al. A multi-proxy approach to unravel late Pleistocene sediment flux and bottom water conditions in the western South Atlantic Ocean. Paleoceanogr. Paleoclimatol. 36, e2020PA004058 (2021).

155. Rodelli, D. et al. Diagenetic fate of biogenic soft and hard magnetite in chemically stratified sedimentary environments of Mamangua Ria, Brazil. J. Geophys. Res. Solid Earth 124, 2313–2330 (2019).

156. Ouyang, T. et al. Variable remanence acquisition efficiency in sediments containing biogenic and detrital magnetites: Implications for relative paleointensity signal recording. Geochem. Geophys. Geosyst. 15, 2780–2796 (2014).

157. Chen, L. et al. Remanence acquisition efficiency in biogenic and detrital magnetite and recording of geomagnetic paleointensity. Geochem. Geophys. Geosyst. 18, 1435–1450 (2017).

158. Li, J. et al. Paleomagnetism of a sediment core taken from the Ontong-Java Plateau: For better understanding of the role of biogenic magnetite in geomagnetic paleointensity recording. Preprint at https://doi.org/10.1002/essoar.10507999.1 (2021).

159. Tarduno, J. A., Tian, W. L. & Wilkison, S. Biogeochemical remanent magnetisation in pelagic sediments of the western equatorial Pacific Ocean. Geophys. Res. Lett. 25, 3987–3990 (1998).

160. Yamazaki, T., Suzuki, Y., Kouduka, M. & Kawamura, N. Dependence of bacterial magnetosome morphology on chemical conditions in deep-sea sediments. Earth Planet. Sci. Lett. 513, 135–143 (2019).

161. Vasiliev, I. et al. Putative greigite magnetofossils from the Pliocene epoch. Nat. Geosci. 1, 782–786 (2008).

162. Pósfai, M. et al. Crystal-size distributions and possible biogenic origin of Fe sulphides. Eur. J. Mineral. 13, 691–703 (2001).

163. Chang, L. et al. Identification and environmental interpretation of diagenetic and biogenic greigite in sediments: A lesson from the Messinian Black Sea. Geochem. Geophys. Geosyst. 15, 3612–3627 (2014).

164. Bazylinski, D. A. & Blakemore, R. P. Nitrogen fixation (acetylene reduction) in Aquaspirillum magnetotacticum. Curr. Microbiol. 9, 305–308 (1983).

165. Jiang, W. et al. Submerged culture of Magnetospirillum gryphiswaldense under N2-fixing condition and regulation of activity of nitrogen fixation. Chin. Sci. Bull. 47, 2095–2099 (2002).

166. Bazylinski, D. A. et al. Chemolithoautotrophy in the marine, magnetotactic bacterial strains MV-1 and MV-2. Arch. Microbiol. 182, 373–387 (2004).

167. Schultheiss, D., Handrick, R., Jendrossek, D., Hanzlik, M. & Schüler, D. The presumptive magnetosome protein Mms16 is a poly(3-hydroxybutyrate) granule-bound protein (phasin) in Magnetospirillum gryphiswaldense. J. Bacteriol. 187, 2416–2425 (2005).

168. Rivas-Lamelo, S. et al. Magnetotactic bacteria as a new model for P sequestration in the ferruginous Lake Pavin. Geochem. Perspect. Lett. 5, 35–41 (2017).

169. Schulz-Vogt, H. N. et al. Effect of large magnetotactic bacteria with polyphosphate inclusions on the phosphate profile of the suboxic zone in the Black Sea. ISME J. 13, 1198–1208 (2019).

170. Tanaka, M. et al. Biomagnetic recovery and bioaccumulation of selenium granules in magnetotactic bacteria. Appl. Environ. Microbiol. 82, 3886–3891 (2016).

171. Isambert, A., Menguy, N., Larquet, E., Guyot, F. & Valet, J.-P. Transmission electron microscopy study of magnetites in a freshwater population of magnetotactic bacteria. Am. Mineral. 92, 621–630 (2007).

172. Cornejo, E., Subramanian, P., Li, Z., Jensen, G. J. & Komeili, A. Dynamic remodeling of the magnetosome membrane is triggered by the initiation of biomineralisation. MBio 7, e01898-15 (2016).

173. Li, J. et al. Bullet-shaped magnetite biomineralisation within a magnetotactic Deltaproteobacterium: Implications for magnetofossil identification. J. Geophys. Res. Biogeosci. 125, e2020JG005680 (2020).

174. Bazylinski, D. A. Structure and function of the bacterial magnetosome. ASM News 61, 337–343 (1995).

175. Simmons, S. L., Bazylinski, D. A. & Edwards, K. J. South-seeking magnetotactic bacteria in the Northern Hemisphere. Science 311, 371–374 (2006).

176. Faivre, D., Fischer, A., Garcia-Rubio, I., Mastrogiacomo, G. & Gehring, A. U. Development of cellular magnetic dipoles in magnetotactic bacteria. Biophys. J. 99, 1268–1273 (2010).

177. Coale, K. H. et al. Southern ocean iron enrichment experiment: Carbon cycling in high- and low-Si waters. Science 304, 408–414 (2004).

178. Jacq, V., Ridame, C., L'Helguen, S., Kaczmar, F. & Saliot, A. Response of the unicellular diazotrophic cyanobacterium Crocosphaera watsonii to iron limitation. PLoS One 9, e86749 (2014).

179. Martínez-García, A. & Winckler, G. Iron fertilization in the glacial ocean. PAGES Mag. 22, 82–83 (2014).

180. Street, J. H. & Paytan, A. Iron, phytoplankton growth, and the carbon cycle. Met. Ions Biol. Syst. 43, 153–193 (2005).

181. Aumont, O. & Bopp, L. Globalizing results from ocean in situ iron fertilization studies. Glob. Biogeochem. Cycles 20, GB2017 (2006).

182. Wambeke, F. van et al. Nutrient limitation of primary productivity in the Southeast Pacific. Biogeosciences 5, 215–225 (2008).

183. Schoffman, H., Lis, H., Shaked, Y. & Keren, N. Iron-nutrient interactions within phytoplankton. Front. Plant Sci. 7, 1223 (2016).

184. Amor, M., Tharaud, M., Gélabert, A. & Komeili, A. Single-cell determination of iron content in magnetotactic bacteria: Implications for the iron biogeochemical cycle. Environ. Microbiol. 22, 823–831 (2020).

185. Vainshtein, M., Suzina, N. & Sorokin, V. A new type of magnet-sensitive inclusions in cells of photosynthetic purple bacteria. Syst. Appl. Microbiol. 20, 182–186 (1997).

186. Sakaguchi, T., Arakaki, A. & Matsunaga, T. Desulfovibrio magneticus sp. nov., a novel sulphate-reducing bacterium that produces intracellular single-domain-sized magnetite particles. Int. J. Syst. Evol. Microbiol. 52, 215–221 (2002).

187. Rahn-Lee, L. et al. A genetic strategy for probing the functional diversity of magnetosome formation. PLoS Genet. 11, e1004811 (2015).

188. Grant, C. R. & Komeili, A. Ferrosomes are iron storage organelles formed by broadly conserved gene clusters in bacteria and archaea. Preprint at https://doi.org/10.1101/2020.01.10.902569 (2020).

189. Amor, M. et al. Magnetotactic bacteria accumulate a large pool of iron distinct from their magnetite crystals. Appl. Environ. Microbiol. 86, 1–20 (2020).

190. Lefèvre, C. T., Frankel, R. B., Abreu, F., Lins, U. & Bazylinski, D. A. Culture-independent characterisation of a novel, uncultivated magnetotactic member of the Nitrospirae phylum. Environ. Microbiol. 13, 538–549 (2011).

191. Lin, W., Li, J. & Pan, Y. Newly isolated but uncultivated magnetotactic bacterium of the phylum Nitrospirae from Beijing, China. Appl. Environ. Microbiol. 78, 668–675 (2012).

192. Spring, S. & Bazylinski, D. A. Magnetotactic bacteria. Prokaryotes 2, 842–862 (2006).

193. Kolinko, S., Richter, M., Gloeckner, F.-O., Brachmann, A. & Schüler, D. Single-cell genomics of uncultivated deep-branching magnetotactic bacteria reveals a conserved set of magnetosome genes. Environ. Microbiol. 18, 21–37 (2016).

194. Sen, J. The role of associated nitrogen-fixing bacteria on nitrogen nutrition of cereal crops. Agric. J. India 24, 967–980 (1929).

195. Rubin-Blum, M., Dubilier, N. & Kleiner, M. Genetic evidence for two carbon fixation pathways (the Calvin-Benson-Bassham Cycle and the Reverse Tricarboxylic Acid Cycle) in symbiotic and free-living bacteria. Msphere 4, e00394-18 (2019).

196. Hoppenrath, M., Elbrächter, M. & Drebes, G. Marine Phytoplankton: Selected Microphytoplankton Species from the North Sea Around Helgoland and Sylt. (E. Schweizerbart'sche Verlagsbuchhandlung, 2009).

197. Matin, A. Organic nutrition of chemolithotrophic bacteria. Annu. Rev. Microbiol. 32, 433–468 (1978).

198. Paoli, G. C., Morgan, N. S., Tabita, F. R. & Shively, J. M. Expression of the cbbLcbbS and cbbM genes and distinct organisation of the cbb Calvin cycle structural genes of Rhodobacter capsulatus. Arch. Microbiol. 164, 396–405 (1995).

199. Williams, T. J., Zhang, C. L., Scott, J. H. & Bazylinski, D. A. Evidence for autotrophy via the reverse tricarboxylic acid cycle in the marine magnetotactic coccus strain MC-1. Appl. Environ. Microbiol. 72, 1322–1329 (2006).

200. Zhang, W., Wang, Y., Liu, L., Pan, Y. & Lin, W. Identification and genomic characterisation of two previously unknown magnetotactic Nitrospirae. Front. Microbiol. 12, 690052 (2021).

201. Monteil, C. L. et al. Intracellular amorphous Ca-carbonate and magnetite biomineralisation by a magnetotactic bacterium affiliated to the Alphaproteobacteria. ISME J. 15, 1–18 (2021).

202. Arakaki, A., Takeyama, H., Tanaka, T. & Matsunaga, T. Cadmium recovery by a sulphate-reducing magnetotactic bacterium, Desulfovibrio magneticus RS-1, using magnetic separation. Appl. Biochem. Biotech. 98, 833–840 (2002).

203. Tajer-Mohammad-Ghazvini, P. et al. Cobalt separation by Alphaproteobacterium MTB-KTN90: Magnetotactic bacteria in bioremediation. Bioprocess Biosyst. Eng. 39, 1899–1911 (2016).

204. Tanaka, M., Arakaki, A., Staniland, S. S. & Matsunaga, T. Simultaneously discrete biomineralisation of magnetite and tellurium nanocrystals in magnetotactic bacteria. Appl. Environ. Microbiol. 76, 5526–5532 (2010).

205. Sannigrahi, S. & Suthindhiran, K. Metal recovery from printed circuit boards by magnetotactic bacteria. Hydrometallurgy 187, 113–124 (2019).

206. Postec, A. et al. Magnetotactic bacteria in microcosms originating from the French Mediterranean coast subjected to oil industry activities. Microb. Ecol. 63, 1–11 (2012).

207. Sewell, R. B. S. & Fage, L. Minimum oxygen layer in the ocean. Nature 162, 949–951 (1948).

208. Cavicchioli, R. et al. Scientists' warning to humanity: Microorganisms and climate change. Nature Rev. Microbiol. 17, 569–586 (2019).

209. Ulloa, O., Canfield, D. E., DeLong, E. F., Letelier, R. M. & Stewart, F. J. Microbial oceanography of anoxic oxygen minimum zones. Proc. Natl. Acad. Sci. U. S. A. 109, 15996–16003 (2012).

210. Schmidtko, S., Stramma, L. & Visbeck, M. Decline in global oceanic oxygen content during the past five decades. Nature 542, 335–339 (2017).

211. Breitburg, D. et al. Declining oxygen in the global ocean and coastal waters. Science 359, eaam7240 (2018).

212. Bertagnolli, A. D. & Stewart, F. J. Microbial niches in marine oxygen minimum zones. Nat. Rev. Microbiol. 16, 723–729 (2018).

213. Wright, J. J., Konwar, K. M. & Hallam, S. J. Microbial ecology of expanding oxygen minimum zones. Nat. Rev. Microbiol. 10, 381–394 (2012).

214. Paulmier, A. & Ruiz-Pino, D. Oxygen minimum zones (OMZs) in the modern ocean. Progr. Oceanogr. 80, 113–128 (2009).

215. Ulloa, O. & Pantoja, S. The oxygen minimum zone of the eastern South Pacific. Deep-Sea Res. II 56, 987–991 (2009).

216. Stevens, H. & Ulloa, O. Bacterial diversity in the oxygen minimum zone of the eastern tropical South Pacific. Environ. Microbiol. 10, 1244–1259 (2008).

217. Lavik, G. et al. Detoxification of sulphidic African shelf waters by blooming chemolithotrophs. Nature 457, 581–584 (2009).

218. Walsh, D. A. et al. Metagenome of a versatile chemolithoautotroph from expanding oceanic dead zones. Science 326, 578–582 (2009).

219. Canfield, D. E. et al. A cryptic sulphur cycle in oxygen-minimum-zone waters off the Chilean coast. Science 330, 1375–1378 (2010).

220. Rhoads, D. C., Mulsow, S. G., Gutschick, R., Baldwin, C. T. & Stolz, J. F. The dysaerobic zone revisited: A magnetic facies? Geol. Soc. Lond. Spec. Publ. 58, 187–199 (1991).

221. Brune, A., Frenzel, P. & Cypionka, H. Life at the oxic-anoxic interface: Microbial activities and adaptations. FEMS Microbiol. Rev. 24, 691–710 (2000).

222. Monteil, C. L. et al. Ectosymbiotic bacteria at the origin of magnetoreception in a marine protist. Nat. Microbiol. 4, 1088–1095 (2019).

223. Reitner, J. et al. Concretionary methane-seep carbonates and associated microbial communities in Black Sea sediments. Palaeogeogr. Palaeoclimatol. Palaeoecol. 227, 18–30 (2005).

224. Dufour, S. C. et al. Magnetosome-containing bacteria living as symbionts of bivalves. ISME J. 8, 2453–2462 (2014).

Chapter 3: Methods

INTRODUCTION

In this chapter, a comprehensive overview is provided of the methods employed in the MTB exploration from two distinct types of extreme aquatic environments: acidic peatlands and marine OMZs. The methodological approach integrates classical microbiological techniques with genomic and bioinformatic tools to elucidate the ecological roles and phylogenetic identities of MTB in low-oxygen, high-redox, and chemically stratified conditions. This is done through a multi-phase strategy that includes field sampling, MTB-specific enrichment techniques, microscopic characterisation, taxonomic validation using molecular tools, high-throughput sequencing, and sophisticated computational workflows for metagenomic assembly, genome binning, quality refinement, metabolic reconstruction, and comparative phylogenomic analyses.

Sample Collection and MTB Enrichment

Sample acquisition was conducted in two contrasting yet complementary environments: (1) acidic peatlands located in the Dajiuhu National Wetland Park, part of the Shennongjia Natural Conservation Region, Hubei Province, China, and (2) marine OMZs sampled globally via publicly available metagenomic datasets. For the Dajiuhu site, duplicate sediment samples were collected using sterile scoops and deposited into 600-mL wide-mouthed polyethylene flasks. Approximately 100 mL of site-specific peatland water was added to maintain microhabitat fidelity and redox conditions. These samples were stored for over five years under dark, room-temperature conditions (~25°C), mimicking the microoxic, anaerobic niches in which MTB typically thrive. Such extended incubation not only preserved native MTB populations but may have enhanced the detectability of slow-growing or rare taxa, as previously

reported in similar studies (Lefèvre et al., 2013). Photographic and spatial documentation of the sampling site is presented in Figure 1a–c.

For magnetic enrichment, two methods were employed. First, the capillary racetrack method (Wolfe et al., 1987) allows for the directional movement of MTB toward the magnetic capillary tip over a period of three hours. Cells were washed repeatedly with autoclaved Milli-Q water to reduce non-target microbial load. Subsequently, the hanging-drop technique enabled visualisation of the enriched, live, motile MTB under a light microscope (Olympus BX53, Tokyo, Japan). These two steps ensured that the enrichment protocol was successful, leading to magnetic separation of active MTB from a mixed diaspora of microbial populations. The resulting concentrated sample was used as input for downstream applications such as microscopy, fluorescence imaging, and molecular profiling. The laboratory setup for this enrichment protocol is illustrated in Figure 1d.

Microscopy and Molecular Identification

Morphological features and magnetosome structures of MTB were characterised using both scanning electron microscopy (SEM) and transmission electron microscopy (TEM). SEM was conducted using the Zeiss Auriga Compact FIB-SEM system (Carl Zeiss, Germany). Specimens were prepared on silicon wafers and fixed in 4% paraformaldehyde. For TEM observation, a 10 µL drop of magnetic enrichment was deposited on a Formvar carbon-coated copper grid and was allowed to air dry in a laminar flow hood. MTB cells were imaged using a JEM-2100 HR TEM (JEOL, Tokyo, Japan) at 200 kV.

For molecular identification, DNA was extracted from magnetically enriched cells and subjected to whole-genome amplification (WGA). WGA was carried out using the GenomiPhi Single Cell DNA Amplification Kit (Cytiva, USA). WGA products were diluted (1:50) and subjected to amplification of the 16S rRNA gene using universal primers

27F (5′-AGA GTT TGA TCC TGG CTC AG-3′) and 1492R (5′-GGT TAC CTT GTT ACG ACT T-3′) (Zhang et al., 2021). PCR products were cloned into pMD19-T vectors (TaKaRa Bio, Japan), followed by random selection and Sanger sequencing of 100 colonies (Sanger et al., 1977). The resulting consensus 16S rRNA gene was queried against the NCBI BLASTn database (McGinnis and Madden, 2004). The top 38 hits were aligned using MEGA v11.0.13 (Tamura et al., 2021) with ClustalW alignment, and low-quality aligned segments were manually trimmed. A phylogenetic tree was constructed using the maximum likelihood approach in W-IQ-TREE with 1,000 bootstrap replicates (Trifinopoulos et al., 2016). Tree visualisation and annotation were performed using the Interactive Tree of Life (iTOL v6) platform (Letunic and Bork, 2024).

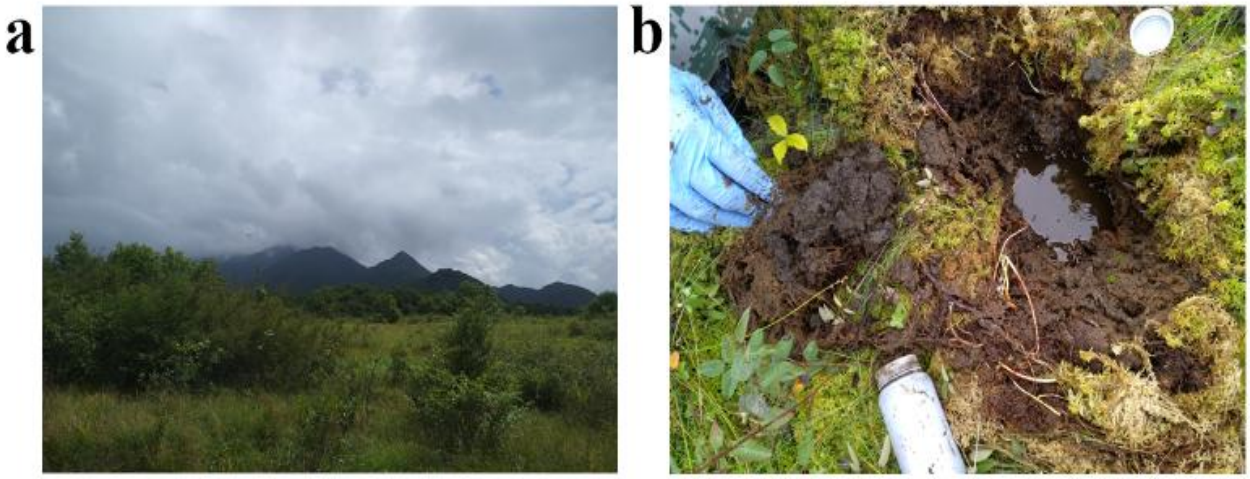

Figure 1: Sample collection and magnetic enrichment of MTB from the Dajiuhu Peatland. (a) View of the Dajiuhu Peatland, located in the southeast Shennongjia Natural Conservation Region, Hubei Province. (b) Sediment sampling site within an acidic, waterlogged soil environment.

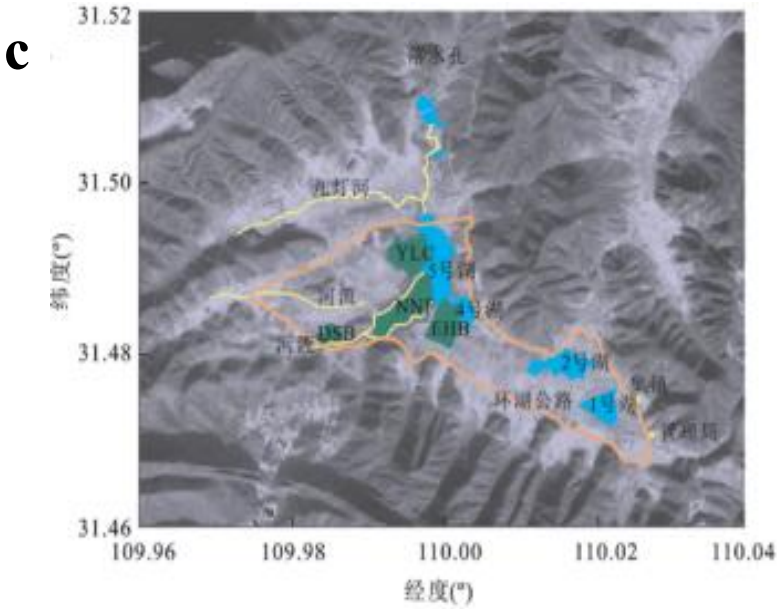

图 4 神农架大九湖盆地

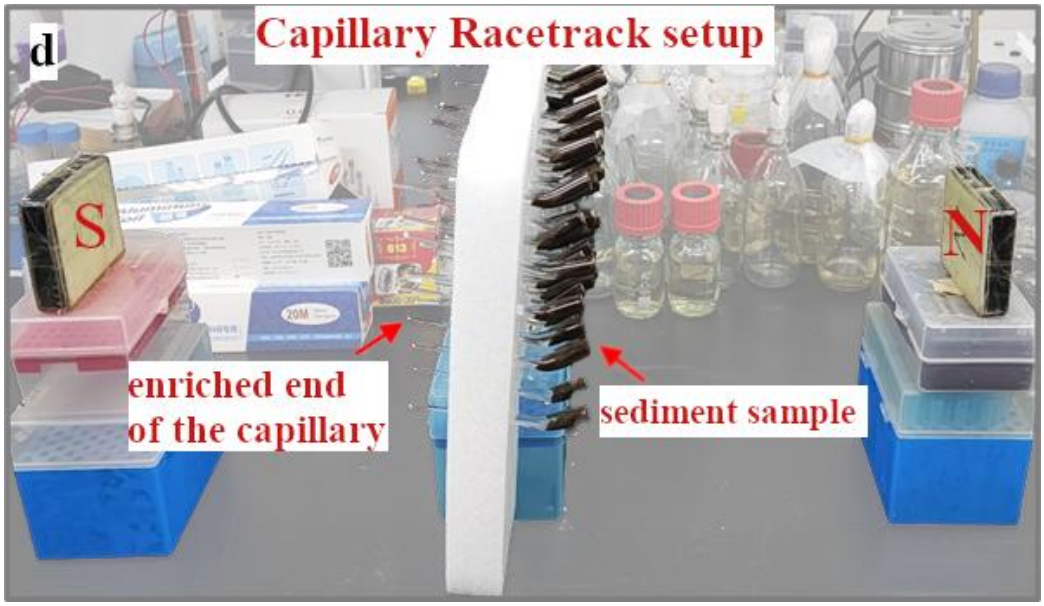

Figure 1: Sample collection and magnetic enrichment of MTB from the Dajiuhu Peatland (continued). (c) Sampling location map of Dajiuhu National Wetland Park. (d) Laboratory setup of the capillary racetrack method used for MTB enrichment from sediment samples.

Taxonomic confirmation was supported by fluorescence *in situ* hybridisation (FISH), using a custom-designed Cy3-labeled oligonucleotide probe targeting *M. dajiuhuensis* 16S rRNA. A universal bacterial FAM-labeled probe (EUB338) was used for cross-validation with *Magnetospirillum gryphiswaldense* (MSR-1) cells as a negative control.

Metagenomic Sequencing and Assembly

Metagenomic sequencing constitutes a cornerstone of this research, enabling analysis of complex microbial communities from environments where traditional cultivation methods are insufficient or inapplicable. For the Dajiuhu MAG, shotgun metagenomic sequencing was conducted using the NovaSeq 6000 platform (Novogene, Beijing, China), employing a paired-end strategy with 150 bp reads. For the OMZ study, a large-scale metagenomic dataset comprising 101 publicly available Sequence Read Archive (SRA) entries associated with OMZs was curated from the European Nucleotide Archive (ENA). These datasets were chosen using the keyword "oxygen minimum zone," and selection criteria focused on ensuring both the geographic diversity of marine samples and data quality relevant to bacterial metagenomic studies. Sequencing and biosample details of the 101 SRA used in this study are detailed in Supplementary Table S1.

Once identified, all raw sequencing files were subjected to a stringent preprocessing pipeline. The metaWRAP v1.1.5 pipeline was employed, beginning with the read_qc module, which performed adapter trimming and low-quality base removal. The '--skip-bmtagger' flag was used to remove low-quality reads and to trim adapter sequences. This quality control step ensured that the remaining reads were of high fidelity, free from sequencing artifacts and adapter contamination, and ready for downstream assembly.

Assembly of high-quality reads was accomplished using two strategies depending on the project subset. For the global OMZ

metagenomes, MEGAHIT was used in the preliminary assembly step due to its efficiency in assembling large and complex environmental datasets. MEGAHIT implements succinct de Bruijn graph algorithms to assemble contigs while managing computational demands efficiently. For Dajiuhu peatland magnetically enriched samples, and subsequent assembly for OMZ samples, metaSPAdes v3.13.0 was selected for its superior performance in assembling microbial communities with lower diversity and higher coverage. Both assemblers were configured with a minimum contig length parameter of 2000 base pairs ('-l 2000'), which filtered out low-confidence, short contigs and retained only substantial sequence fragments suitable for binning and annotation.

Genome Binning and Refinement

The transition from assembled contigs to draft genomes, or MAGs, was achieved through a multi-tiered genome binning process that incorporated three independent algorithms: MaxBin2 (Wu et al., 2016), MetaBAT2 (Kang et al., 2019) and CONCOCT (Alneberg et al., 2014). These tools use complementary approaches for clustering contigs. MetaBAT2 relies on contig coverage and tetranucleotide frequency patterns; MaxBin2 incorporates a probabilistic model integrating contig coverage and essential gene presence; and CONCOCT uses Gaussian mixture models and variational Bayesian inference to bin contigs based on sequence composition and read coverage.

The binning workflow was executed using the Binning module of metaWRAP v1.1.5. Each of the three algorithms was applied independently to the same contig datasets, ensuring redundancy in bin predictions. The metaWRAP Bin_refinement module was then used to resolve binning inconsistencies and to generate a consensus bin set with improved accuracy. The criteria for bin retention were stringent: only bins with ≥70% estimated completeness and ≤10% contamination were kept. These thresholds align with the medium- and high-quality MAG

definitions outlined by the Minimum Information about a Metagenome-Assembled Genome (MIMAG) standards (Bowers et al., 2017).

The refinement process significantly improved MAG quality by selecting contigs that consistently grouped within bins across all three algorithms. Bin quality was also evaluated using CheckM v1.0.12 (Parks et al., 2015) and CheckM2 (Chklovski et al., 2023), with evaluation metrics including completeness, contamination, GC content, N50/L50 statistics and maximum contig size. QUAST v5.0.2 (Quast et al., 2012) was used for further quality control. Bins that failed to meet the quality criteria were either discarded or re-binned with adjusted parameters.

To ensure that downstream analyses were not biased by redundancy, dereplication was performed using dRep v3.4.0. This step involved clustering bins based on Average Nucleotide Identity (ANI), which is a measure of genomic similarity. Two ANI thresholds were used: 90% for primary clusters and 99% for secondary clustering, which allows representative genomes to be selected without over-representing closely related strains. The dereplication output consisted of a curated set of non-redundant, high-quality MTB genomes suitable for taxonomic, functional and phylogenetic analysis.

Together, the binning and refinement steps transformed complex metagenomic assemblies into biologically meaningful genomic units, offering high-resolution insights into MTB community structure and evolutionary relationships across contrasting environmental regimes.

Genome Screening and Magnetosome Gene Cluster Annotation

To identify and characterise MTB within the reconstructed genome bins, a comprehensive genome annotation and screening strategy was implemented. Identification of MGCs, responsible for the biomineralisation and alignment of magnetic particles was the central focus of this phase. The strategy employed a combination of automated

tools, manual validation and database cross-checks to ensure the accuracy and completeness of MGC detection.

The workflow began with MAG annotation using Prokka v1.13.4, a widely adopted bacterial genome annotation tool. Prokka integrates a suite of programs including Prodigal for gene prediction, Barrnap for rRNA gene detection and HMMER for functional domain searches. In this study, parameters were optimised with an e-value threshold of 1e-05 to reduce noise and increase annotation specificity. Annotated protein-coding genes were exported in GFF and FAA formats, which formed the input for downstream MGC-specific screening. Next, MagCluster v0.2.11 was employed for MGC screening. This specialised tool consists of three core modules: (1) Prokka for genome annotation; (2) mgc_screen to detect MGCs; and (3) a visualisation module integrated with clinker v0.0.23 for synteny analysis. The mgc_screen module scans genomes for hallmark magnetosome genes such as *mam*, *man*, *mms* and *mad*. Screening was conducted with default parameters to balance sensitivity and specificity across the phylogenetically diverse bins derived from OMZs and acidic peatlands.

Putative MGCs identified by MagCluster were subsequently validated through manual inspection. This was achieved by comparing predicted magnetosome proteins against entries in the NCBI non-redundant (nr) protein database using PSI-BLAST (Position-Specific Iterated BLAST) implemented through the NCBI BLAST+ suite v2.12.0. Each candidate protein underwent a single iteration of PSI-BLAST (-num_iterations 1) to avoid model overfitting while enhancing domain-level resolution. PSI-BLAST outputs were verified manually using keywords, “mam”, “mad”, “man” and “magnetosome”. This ensures MTB genome identification from the dataset.

To visualise gene synteny and structural conservation across genomes, clinker was used to render annotated MGCs into easily

interpretable gene maps. This step allowed cross-genomic comparison of gene order and proximity, which is critical for detecting rearrangements or truncations in MGC regions and an added step for manual curation. Outputs were saved in Scalable Vector Graphics (SVG) format and were further refined using Inkscape v1.2.2 for figure preparation.

Overall, this multi-step pipeline starting with genome annotation to MGC validation, ensured accurate identification of magnetotactic functionality in novel and known bacterial genomes. It also enabled discovery of unusual gene arrangements and highlighted phylogenetic groups harbouring potential MGCs.

Phylogenomic Tree Construction and Average Nucleotide Identity Prediction

Phylogenomic analysis was conducted to resolve evolutionary placement of identified MAGs compared to other MTB and non-MTB relatives. For the Dajiuhu MAG and reference genomes, protein sequences from 120 conserved, single-copy genes were identified using GTDB-Tk v2.1.0 (Chaumeil et al., 2020) and concatenated. IQ-TREE v2.0.3 (Nguyen et al., 2015) was employed for phylogenetic inference, with the optimal substitution model determined via the TEST function. Ultrafast bootstrap analysis was performed with 1,000 replicates to assess branch support.

For the OMZ MAGs, a phylogenomic tree was generated using the anvi'o platform (Eren et al., 2021). Twenty-four reference genomes were considered for this analysis based on close proximity from the GTDB website's "Taxonomy Tree" (https://gtdb.ecogenomic.org/tree). Genome FASTA files (both for MAGs and reference genomes) were first converted into anvi'o-compatible contigs databases. A genomes storage database was then created from these using anvi-gen-genomes-storage. To identify conserved phylogenetic markers, HMM searches were run for bacterial single-copy core genes using the anvi'o default bacterial HMM profile. Protein sequences of these markers were extracted and concatenated across

all genomes. This concatenated alignment was used to construct a maximum likelihood tree using FastTree2 (Price et al., 2010), implemented through anvi-gen-phylogenomic-tree. The resulting phylogeny in both instances were visualised using iTOL v6 (Letunic and Bork, 2024), and figure modifications were carried out in Inkscape (https://inkscape.org/).

To further quantify genomic similarity and to classify putative MTB at the species level, ANI analysis was carried out using the ANImf algorithm in dRep v3.4.0. Dereplication thresholds were set at 90% ANI for genus-level and 99% ANI for strain-level clustering. These thresholds conform to widely accepted criteria for microbial taxonomy. PairwiseANIviz (Ji et al., 2024) was used to generate a matrix heatmap, colour-coded by identity scores and accompanied by hierarchical clustering. This visualisation aided in identifying unique MTB genomes and closely related clusters.

Metabolic Predictions

Functional profiling was performed using KofamScan v1.3.0, which assigns KEGG Orthologs (KO) to genes based on Hidden Markov Models. Each KO assignment was accompanied by a confidence score. Metabolic module completeness was then assessed using KEGGDecoder v1.3.0, which interprets KO assignments to evaluate the integrity of functional pathways such as carbon fixation (e.g., Wood–Ljungdahl pathway), denitrification, sulphate reduction, and other energy-generating cycles. These metabolic modules were visualised using KEGG Mapper Reconstruct (https://www.genome.jp/kegg/mapper/reconstruct.html), and final diagrams were curated manually to ensure biological plausibility. For visualisation, the matrix was also processed using Python (matplotlib v3.5.2 (https://matplotlib.org/), seaborn v0.11.2 (https://seaborn.pydata.org/) and pandas) to plot a bubble heatmap, where

bubble size and colour indicate the presence and completeness of specific metabolic pathways across bins.

Taxonomic Classification and Nomenclature

The classification process began with use of the GTDB-Tk version 2.1.0, a widely recognised framework for microbial taxonomy based on genome phylogeny. GTDB-Tk compares genomes to a reference tree derived from the Genome Taxonomy Database (GTDB) release 207_v2, which contains over 200,000 bacterial and archaeal genomes categorised based on 120 single-copy marker genes. These genes are phylogenetically informative and provide robust resolution across bacterial taxa. The 'classify_wf' workflow in GTDB-Tk was employed, aligning marker genes using HMMER, placing them into the reference tree using pplacer, and assigning taxonomy based on relative evolutionary divergence (RED) metrics.

Following taxonomic assignment, species delineation was further supported through ANI analysis, a high-resolution metric that compares genome-wide sequence identity. ANI values exceeding 95–96% typically indicate conspecific genomes. To this end, FastANI was employed to compare newly recovered MTB genomes with published reference datasets and to identify distinct genomic species clusters. These ANI-based groupings were visualised using hierarchical heatmaps to facilitate interpretation and support dereplication of redundant MAGs before formal naming. For novel lineages determined to be sufficiently distinct from previously described species, formal names were assigned in accordance with the standards established by the SeqCode initiative, which is a genomic nomenclature system designed to accommodate uncultured prokaryotes. The genus name *Magnetominusculus* was proposed to reflect the small genome size and magnetotactic nature of the type strain, while the species name *dajiuhuensis* refers to its origin from the Dajiuhu Peatland. The full designation *Magnetominusculus dajiuhuensis* DJH-1^{Ts} was given to the type genome and registered under the SeqCode registry

at seqco.de/r:5k0ci1ce. This registry ensures that the name is publicly available, citable, and traceable in genomic and taxonomic databases.

REFERENCES

Alneberg, J. et al. Binning metagenomic contigs by coverage and composition. Nat. Methods 11, 1144–1146 (2014).

Altschul, S. F. et al. Gapped BLAST and PSI-BLAST: a new generation of protein database search programs. Nucleic Acids Res. 25, 3389–3402 (1997).

Aramaki, T. et al. KofamKOALA: KEGG ortholog assignment based on profile HMM and adaptive score threshold. Bioinformatics 36, 2251–2252 (2020).

Bowers, R. M. et al. Minimum information about a metagenome-assembled genome (MIMAG) of bacteria and archaea. Nat. Biotechnol. 35, 725–731 (2017).

Chaumeil, P. A., Mussig, A. J., Hugenholtz, P. & Parks, D. H. GTDB-Tk: a toolkit to classify genomes with the Genome Taxonomy Database. Bioinformatics 36, 1925–1927 (2020).

Chklovski, A. et al. CheckM2: A rapid, scalable and accurate tool for assessing microbial genome quality using machine learning. Nat. Methods 20, 1203–1212 (2023).

Eren, A. M. et al. Community-led, integrated, reproducible multi-omics with anvi'o. Nat. Microbiol. 6, 3–6 (2021).

Gilchrist, C. L. M. & Chooi, Y. H. clinker & clustermap.js: automatic generation of gene cluster comparison figures. Bioinformatics 37, 2473–2475 (2021).

Gurevich, A., Saveliev, V., Vyahhi, N. & Tesler, G. QUAST: Quality assessment tool for genome assemblies. Bioinformatics 29, 1072–1075 (2013).

Ji, R. et al. Linking morphology, genome, and metabolic activity of uncultured magnetotactic Nitrospirota at the single-cell level. Microbiome 12, 158 (2024).

Ji, R., Zhang, W., Pan, Y. & Lin, W. MagCluster: A tool for identification, annotation, and visualisation of magnetosome gene clusters. Microbiol. Resour. Announc. 11, e01031-21 (2022).

Kang, D. D. et al. MetaBAT 2: An adaptive binning algorithm for robust and efficient genome reconstruction from metagenome assemblies. PeerJ 7, e7359 (2019).

Lefèvre, C. T. & Wu, L. F. Evolution of the bacterial organelle responsible for magnetotaxis. Trends Microbiol. 21, 534–543 (2013).

Letunic, I. & Bork, P. Interactive Tree of Life (iTOL) v6: Recent updates and new developments. Nucleic Acids Res. 52, W78–W82 (2024).

McGinnis, S. & Madden, T. L. BLAST: At the core of a powerful and diverse set of sequence analysis tools. Nucleic Acids Res. 32, W20–W25 (2004).

Nguyen, L. T., Schmidt, H. A., von Haeseler, A. & Minh, B. Q. IQ-TREE: A fast and effective stochastic algorithm for estimating maximum-likelihood phylogenies. Mol. Biol. Evol. 32, 268–274 (2015).

Olm, M. R., Brown, C. T., Brooks, B. & Banfield, J. F. dRep: A tool for fast and accurate genomic comparisons that enables improved genome recovery from metagenomes through de-replication. ISME J. 11, 2864–2868 (2017).

Parks, D. H. et al. CheckM: Assessing the quality of microbial genomes recovered from isolates, single cells, and metagenomes. Genome Res. 25, 1043–1055 (2015).

Price, M. N., Dehal, P. S. & Arkin, A. P. FastTree 2 – approximately maximum-likelihood trees for large alignments. PLoS One 5, e9490 (2010).

Seemann, T. Prokka: Rapid prokaryotic genome annotation. Bioinformatics 30, 2068–2069 (2014).

Trifinopoulos, J., Nguyen, L. T., von Haeseler, A. & Minh, B. Q. W-IQ-TREE: A fast online phylogenetic tool for maximum likelihood analysis. Nucleic Acids Res. 44, W232–W235 (2016).

Wu, Y. W., Simmons, B. A. & Singer, S. W. MaxBin 2.0: An automated binning algorithm to recover genomes from multiple metagenomic datasets. Bioinformatics 32, 605–607 (2016).

Zhang, W. et al. Identification and genomic characterisation of two previously unknown magnetotactic Nitrospirae. Front. Microbiol. 12, 690052 (2021).

Chapter 4: Genomic and metabolic characterisation of a novel species *Magnetominusculus dajiuhuensis* DJH-1^{Ts} sp. nov. from an acidic peatland

SUMMARY OF CHAPTER

Introduction to *Nitrospirota* MTB

The *Nitrospirota* phylum (formerly *Nitrospirae*) encompasses diverse bacterial lineages involved in key geochemical processes, particularly sulphur and nitrogen cycling. Among them, *Nitrospirota*-affiliated MTB remain underrepresented and largely uncultured. These bacteria are known for forming magnetosome chains containing large numbers of intracellular magnetite crystals and for possessing genes indicative of sulphate reduction and autotrophic carbon fixation (Jogler et al., 2010; Lin et al., 2014b). Notable strains such as *Candidatus Magnetobacterium bavaricum* and *Candidatus Magnetobacterium casensis* can produce hundreds of magnetosomes per cell and accumulate intracellular elemental sulphur, suggesting their significant involvement in environmental redox dynamics (Spring et al., 1993; Lin et al., 2014b). Despite their ecological relevance, these MTB have not yet been brought into pure culture, and much of their genomic architecture, population diversity, and magnetosome formation mechanisms remain unresolved.

Role in Biogeochemical Cycling

Nitrospirota MTB are integral to the cycling of key elements, particularly nitrogen and sulphur, in anaerobic and microaerophilic environments. These bacteria contribute to nitrogen cycling primarily through processes such as denitrification and nitrogen fixation. In denitrification, *Nitrospirota* MTB convert nitrate (NO_3^-) into nitrogen gas (N_2), effectively removing bioavailable nitrogen from ecosystems and preventing its overaccumulation, which could otherwise lead to

eutrophication and associated environmental problems (Lin et al., 2020). Additionally, some *Nitrospirota* MTB have the capability to fix atmospheric nitrogen, converting it into ammonia (NH_3), which is then accessible to other organisms within the ecosystem (Zhang et al., 2021). In sulphur cycling, *Nitrospirota* MTB are involved in the reduction of sulphate (SO_4^{2-}) to sulphide (S^{2-}), a process critical in many anaerobic environments. The ability of these bacteria to reduce sulphur compounds is not only vital for their own metabolism but also influences the sulphur balance in the broader ecosystem, contributing to the formation of mineral deposits and affecting the availability of sulphur for other microbial processes (Jørgensen et al., 2019; Zhao et al., 2023). The ecological roles of *Nitrospirota* MTB are of particular interest because of their ability to inhabit a wide spectrum of extreme environments, including acidic peatlands, hydrothermal vents, and saline basins (Goswami et al., 2022; Lefèvre et al., 2010; Lin et al., 2018; Liu et al., 2020). These organisms often display highly versatile metabolic profiles, such as the capacity for nitrogen fixation, sulphate reduction, and CO_2 fixation via the Wood–Ljungdahl pathway, enabling survival in nutrient-limited and redox-dynamic niches (Qian et al., 2019; Uzun et al., 2020; Zhao et al., 2023). Notably, members of this group have been observed to biomineralise significantly more magnetosomes than other MTB taxa, with individual cells producing 10 to 100 times more crystals (Jogler et al., 2010). Furthermore, their intracellular iron content can be several hundred times higher than that of non-magnetotactic counterparts, underscoring their potential role as iron sinks in natural systems (Zhao et al., 2023).

Novel *Nitrospirota* MTB Strain: *Magnetominusculus dajiuhuensis* DJH-1^{Ts}

The key finding from this chapter encompasses a novel MTB species, *Magnetominusculus dajiuhuensis* DJH-1^{Ts}, within the *Nitrospirota* phylum, isolated from the acidic Dajiuhu Peatland in central China. This strain is notable for its genomic and metabolic characteristics,

which include the presence of a nearly complete MGC and the ability to participate in both nitrogen and sulphur cycling, adding to the lineage-specific characteristics of *Nitrospirota* MTB (Lin et al., 2020b; Goswami et al., 2022). *Magnetominusculus dajiuhuensis* DJH-1^{Ts} is adapted to the acidic conditions of the Dajiuhu Peatland, where it potentially contributes to sulphur reduction and denitrification, as suggested by its genomic content. This bacterial genome indicates that it utilises the Wood-Ljungdahl pathway for carbon fixation, a metabolic route common among acetogenic bacteria in anaerobic environments.

Implications for Environmental and Climate Studies

The discovery and characterisation of *Magnetominusculus dajiuhuensis* DJH-1^{Ts} underscore the importance of *Nitrospirota* MTB in understanding and managing biogeochemical cycles in peatland ecosystems. The ability of these bacteria to participate in nitrogen and sulphur cycling highlights their potential role in biogeochemical cycling in redox-stressed acidic peatlands, which represent isolated, terrestrial microoxic/anoxic environments with high organic contents and extreme pH. Moreover, the study of *Nitrospirota* MTB provides valuable insights into the evolutionary processes that have enabled these bacteria to thrive in extreme environments. By understanding the genomic adaptations that allow *Nitrospirota* MTB to participate in complex biogeochemical cycles, researchers can better predict how these processes might change in response to environmental shifts, such as those driven by climate change.

The following chapter appears as published in: Goswami, P., Ji, R., Shen, J., Roberts, A. P., & Lin, W. (2025). Genomic and metabolic characterisation of a novel species *Magnetominusculus dajiuhuensis* DJH-1Ts sp. nov. from an acidic peatland. *Systematic and Applied Microbiology*, 48, 126605; https://doi.org/10.1016/j.syapm.2025.126605

Genomic and metabolic characterisation of a novel species *Magnetominusculus dajiuhuensis* DJH-1^{Ts} sp. nov. from an acidic peatland

Pranami Goswami[1,2,3,4#], Runjia Ji[1,2,3#], Jianxun Shen[1,2], Andrew P. Roberts[4*] and Wei Lin[1,2,3*]

[1]Key Laboratory of Earth and Planetary Physics, Institute of Geology and Geophysics, Chinese Academy of Sciences, Beijing 100029, China.

[2]France-China Joint Laboratory for Evolution and Development of Magnetotactic Multicellular Organisms, Chinese Academy of Sciences, Beijing 100029, China.

[3]College of Earth and Planetary Sciences, University of Chinese Academy of Sciences, Beijing 100049, China.

[4]Research School of Earth Sciences, Australian National University, ACT, Canberra 2601, Australia.

[#]These authors contributed equally to this work

[*]Corresponding authors: weilin@mail.iggcas.ac.cn (Wei Lin), andrew.roberts@anu.edu.au (Andrew P. Roberts)

ABSTRACT

Magnetotactic bacteria (MTB) are recognised widely for their ability to synthesise intracellular magnetite (Fe_3O_4) and/or greigite (Fe_3S_4) nanocrystals and align with Earth's magnetic field. They are crucial for understanding prokaryotic organelle biogenesis. MTB members of the *Nitrospirota* phylum (previously known as the *Nitrospirae* phylum) are of interest due to their important ecological roles in the biogeochemical

cycling of iron and sulphur. Here, we introduce *Magnetominusculus dajiuhuensis* DJH-1^{Ts}, a newly discovered *Nitrospirota* MTB species that thrives in the acidic Dajiuhu Peatland of central China. By combining electron microscopy, 16S rRNA gene-based analysis and genome-resolved metagenomics, we elucidate its distinctive morphology, genomic features, and metabolic functions. The metagenome-assembled genome, assigned to the genus *Magnetominusculus*, family *Magnetobacteriaceae*, order *Thermodesulfovibrionales*, class *Thermodesulfovibrionia* according to the GTDB taxonomy, reveals an obligate anaerobe that lives in central China's largest wetland. We propose the formal name *Magnetominusculus dajiuhuensis* DJH-1^{Ts} sp. nov. following the SeqCode system. Genomic and metabolic characterisation of this novel species suggests its potential role in nitrogen, sulphur, and carbon metabolism in aquatic biogeochemistry, particularly in peatlands. The genome of this novel strain indicates that it harnesses the Wood-Ljungdahl pathway for carbon fixation and acetate metabolism in anaerobic conditions, while its potential role in nitrogen cycling is characterised by denitrification and nitrogen fixation. It also participates in reduction of sulphate to sulphide, indicating a role in sulphur cycling in its ecological niche. Taken together, the discovery and characterisation of *Magnetominusculus dajiuhuensis* DJH-1^{Ts} provide new insights into MTB diversity and ecological functions, particularly in peatland biogeochemistry.

Keywords: magnetotactic bacteria; *Nitrospirota*; magnetosome; acidic peatland; metagenomics; metabolic function

INTRODUCTION

MTB are a group of microorganisms that synthesise intracellular magnetite (Fe_3O_4) and/or greigite (Fe_3S_4) nanocrystals, which enable them to align with magnetic fields (Bazylinski and Frankel, 2004; Uebe and Schüler, 2016). MTB can produce membrane-bounded organelles (i.e., magnetosomes) and, thus, serve as excellent models for investigating

organelle biogenesis in prokaryotes (Grant et al., 2018). MTB genomes contain sequence segments of MGCs, which are responsible for magnetosome biosynthesis and arrangement, comprising a series of *mam*, *mms*, *mad* and *man* genes (Lin et al., 2017; Müller et al., 2020). MTB typically inhabit natural aquatic oxic-anoxic transition zones and commute primarily based on magnetic orientation and oxygen contents to navigate and find optimal microhabitats for nutrient foraging and growth (Goswami et al., 2022; Li et al., 2020; Spring and Bazylinski, 2006). Despite their widespread distribution, the ecological roles of many MTB remain underexplored (Shen et al., 2023a).

Some *Nitrospirota* members with magnetotactic behaviours are suggested to have an expanded role in iron, sulphur, and nitrogen cycling, especially in low-oxygen conditions (Jogler et al., 2010; Lin et al., 2014; Spring et al., 1993; Zhang et al., 2021; Zhao et al., 2023). The magnetotactic *Nitrospirota* identified to date belong to the class *Thermodesulfovibrionia*. Their dual role in sulphur and iron cycling, combined with their resilience in extreme environments, underscores their ecological significance and the need for further research into their diverse functions across the nitrogen, iron and sulphur cycles.

Nitrospirota MTB have high diversity and adaptability and are found in various settings including peatlands and hot springs (Goswami et al., 2022; Lefèvre et al., 2010; Lin et al., 2020b, 2018; Liu et al., 2020; Nash, 2008; Qian et al., 2019; Uzun et al., 2020; Zhao et al., 2023). From the Dajiuhu Peatland, the largest and highest wetland in central China, *Nitrospirota* MTB were previously found to be predominant in waterlogged soils with a pH range of 4.3-5.7 (Lin et al., 2020b). To make use of spatial oxygen/light/nutrient content gradients for biological denitrification, sulphur oxidation and sulphate reduction, *Nitrospirota* MTB ingest reduced/oxidised forms of elemental nitrogen and sulphur and shuttle to appropriate locations for completion of corresponding biochemical reactions (Li et al., 2020; Lin et al., 2014; Spring and

Bazylinski, 2006). Notably, *Nitrospirota* MTB generally produce ~10- to 100-fold more abundant magnetosomes than other MTB taxa (Jogler et al., 2010) and likely take up hundreds of times more iron than non-MTB (Zhao et al., 2023). These abilities make it valuable to understand the ecological roles of *Nitrospirota* MTB species.

Despite growing categorisation of MTB-containing phyla, the connection between morphotype and genomic data for *Nitrospirota* MTB is not well established, highlighting a gap in understanding of their ecological roles and environmental interactions (Goswami et al., 2022; Shen et al., 2023b). Here, we combine magnetic enrichment techniques with electron microscopy and metagenomic analyses to identify and characterise a new MTB *Nitrospirota* population from the acidic Dajiuhu Peatland. We aim to elucidate their genome and metabolic functions in the context of their living environments, thereby advancing our understanding of these microbes.

MATERIALS AND METHODS

Sample Collection and Magnetotactic Bacteria Enrichment

The Dajiuhu Peatland, which is located in the Dajiuhu National Wetland Park within the southeast Shennongjia Natural Conservation Region, Hubei Province, harbours diverse microbial communities that play a role in biogeochemical cycling (Xiang et al., 2014). Various MTB groups have been detected in the acidic, waterlogged soils of this peatland (Lin et al., 2020b). Duplicate sediment samples were collected from the same location and were transferred to 600-mL plastic flasks, with approximately 100 mL of water from the same location added to each flask. The samples were stored in the laboratory under dark conditions at room temperature (~25°C) for nearly five years. MTB are known to remain viable over extended periods in microaerobic, dark conditions, as reported in previous studies (Zhao et al., 2023). In some cases, prolonged storage may also

facilitate proliferation of minority MTB populations within the micro-environment (Lefèvre et al., 2013, 2011).

MTB were examined using the hanging-drop method (Greenberg et al., 2005) and observed under an Olympus BX53 microscope (Olympus, Tokyo, Japan). For MTB isolation within the sediment, the 'capillary racetrack' method was employed (Wolfe et al., 1987). After a three-hour collection, enriched cells were washed twice with double-distilled water and then used for further analysis.

Morphological Characterisation, Phylogenetic Analysis and Fluorescence in situ Hybridisation

To investigate the morphology and magnetosome structure of the novel MTB species, *Magnetominusculus dajiuhuensis* DJH-1^{Ts}, we employed transmission electron microscope (TEM) (JEM-2100 HR TEM, JEOL, Tokyo, Japan) and scanning electron microscope (SEM) (Zeiss Auriga Compact FIB-SEM, Germany) observations. Whole-genome amplification (WGA) was carried out on magnetically enriched cells using the GenomiPhi Single Cell DNA Amplification Kit (Cytiva, United States). WGA products were diluted (~1:50 ratio) and subsequently employed as a template for amplification of the 16S rRNA gene using the universal bacterial primers 27F (5′-AGA GTT TGA TCC TGG CTC AG-3′) and 1492R (5′-GGT TAC CTT GTT ACG ACT T-3′) as described by Zhang et al. (2021). The PCR product was cloned into pMD19-T vector (TaKara Bio, Japan) and 100 colonies were selected at random and subsequently sequenced using Sanger sequencing (Sanger et al., 1977). The consensus 16S rRNA gene sequence was compared using NCBI BLASTn (McGinnis and Madden, 2004). The top thirty-eight BLASTn hits were selected, and the sequences were imported into MEGA v11.0.13 (Tamura et al., 2021). The sequences were aligned using the built-in **ClustalW** algorithm (Thompson et al., 1994) and trimmed to remove the poorly aligned regions. A phylogenetic tree was constructed using the maximum likelihood model **in** W-IQ-TREE**,** with bootstrap values set to

1000 (Trifinopoulos et al., 2016). For visualisation and manual annotation adjustments, the tree was processed using the Interactive Tree Of Life (iTOL v6) (Letunic and Bork, 2024).

To identify the newly discovered MTB cells, an oligonucleotide probe (Mdaj probe, 5'-TTC GGA TCG CTA CCA TCT GC-3') specific for the 16S rRNA gene sequence of *M. dajiuhuensis* DJH-1^{Ts} was designed. Probe specificity and quality were assessed using SILVA (Quast et al., 2012). The Cy3-labeled probe was then used in the *in situ* hybridisation of enriched MTB cells. The universal bacterial probe EUB338 (5′-GCT GCC TCC CGT AGG AGT-3′) (Amann et al., 1990), labelled fluorescently with fluorescein phosphoramidite FAM at the 5′ end, was used to target *Magnetospirillum gryphiswaldense* strain MSR-1 cells (MSR-1 hereafter), which served as a negative control. The fluorescence *in situ* hybridisation (FISH) procedure was carried out following the protocol described previously (Pernthaler et al., 2001; Spring et al., 1993). In brief, cell mixtures of both *M. dajiuhuensis* DJH-1^{Ts} and MSR-1 were deposited onto silicon wafers, fixed with 4% paraformaldehyde solution for 1 hour at room temperature, washed three times with 1x phosphate buffered saline, followed by dehydration with 50%, 80% and 96% ethanol, and then hybridised at 46°C for 3 hours. Optical sections were recorded with an Olympus BX53 fluorescence microscope (Olympus, Tokyo, Japan) and SEM.

Metagenomic Sequencing, Assembly and Genome Binning

Metagenomic sequencing was performed using the NovaSeq 6000 platform (Novogene, Beijing, China) with a 150 × 150 paired-end library strategy. Metagenomic raw reads were processed and binned using metaWRAP v1.1.5 (Uritskiy et al., 2018). The read_qc module was used to trim and screen metagenomic raw reads. Clean reads were then assembled for each metagenome using metaSPAdes v3.13.0 (Nurk et al., 2017), with a minimum contig length set to 2000 (-l 2000). Subsequently, binning was performed on each metagenome assembly using MetaBAT2

(Kang et al., 2019), MaxBin2 (Wu et al., 2016) and CONCOCT (Alneberg et al., 2014). Resulting bins for each metagenome were compared, and a refined bin set comprising 42 metagenome-assembled genomes (MAGs) was obtained using the bin_refinement module, with 70% (-c 70) minimum bin completion and 10% (-x 10) maximum bin contamination.

Identification and annotation of MTB genomes were conducted using MagCluster v0.2.11 (Ji et al., 2022), following a process outlined in https://github.com/RunJiaJi/magcluster. Initially, genome bins were annotated with Prokka v1.13.4 (Seemann, 2014), employing an e-value threshold of 1e-05. Subsequently, the mgc_screen module of MagCluster was applied with default parameters to screen for potential MGCs. Putative magnetosome gene sequences were screened manually and cross-checked to verify the presence of MGCs. MGCs were visualised using clinker v0.0.21 (Gilchrist and Chooi, 2021).

MTB genome quality was assessed using CheckM v1.0.12 (Parks et al., 2015) and CheckM2 (Chklovski et al., 2023) to estimate completeness and contamination levels. Genomic statistics, including size, GC content, contig N50/L50 and maximum contig length, were determined using QUAST v5.0.2 (Quast et al., 2012). A non-redundant MTB genome dataset was created using dRep v3.4.0 (Olm et al., 2017) from the 42 MAGs obtained after bin refinement. After dereplication at 95% ANI, six species-level genomes were obtained. ANI analysis was conducted using fastANI (Jain et al., 2018) with default parameters; results are visualised in conjunction with GTDB-Tk v2.1.0 (Chaumeil et al., 2020) classification outcomes using pairwiseANIviz (Ji et al., 2024) (https://github.com/RunJiaJi/pairwiseANIviz). The *M. dajiuhuensis* DJH-1^{Ts} genome was compared to 41 published *Nitrospirota* MTB genomes. Genomes with no significant similarity are denoted in grey, enhancing the clarity of distinct taxonomic affiliations. The final figure was generated using Inkscape (https://inkscape.org/). The relative abundance of *M.*

dajiuhuensis DJH-1^{Ts} was calculated using Bowtie2 v2.3.4.3 (Langmead and Salzberg, 2012) and SAMtools (Li et al., 2009).

Phylogenomic Analyses, Pangenome Analysis and Metabolic Predictions

A maximum-likelihood phylogenomic tree was constructed for the *M. dajiuhuensis* DJH-1Ts genome, alongside 41 MTB Nitrospirota genomes and 101 non-MTB Nitrospirota genomes, using IQ-TREE v2.0.3 (Nguyen et al., 2015). The analysis was based on a concatenated alignment of 120 single-copy marker proteins generated using GTDB-Tk v2.1.0 (Chaumeil et al., 2020). The best-fit substitution model was determined using the "TEST" option in IQ-TREE. Ultrafast bootstrap analysis with 1000 replicates was performed to assess branch support. The resulting tree was visualised with iTOL v6 (Letunic and Bork, 2024), with final edits made using Inkscape (https://inkscape.org/).

For pangenome analysis, Anvi'o v7.1 was used (Eren et al., 2021) to explore the genomic diversity of *M. dajiuhuensis* DJH-1^{Ts} compared to ten *Nitrospirota* MTB genomes (*Ca.* M. xianensis strain HCH-1, Nitrospirae bacterium nDJH13bin15, Nitrospirae bacterium MYbin3, Nitrospirae bacterium nDJH14bin9, *Ca.* Magnetoovum chiemensis strain CS-04, *Ca*. Magnetomicrobium cryptolimnococcus strain XYC, *Ca.* Magnetocorallium paracelense strain XS-1, *Ca.* Magnetobacterium bavaricum, *Ca.* Magnetobacterium casensis, and *Ca.* Magnetobacterium cryptolimnobacter strain XYR). Briefly, genomic data were organised into a unified storage database (GENOMES.db) and a pangenome database (Pangenome-PAN.db) was created to cluster genes into homologous groups and calculate key metrics such as core and accessory gene content and redundancy. Hidden Markov Models (HMMs) were incorporated into contigs databases to identify single-copy core genes. The resulting pangenome structure was visualised in Anvi'o's interactive display, which

highlights gene presence-absence patterns and associated genomic statistics through a circular, colour-coded representation.

The same ten genomes were selected for metabolic predictions and were annotated against the KEGG database using the KofamKOALA server (Aramaki et al., 2020). Metabolic pathway completeness was estimated and visualised with KEGG-Decoder (Graham et al., 2018). A schematic cell diagram illustrating the potential metabolic network of M. dajiuhuensis DJH-1Ts was created using Inkscape (https://inkscape.org/).

SeqCode Nomenclature

The SeqCode nomenclature was applied to assign a unique and precise identifier to the novel MTB species. This nomenclature system adheres to standardised guidelines outlined in the SeqCode documentation (Hedlund et al., 2022; Whitman et al., 2022, 2024), ensuring consistency and compatibility in species/strain identification practices. The genus, *Magnetominusculus*, and the novel species, *Magnetominusculus dajiuhuensis* DJH-1^{Ts}, have been submitted to the SeqCode registry with accession number seqco.de/r:5k0ci1ce.

RESULTS AND DISCUSSION

Morphological Diversity of MTB Community in the Dajiuhu Peatland

Initial microscopic screening of surface sediments from the Dajiuhu Peatland revealed several MTB morphotypes (Figure 1a). Magnetic enrichment allowed detailed morphological examination with TEM and SEM (Figure 1b-e), which revealed that the predominant cell type is coccobacilli-shaped, with either single or dual bullet-shaped magnetosome chains (Figure 1b, d). These cells are approximately 0.5 μm in width and 1 μm in length. Each magnetosome chain or cluster within a cell consistently contains 10-14 magnetosomes, with some cells having one intact chain alongside a clustered magnetosome group (Figure 1b, d).

Fluorescence *in situ* Hybridisation (FISH) and Phylogenetic Analysis

Nearly complete 16S rRNA gene sequences of magnetically enriched MTB were amplified, cloned and sequenced. A cross-check of 16S rRNA gene sequences with reconstructed genome bins (see below) revealed one 16S rRNA sequence (1435 bp) with a 99% similarity to the

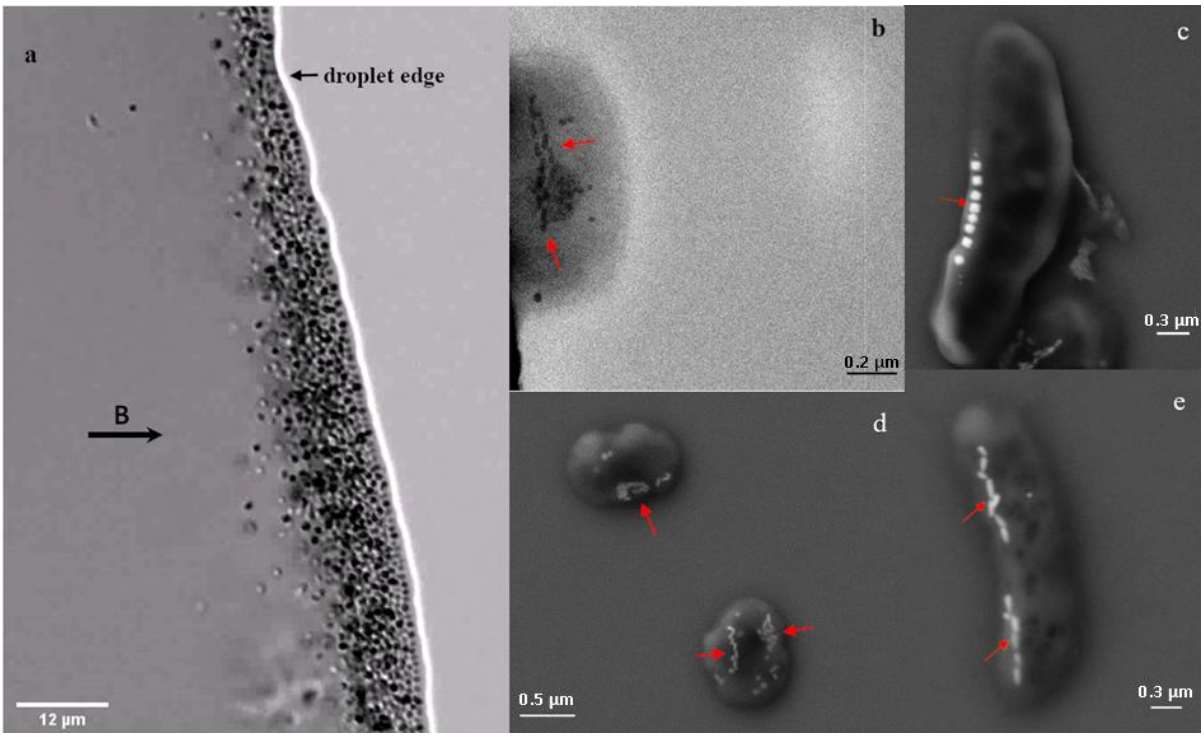

Figure 1: Microscopic characterisation of MTB cells from the Dajiuhu Peatland. (a) Image at 100x magnification with MTB cells congregating at the water droplet edge. The applied field (B) direction is from left to right. (b) TEM image of coccobacilli-shaped cells with bullet-shaped magnetosomes and (c, d, e) SEM images of three distinct morphotypes, including (c) spirillum cells with octahedral magnetosomes, (d) coccobacilli-shaped cells with bullet-shaped magnetosomes and (e) spirillum cells with bullet-shaped magnetosomes. Red arrows indicate magnetosome chains.

16S rRNA region in the *Nitrospirota* genome. BLASTn analysis of this 16S rRNA sequence against the NCBI database identified the closest match as an uncultured *Nitrospirae* bacterium MY3-11A genomic sequence (GenBank accession HM454282.1) with 97.98% identity and 99% query coverage. A specific probe, Mdaj (5'-TTC GGA TCG CTA CCA TCT GC-3'), was designed, targeting the 16S rRNA gene of *M. dajiuhuensis* DJH-1^{Ts}, the dominant population in Dajiuhu sediment. FISH analysis confirmed the specific binding of both the universal bacterial probe EUB338 and Mdaj to *M. dajiuhuensis* DJH-1^{Ts} cells, whereas control cells (MSR-1) bound only to EUB338. These results validated the coccobacilli morphology of *M. dajiuhuensis* DJH-1^{Ts} (Figure 2).

Thirty-eight 16S rRNA gene sequences with over 98% query coverage and higher than 87% identity were selected for phylogenetic analysis. Also, both Nitrospirota bacterium HSMV-1 (Lefèvre et al., 2010) and *M. dajiuhuensis* DJH-1^{Ts} are classified within the same order, *Thermodesulfovibrionales*, so the sequence of HSMV-1 is also included in this analysis. The phylogenetic tree reveals a close association of *M. dajiuhuensis* DJH-1^{Ts} to Uncultured Nitrospirae bacterium clone LBB_02 16S ribosomal RNA gene (GenBank accession number MK632186), Uncultured magnetotactic coccus partial 16S rRNA gene clone CF3 (AJ863136) and Uncultured Nitrospirae bacterium clone OTU1 16S ribosomal RNA gene (GQ468508) (Figure 2f). The phylogenetic tree also highlights habitat differentiation and morphological variation among the *Nitrospirota* MTB by comparison, with most sequences associated with freshwater environments and coccoid-to-ovoid morphology. Although both HSMV-1 and *M. dajiuhuensis* DJH-1^{Ts} are classified within the same order, *Thermodesulfovibrionales*, their phylogenetic placement in the tree suggests a more distant evolutionary relationship compared to other closely clustered magnetotactic Nitrospirota.

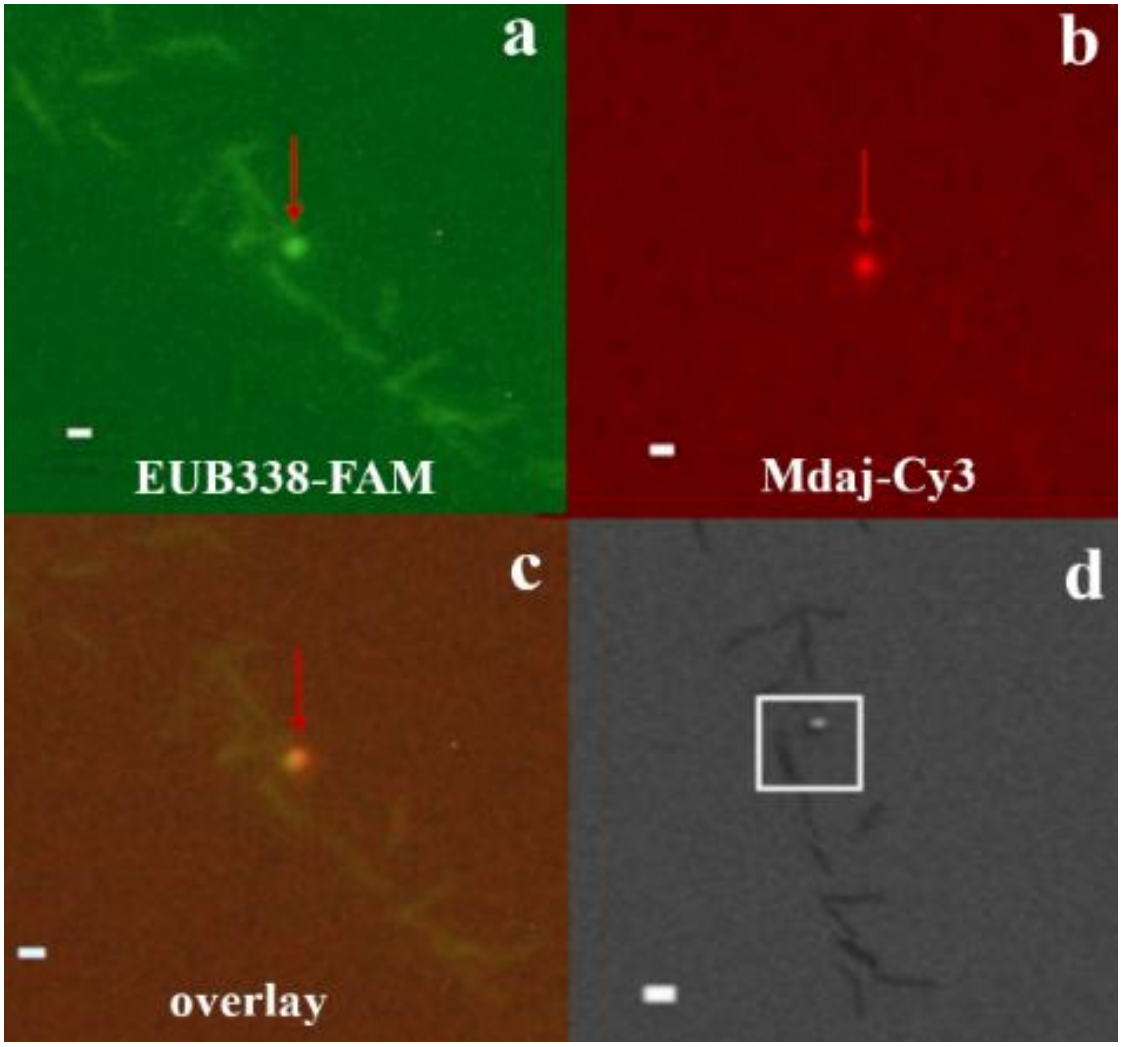

Figure 2: Fluorescence *in situ* hybridisation (FISH) coupled with scanning electron microscope (SEM) and phylogenetic analysis of *M. dajiuhuensis* DJH-1^{Ts}. (a) Fluorescence image with EUB338-FAM probe and universal bacterial staining. (b) Fluorescence image with Mdaj-Cy3 probe specific for *M. dajiuhuensis* DJH-1^{Ts}. (c) Overlay of (a) and (b) with co-localisation of universal bacterial and species-specific signals. (d) Corresponding SEM image of the same field of view, detailing cellular morphology. Scale bars in (a), (b), (c) and (d) are 2 µm each.

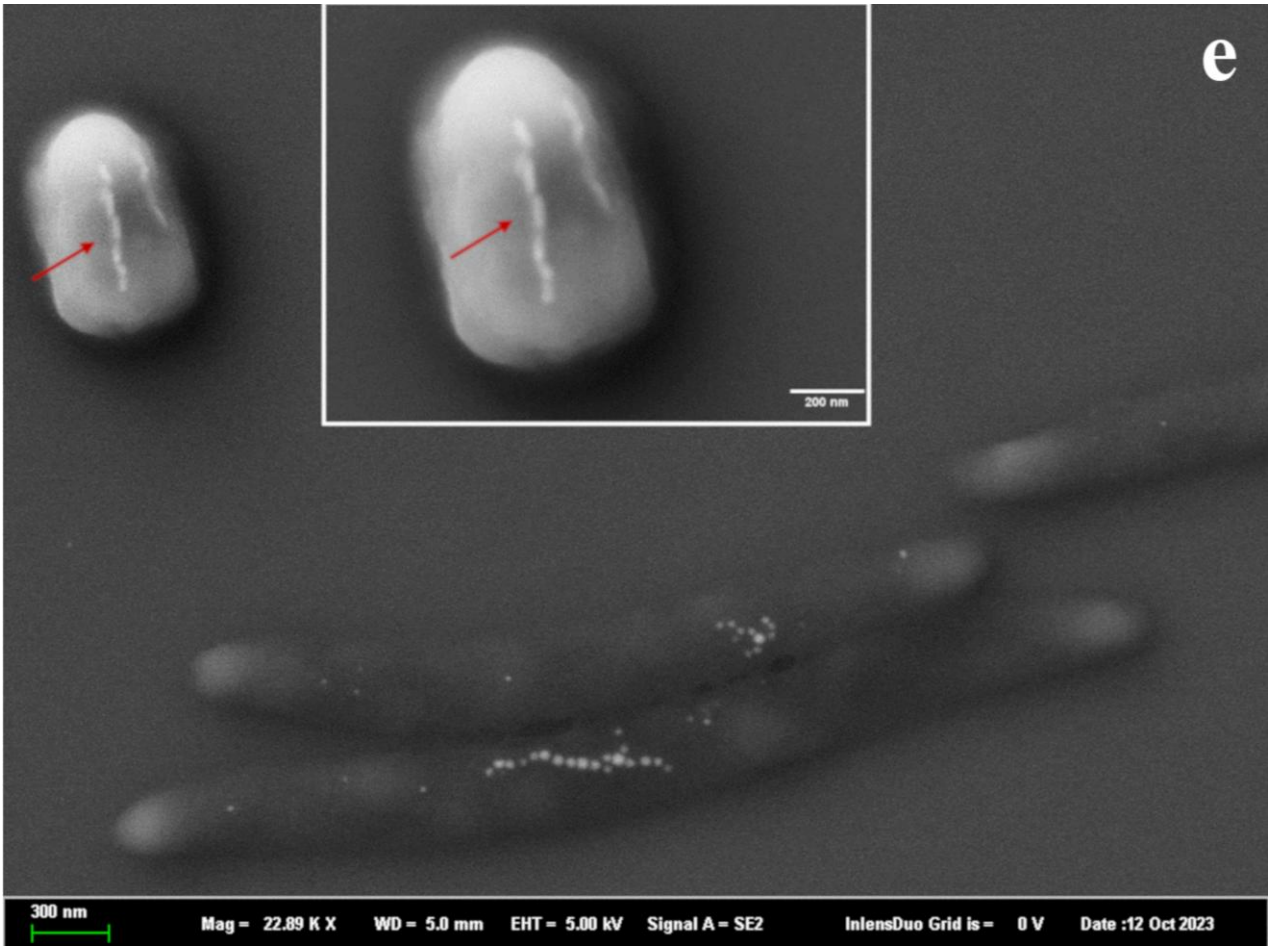

Figure 2: Fluorescence *in situ* hybridisation (FISH) coupled with scanning electron microscope (SEM) and phylogenetic analysis of *M. dajiuhuensis* DJH-1^{Ts} (continued). (e) Magnified SEM inset from (d), 300 nm, with detailed structural features of a single bacterium with magnetosome chains (red arrows). The inset in (e), 200 nm, is of a magnified *M. dajiuhuensis* DJH-1^{Ts} cell**.**

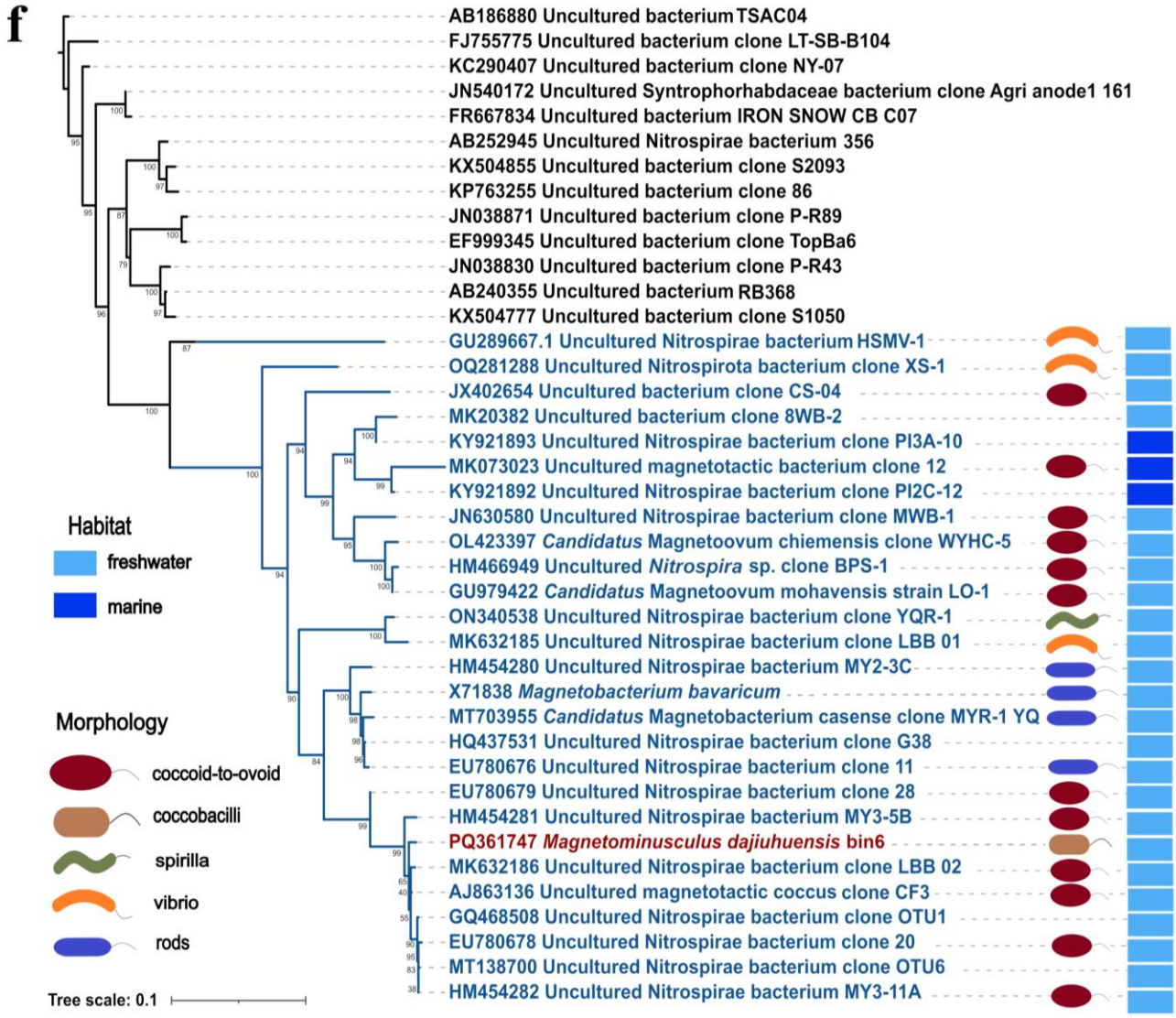

Figure 2: Fluorescence *in situ* hybridisation (FISH) coupled with scanning electron microscope (SEM) and phylogenetic analysis of *M. dajiuhuensis* DJH-1^{Ts} (continued). (f) A maximum likelihood phylogenetic tree rooted to AB186880 (uncultured bacterium gene for 16S rRNA clone TSAC04) with *M. dajiuhuensis* DJH-1^{Ts} indicated in bold red, illustrating its phylogenetic proximity to other *Nitrospirota* MTB in blue and non-MTB populations in black, with bootstrap values shown at each node. Habitat types (freshwater or marine) and morphologies (coccoid-to-ovoid, cocci, spirilla, vibrio and rods) are depicted alongside the tree, highlighting the ecological and phenotypic diversity of related *Nitrospirota* MTB species.

Genome Quality Assessment and Phylogenomic Characterisation of *M. dajiuhuensis* DJH-1Ts

Out of the 42 MAGs obtained after bin refinement, *M. dajiuhuensis* DJH-1^{Ts} was identified as a high-quality genome with 3.64 Mbp size (Table 1). This genome has 99.61% completeness and 1.94% contamination, as determined from CheckM2 (Chklovski et al., 2023) analysis. Moreover, the average relative abundance of *M. dajiuhuensis* DJH-1^{Ts} across all sequenced metagenomic raw reads is ~52.36%. The genome consists of 218 contigs with a 47.53% average GC content (Table 1), includes a full complement of 23S, 16S and 5S rRNA genes, along with 19 tRNAs and meets the high-quality standards of the MIMAG (Bowers et al., 2017). Phylogenomic analysis places *M. dajiuhuensis* DJH-1^{Ts} within the class *Thermodesulfovibrionia*, clustering with other *Nitrospirota* MTB (Figure 3a).

ANI analysis reveals that *M. dajiuhuensis* DJH-1^{Ts} shares 95.8% similarity with its closest related genome, Nitrospirota bacterium nDJH13bin15 (GenBank assembly GCA_015233685.1), a metagenomic bin previously assembled from Dajiuhu Peatland (Lin et al., 2020b) (Figure 3b). While this ANI value exceeds the 95% threshold commonly used to delineate species boundaries, the genome completeness and quality indicate a clear distinction (Table 1). The *M. dajiuhuensis* DJH-1^{Ts} genome is nearly complete. In contrast, the nDJH13bin15 genome is only 66.54% complete, despite having no detectable contamination. The disparity in total length, number of genes, and completeness suggests that the nDJH13bin15 genome is incomplete and may lack essential functional elements. According to the MIMAG standards, the nDJH13bin15 genome is medium-quality with no 16S or 23S rRNA genes, which raises concerns about its reliability as a representative genome (Bowers et al., 2017).

Magnetosome Genes of *M. dajiuhuensis* DJH-1Ts

The draft genome of *M. dajiuhuensis* DJH-1^{Ts} contains a nearly complete MGC (Figure 4), including homologous magnetosome genes such as *man1*, *mamK*, *man2*, *mad10*, *man3*, *mamP*, *mamM*, *mad31*, *mamQ-II*, *mamB*, *mad2*, *mamA*, *mamI*, *mamE*, *mamQ-I*, *man4, man5, man6, mamO-Cter, mad23, mad24, mad25,* and *mad26.* Use of the --clinker module of MagCluster (Ji et al., 2022) facilitated comparative analysis of MGC arrangements between *M. dajiuhuensis* DJH-1^{Ts} and ten closely related *Nitrospirota* MTB. Notably, the gene content and MGC organisation of *M. dajiuhuensis* DJH-1^{Ts} have significant similarity to nDJH13bin15 (Figure 4).

Pangenome Analysis, Metabolic Potential and Environmental Implications of M. dajiuhuensis DJH-1Ts

The pangenome structure of *M. dajiuhuensis* DJH-1^{Ts} (Figure 5a) was analysed alongside ten closely related genomes to identify gene conservation and variability patterns. *M. dajiuhuensis* DJH-1^{Ts} serves as the reference genome (forced synteny), and is represented as a continuous red ring, which provides a baseline for comparing gene presence and absence. *Ca.* Magnetominusculus xianensis strain HCH-1 and *Ca.* Magnetomicrobium cryptolimnococcus strain XYC genomes are closest in composition to *M. dajiuhuensis* DJH-1^{Ts} in terms of gene cluster conservation, GC content and functional homogeneity, which underscores their evolutionary proximity. In contrast, the *Ca.* Magnetobacterium bavaricum genome is the most distantly related.

The *M. dajiuhuensis* DJH-1^{Ts} genome includes genes for essential metabolic pathways such as carbon, nitrogen and sulphur cycles, among others. The carbon metabolism of *M. dajiuhuensis* DJH-1^{Ts} includes key biochemical pathways such as glycolysis, where glucose is converted to pyruvate, generating ATP and NADH (Figures 5b and c). This is complemented by the non-oxidative branch of the pentose phosphate

pathway, which likely contributes to nucleotide synthesis and redox balance through NADPH production. Pyruvate undergoes oxidative decarboxylation to form acetyl-CoA, which likely participates in a truncated TCA cycle, and suggests a probable biosynthetic emphasis rather than complete catabolic oxidation.

The presence of the phosphate acetyltransferase-acetate kinase pathway indicates potential acetate utilisation under anaerobic conditions. Also, the Wood-Ljungdahl pathway suggests autotrophic carbon fixation, a trait common in anaerobic acetogenic bacteria.

The presence of the gene encoding hydroxylamine dehydrogenase (HAO) suggests that *M. dajiuhuensis* DJH-1^{Ts} might be involved in hydroxylamine detoxification. HAO is also a key enzyme in nitrification because it oxidises hydroxylamine to nitrite. However, the absence of the *AmoCAB* (ammonia monooxygenase) and *NxrAB* (nitrite oxidoreductase) genes in *M. dajiuhuensis* DJH-1^{Ts} indicates that it cannot perform nitrification metabolism. Similar to previously studied *Nitrospirota* MTB (Kolinko et al., 2016; Lin et al., 2014), this bacterium might be able to reduce nitric oxide to nitrous oxide and further to nitrogen gas, suggesting a potential role in the denitrification pathway (Lin et al., 2014). The presence of nitrogen fixation genes indicates that *M. dajiuhuensis* DJH-1^{Ts} may also contribute to conversion of atmospheric nitrogen into ammonia, making nitrogen available to living organisms.

M. dajiuhuensis DJH-1^{Ts} may engage in dissimilatory sulphate reduction, converting sulphate to Adenosine 5'-phosphosulphate (APS) as an intermediate, and subsequently reducing APS to sulphite and sulphide. This complete sulphate reduction pathway, often found in anaerobic environments, enables energy production through chemolithotrophy (Jørgensen et al., 2019).

Table 1: Genomic statistics of *M. dajiuhuensis* DJH-1^{Ts} and its closest related genome Nitrospirota bacterium nDJH13bin15.

Genomic features	*Magnetominusculus dajiuhuensis* DJH-1^{Ts}	Nitrospirota bacterium nDJH13bin15
Number of contigs	218	121
Largest contig (bp)	101549	58913
Total length (bp)	3635779	2034618
GC (%)	47.53	48.07
N50 (bp)	23014	27741
CheckM Completeness (%)	99.09	66.54
CheckM Contamination (%)	1.82	0
CheckM2 Completeness (%)	99.61	65.86
CheckM2 Contamination (%)	1.94	0
Number of CDS	3368	1951
Number of tRNAs	19	15
Number of 16S rRNA gene	1	0
Number of 23S rRNA gene	1	0
Number of 5S rRNA gene	1	1

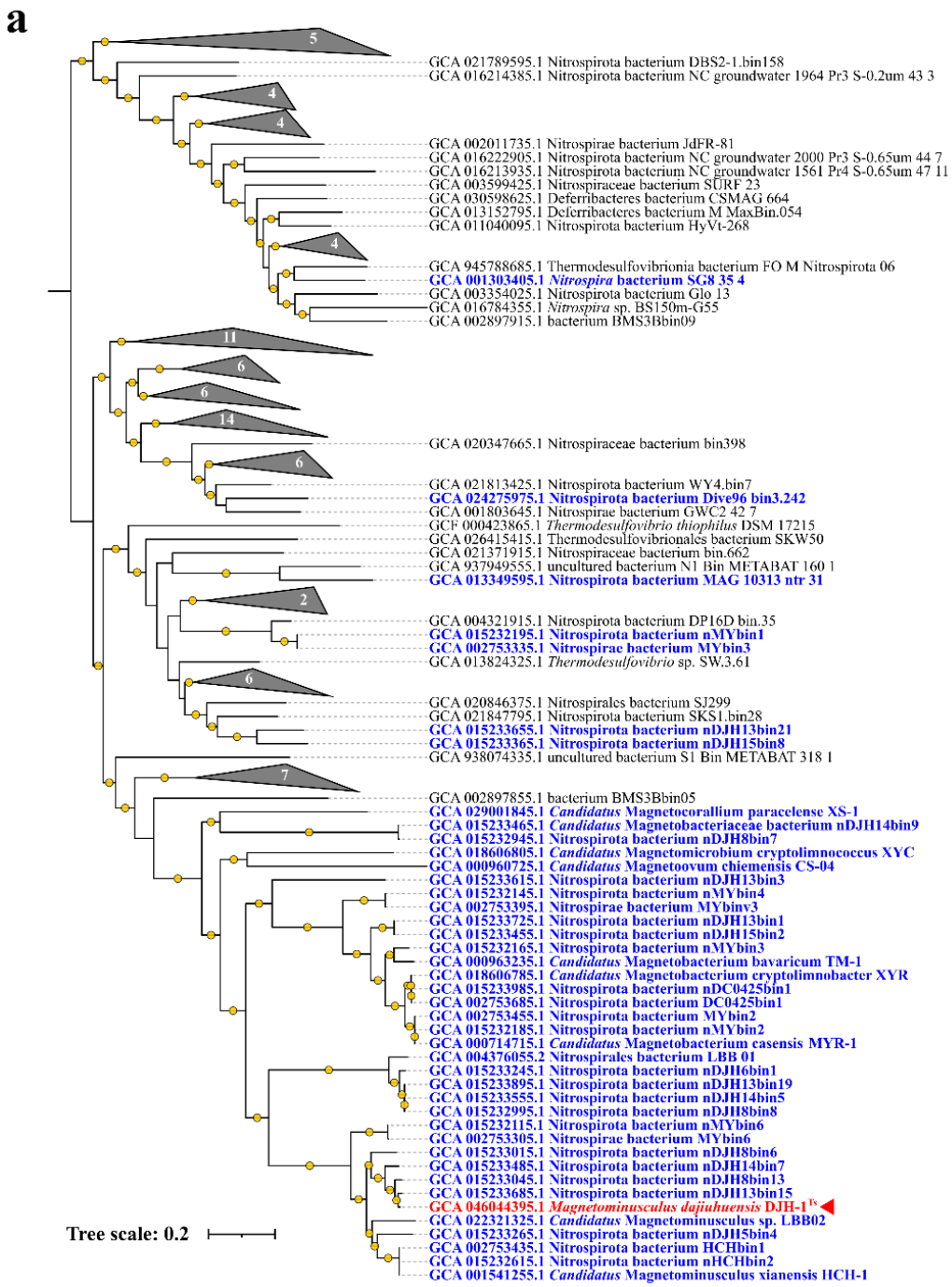

Figure 3: Phylogenomic tree and average nucleotide identity (ANI) heatmap of *M. dajiuhuensis* DJH-1^{Ts} within the *Nitrospirota* phylum. (a) Phylogenomic analysis of *M. dajiuhuensis* DJH-1^{Ts} (indicated in red and bold) within the class *Thermodesulfovibrionia* and 142 *Nitrospirota* genomes. All MTB *Nitrospirota* genomes are indicated in blue. Nodes with bootstrap values larger than 75 are indicated with dots.

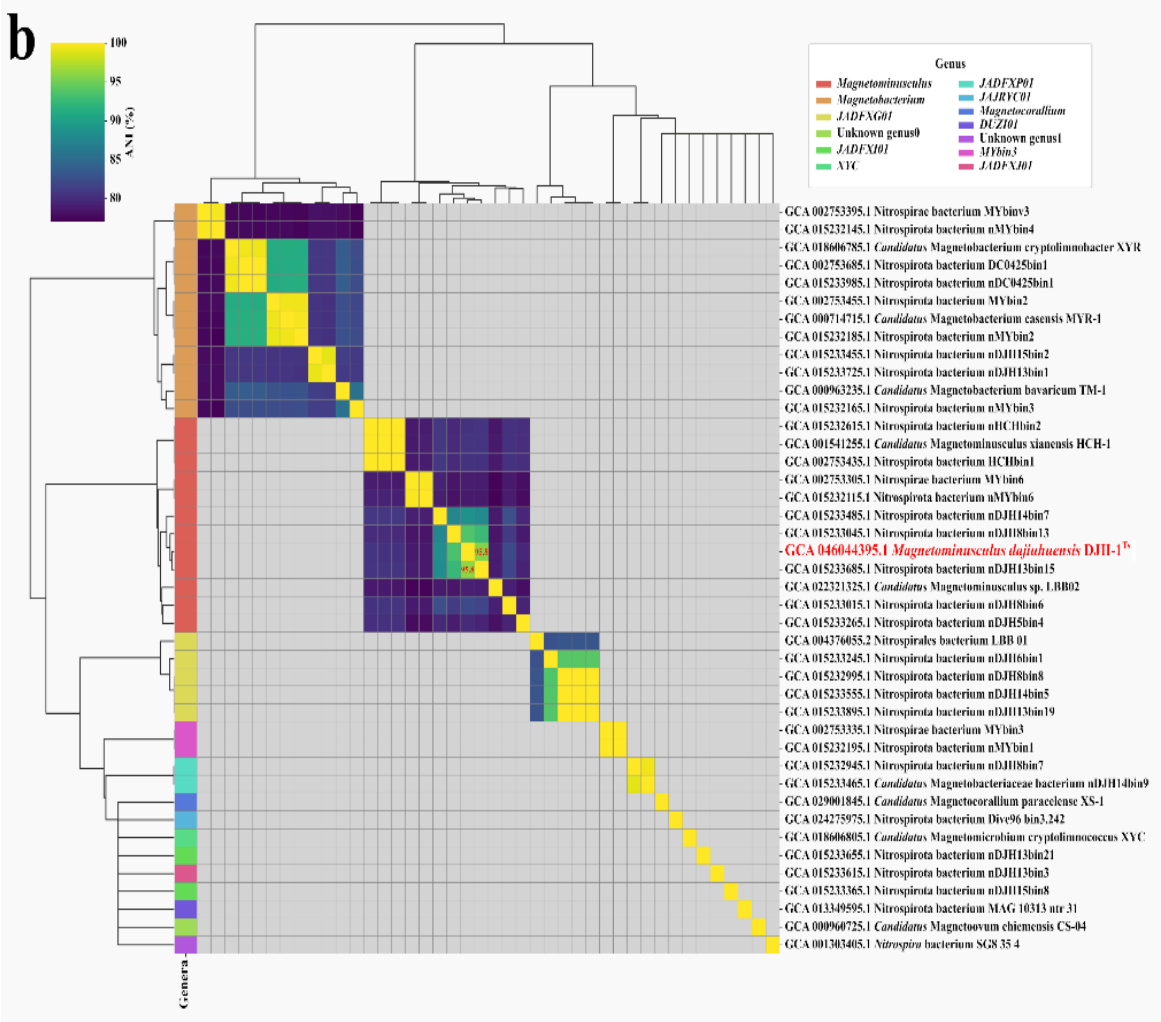

Figure 3: Phylogenomic tree and average nucleotide identity (ANI) Heatmap of *M. dajiuhuensis* DJH-1^{Ts} within the *Nitrospirota* Phylum (continued). (b) Pairwise ANI heatmap comparison of ANI percentages between *M. dajiuhuensis* DJH-1^{Ts} and 41 *Nitrospirota* MTB populations. High ANI values are depicted in warmer colours, which suggest closer genetic relationships, while lower ANI values are shown in cooler colours, which suggest greater genetic distance. Populations on the left are grouped based on overall genetic relatedness, which provides insights into phylogenetic relationships and genetic diversity within the group.

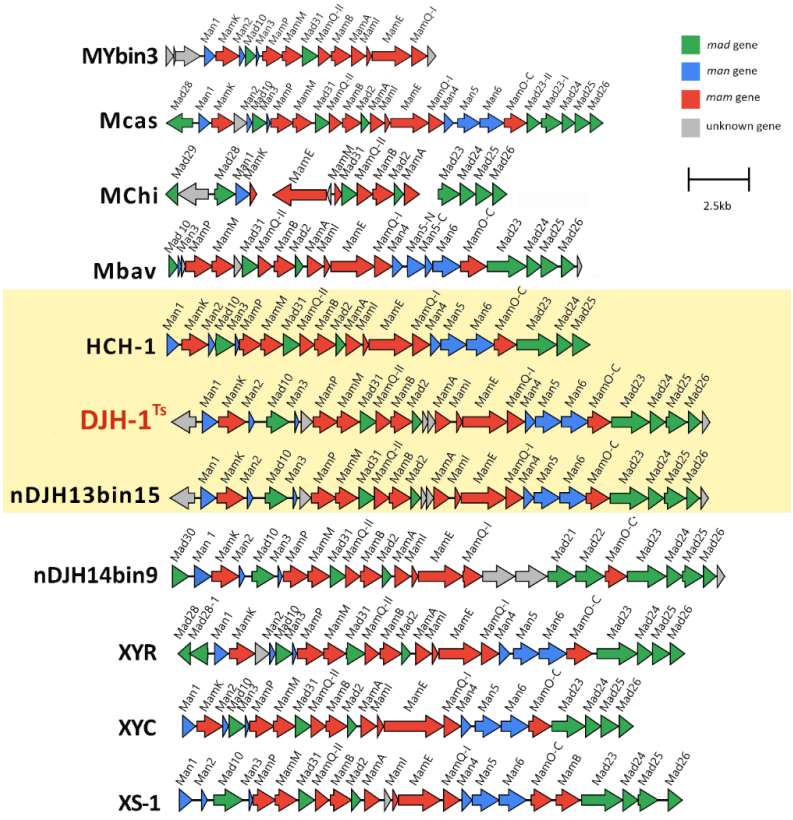

Figure 4: Comparative genomic organisation of magnetosome gene clusters (MGCs) in *M. dajiuhuensis* DJH-1^{Ts} and previously reported related MTB populations. Genes are colour-coded to indicate *mam* genes (red), *mad* genes (green), *man* genes (blue) and unknown genes (grey). The genomes used for comparison are Mcas, *Candidatus* Magnetobacterium casensis; MChi, *Candidatus* Magnetoovum chiemensis strain CS-04; Mbav, *Candidatus* Magnetobacterium bavaricum; HCH-1, *Candidatus* Magnetominusculus xianensis strain HCH-1; MYbin3, Nitrospirae bacterium MYbin3; nDJH13bin15, Nitrospirae bacterium nDJH13bin15; nDJH14bin9, Nitrospirae bacterium nDJH14bin9; XYR, *Candidatus* Magnetobacterium cryptolimnobacter strain XYR; XYC, *Candidatus* Magnetomicrobium cryptolimnococcus strain XYC; and XS-1, *Candidatus* Magnetocorallium paracelense strain XS-1. The highlighted three MGCs belong to the same genus, *Magnetominusculus*.

M. dajiuhuensis DJH-1^{Ts} also has the genetic potential to synthesise essential vitamins like thiamine (B1), riboflavin (B2) and cobalamin (B12). The presence of various ABC transporters suggests sophisticated mechanisms for essential ion and nutrient uptake, which is critical for survival and competition (Tanaka et al., 2018). Flagella and chemotaxis machinery suggest motility and the ability to respond to chemical gradients in association with magnetotaxis, which is crucial for finding optimal environmental niches for MTB (Frankel et al., 1997). The presence of Type II secretion systems, along with the Sec-SRP and Tat pathways, suggests that *M. dajiuhuensis* DJH-1^{Ts} could secrete a variety of proteins and compounds, which are specialised for functions related to interactions with biotic and abiotic environments, including nutrient acquisition and interactions with other organisms (Tseng et al., 2009). Although *M. dajiuhuensis* DJH-1^{Ts} has a partially complete methanogenesis pathway via acetate, further studies are needed to determine whether it can perform methanogenesis in anaerobic environments.

The metabolic complexity of *M. dajiuhuensis* DJH-1^{Ts} allows it to participate actively in both the nitrogen and sulphur cycles, handle various substances through its secretion systems, and manage environmental stresses through specific transporters and biosynthetic pathways. This metabolic versatility likely confers ecological competitiveness and adaptability to *M. dajiuhuensis* DJH-1^{Ts}.

CONCLUSIONS

In this study, we identify and characterise a novel *Nitrospirota* MTB species, which we name *Magnetominusculus dajiuhuensis* DJH-1^{Ts} following the SeqCode nomenclature guidelines (Hedlund et al., 2022; Whitman et al., 2022, 2024). Use of the SeqCode-style nomenclature for precise strain identification reflects how microbial taxonomy and classification are evolving. SeqCode-style nomenclature gives each strain a structured and unique identifier, which avoids naming conflicts. It also promotes standardisation. The species epithet, *dajiuhuensis* DJH-1^{Ts}, is

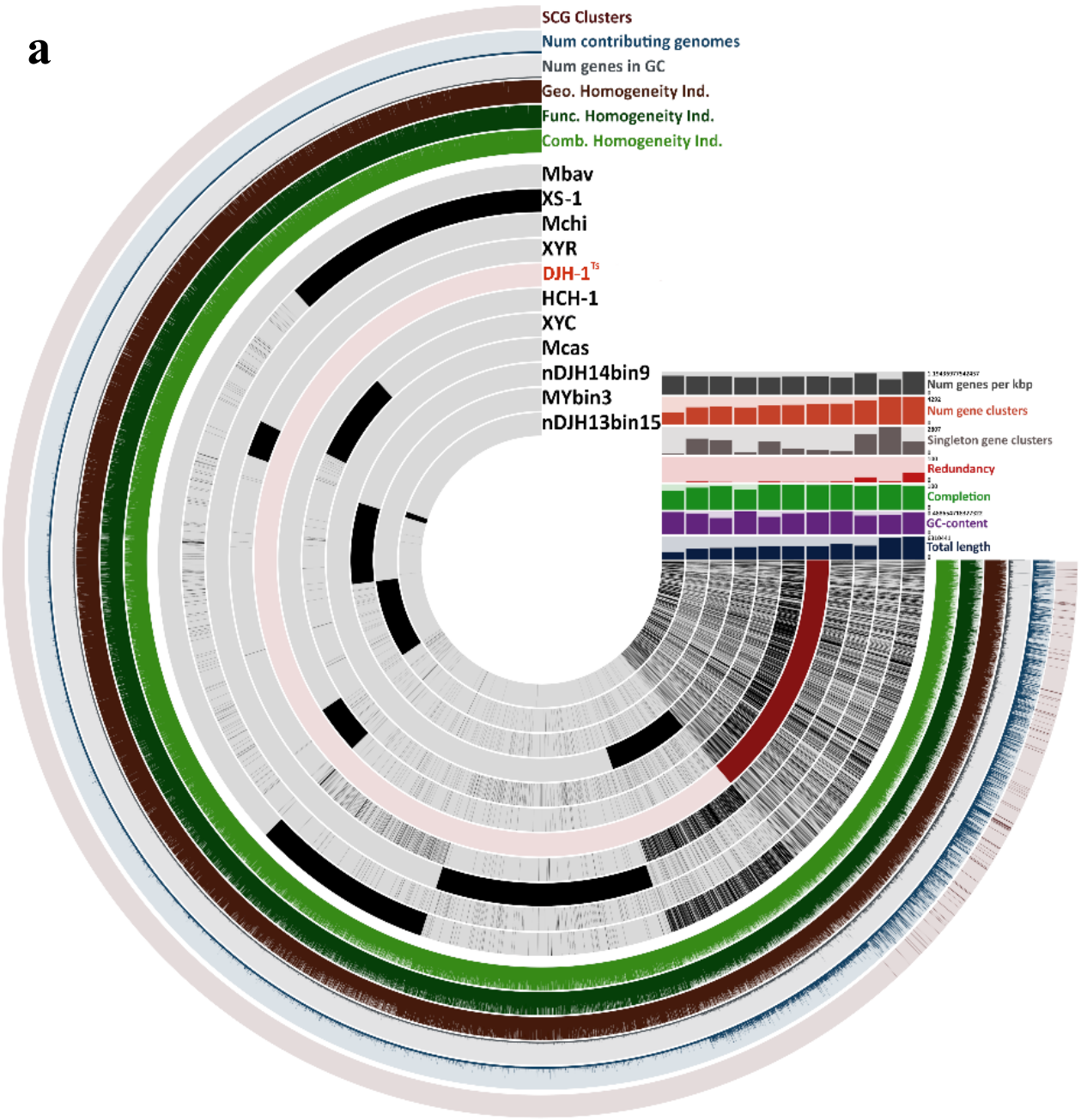

Figure 5: Pangenome analysis and metabolic potential of *M. dajiuhuensis* DJH-1^{Ts}. (a) Pangenome structure of *M. dajiuhuensis* DJH-1^{Ts}, visualised using the Anvi'o forced synteny model set to "gene_cluster_presence_absence" view, alongside ten *Nitrospirota* MTB genomes (Mbav, *Ca.* Magnetobacterium bavaricum; XS-1, *Ca.* Magnetocorallium paracelense strain XS-1; CS-04, *Ca.* Magnetobacterium chiemensis strain CS-04; XYR, *Ca.*

Magnetobacterium cryptolimnobacter strain XYR; HCH-1, *Ca.* Magnetominusculus xianensis strain HCH-1; XYC, *Ca.* Magnetomicrobium cryptolimnococcus strain XYC; Mcas, *Ca.* Magnetobacterium casensis; *nDJH14bin9, Nitrospirae bacterium nDJH14bin9*; *MYbin3, Nitrospirae bacterium MYbin3* and *nDJH13bin15, Nitrospirae bacterium nDJH13bin15).* Outermost rings denote key metrics, such as the number of genomes contributing to each gene cluster, single-copy gene (SCG) clusters, the number of genes in gene clusters, geographical homogeneity, functional homogeneity, and combined homogeneity, while the inset bar charts summarise genomic features, including redundancy, completion, singleton gene clusters, GC content, total genome length, and number of genes per kbp.

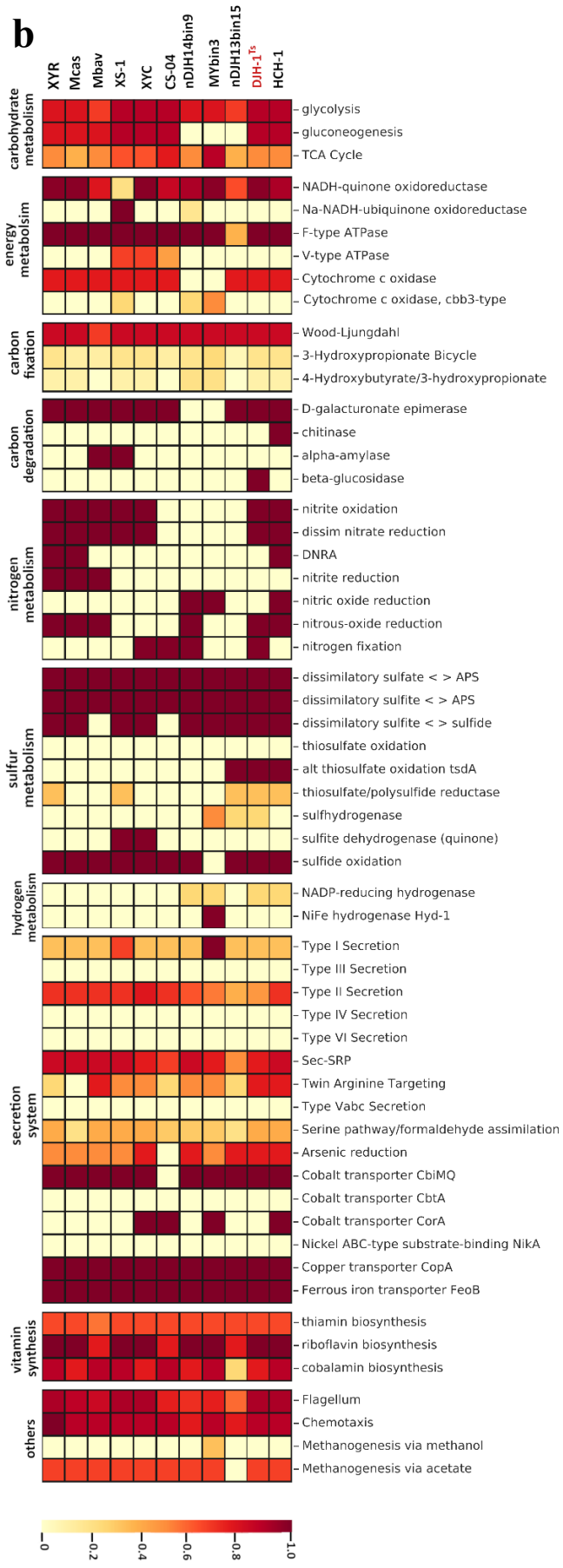
b
XYR
Mcas
Mbav
XS-1
XYC
CS-04
nDJH14bin9
MYbin3
nDJH13bin15
DJH-1^Ts
HCH-1
carbohydrate metabolism
glycolysis
gluconeogenesis
TCA Cycle
energy metabolism
NADH-quinone oxidoreductase
Na-NADH-ubiquinone oxidoreductase
F-type ATPase
V-type ATPase
Cytochrome c oxidase
Cytochrome c oxidase, cbb3-type
carbon fixation
Wood-Ljungdahl
3-Hydroxypropionate Bicycle
4-Hydroxybutyrate/3-hydroxypropionate
carbon degradation
D-galacturonate epimerase
chitinase
alpha-amylase
beta-glucosidase
nitrogen metabolism
nitrite oxidation
dissim nitrate reduction
DNRA
nitrite reduction
nitric oxide reduction
nitrous-oxide reduction
nitrogen fixation
sulfur metabolism
dissimilatory sulfate < > APS
dissimilatory sulfite < > APS
dissimilatory sulfite < > sulfide
thiosulfate oxidation
alt thiosulfate oxidation tsdA
thiosulfate/polysulfide reductase
sulfhydrogenase
sulfite dehydrogenase (quinone)
sulfide oxidation
hydrogen metabolism
NADP-reducing hydrogenase
NiFe hydrogenase Hyd-1
secretion system
Type I Secretion
Type III Secretion
Type II Secretion
Type IV Secretion
Type VI Secretion
Sec-SRP
Twin Arginine Targeting
Type Vabc Secretion
Serine pathway/formaldehyde assimilation
Arsenic reduction
Cobalt transporter CbiMQ
Cobalt transporter CbtA
Cobalt transporter CorA
Nickel ABC-type substrate-binding NikA
Copper transporter CopA
Ferrous iron transporter FeoB
vitamin synthesis
thiamin biosynthesis
riboflavin biosynthesis
cobalamin biosynthesis
others
Flagellum
Chemotaxis
Methanogenesis via methanol
Methanogenesis via acetate
0
0.2
0.4
0.6
0.8
1.0

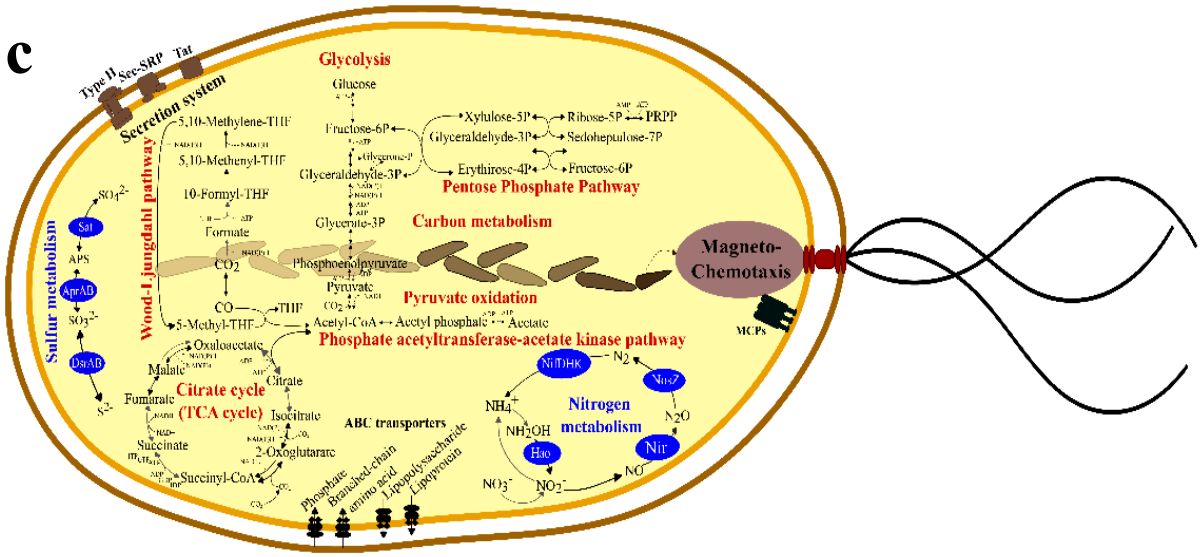

Figure 5: Pangenome analysis and metabolic potential of *M. dajiuhuensis* DJH-1^{Ts} (continued)**.** **(**b) Comparative metabolic pathways of *M. dajiuhuensis* DJH-1^{Ts} with the same ten related *Nitrospirota* MTB. The colour gradient represents major metabolic pathway completeness inferred from the presence or absence of genes. Dark red indicates a complete or nearly complete pathway, while yellow signifies a pathway that is either absent or mostly incomplete.

(c) Schematic diagram of the overall metabolic network of *M. dajiuhuensis* DJH-1^{Ts}.

named after its discovery location, the acidic Dajiuhu Peatland. Microscopic examination, including light and electron microscopy, reveal the coccobacilli morphology and distinctive magnetosome structures of *M. dajiuhuensis* DJH-1^{Ts}.

Table 2: Protologue table of *Magnetominusculus* gen. nov. and *Magnetominusculus dajiuhuensis* DJH-1^{Ts} sp. nov.

	Genus	**Species**
Guiding Code for Nomenclature	-	SeqCode
Nature of the type material	-	MAG
Category epithet	Magnetominusculus	Magnetominusculus dajiuhuensis DJH-1Ts
Category status	gen. nov.	sp. nov.
Category etymology	Mag.ne.to.mi.nus`cu.lus. from L. magnetum, magnet; L. adj. minusculus, small; N.L. masc. n. Magnetominusculus, small magnetosome-bearing bacterium.	da.jiu.hu.en′sis. N.L. adj. dajiuhuensis, named after Dajiuhu, the peatland in China where it was discovered.
Type species of the genus	Magnetominusculus dajiuhuensis DJH-1Ts	-
Description of the new taxon and diagnostic traits	The description of the genus is identical to that of the type species.	Magnetominusculus dajiuhuensis DJH-1Ts is an obligate anaerobic magnetotactic bacterium (MTB), inferred from genomic data. Cells are coccobacilli-shaped (~0.5 µm wide and 1 µm long) and possess single or dual

		bullet-shaped magnetosome chains, each containing 10–14 magnetosomes. It was isolated from acidic surface sediments (pH 4.3–5.7) of the Dajiuhu Peatland, China. Its genome includes key metabolic pathways involved in carbon, nitrogen, and sulphur cycling. Carbon metabolism comprises glycolysis, the non-oxidative pentose phosphate pathway, and acetate production via the phosphate acetyltransferase-acetate kinase pathway, suggesting a biosynthetic focus rather than complete catabolic oxidation. The presence of the Wood-Ljungdahl pathway suggests autotrophic carbon fixation. Nitrogen metabolism includes hydroxylamine oxidation and nitrate reduction contributing to potential denitrification. Genes for nitrogen fixation suggest its likely ability to convert atmospheric nitrogen into

		ammonia. Sulphur metabolism involves complete dissimilatory sulphate reduction, producing sulphite and sulphide via adenosine 5′-phosphosulphate (APS). The species has genetic potential to synthesize essential vitamins such as thiamine (B1), riboflavin (B2), and cobalamin (B12), and encodes ABC transporters for nutrient uptake. Motility is inferred from flagella and chemotaxis genes. Type II secretion systems suggest environmental interactions. Although the genome suggests a partial methanogenesis pathway via acetate, further studies are needed to confirm its functionality. This metabolic versatility indicates an active role in carbon, nitrogen, and sulphur cycling in anaerobic environments, particularly acidic peatlands.
Designated Genome, MAG or SAG	-	Magnetominusculus dajiuhuensis DJH-1Ts

Type Genome, MAG or SAG accession number	-	GCA_046044395.1Ts
Access to raw data (SRA accession numbers)	-	SRR31558115-SRR31558128
SeqCode registry number	seqco.de/r:5k0ci1ce	-
Genome status	-	Incomplete (99.61% complete according to CheckM2)
Genome size	-	3.64 Mbp
GC mol%	-	47.53%
16S rRNA gene accession number	-	PQ361747
Country of origin	-	China
Region of origin	-	Dajiuhu Peatland, Hubei Province
Source of isolation	-	Sediment
Latitude	-	31°34′ - 31°33′N
Longitude	-	109°56′ - 110°11′E
Depth	-	Surface sediments

Number of strains in study	-	1 (Magnetominusculus dajiuhuensis DJH-1Ts)
Information related to the Nagoya Protocol	-	Not applicable

DATA AVAILABILITY

The 16S rRNA gene sequence has been deposited in GenBank under accession number PQ361747. The genome sequence is deposited in NCBI under genome accession number GCA_046044395.1, BioSample ID SAMN42912234 and BioProject ID PRJNA400260. Raw sequencing reads are available under SRA accession numbers SRR31558115-SRR31558128.

ACKNOWLEDGEMENTS

We thank Xianyu Huang (State Key Laboratory of Biogeology and Environmental Geology, China University of Geosciences, Wuhan), and Zhiqi Zhang (Shennongjia National Park Administration) for contributions to the collection of acidic peatland soil samples, Wensi Zhang and Li Liu for sample collection, and Lixin Gu and Xu Tang for help with TEM and SEM data collection. We also thank the Supercomputing Laboratory, Institute of Geology and Geophysics, Chinese Academy of Sciences (IGGCAS), for assistance with data analysis. This work was supported by the National Natural Science Foundation of China (grant numbers 42388101 and T2225011), a CAS-TWAS President's Fellowship (Series No 2019-054), and the CAS Project for Young Scientists in Basic Research (YSBR-097).

AUTHOR CONTRIBUTIONS

P.G., R.J., W.L. and A.P.R. conceptualised the work; P.G. and R.J. designed and carried out the experiments and carried out bioinformatics analyses; P.G., J.S., R.J. and W.L. wrote the paper, with input from all authors; W.L. secured the funding. All authors revised the manuscript and approved the final version.

REFERENCES

Alneberg, J. et al. Binning metagenomic contigs by coverage and composition. Nat. Methods 11, 1144–1146 (2014).

Amann, R. I. et al. Combination of 16S rRNA-targeted oligonucleotide probes with flow cytometry for analyzing mixed microbial populations. Appl. Environ. Microbiol. 56, 1919–1925 (1990).

Aramaki, T. et al. KofamKOALA: KEGG Ortholog assignment based on profile HMM and adaptive score threshold. Bioinformatics 36, 2251–2252 (2020).

Bazylinski, D. A. & Frankel, R. B. Magnetosome formation in prokaryotes. Nat. Rev. Microbiol. 2, 217–230 (2004).

Bowers, R. M. et al. Minimum information about a single amplified genome (MISAG) and a metagenome-assembled genome (MIMAG) of bacteria and archaea. Nat. Biotechnol. 35, 725–731 (2017).

Chaumeil, P.-A. et al. GTDB-Tk: A toolkit to classify genomes with the Genome Taxonomy Database. Bioinformatics 36, 1925–1927 (2020).

Chklovski, A. et al. CheckM2: A rapid, scalable and accurate tool for assessing microbial genome quality using machine learning. Nat. Methods 20, 1203–1212 (2023).

Delmont, T. O. & Eren, A. M. Linking pangenomes and metagenomes: the Prochlorococcus metapangenome. PeerJ 6, e4320 (2018).

Eren, A. M. et al. Community-led, integrated, reproducible multi-omics with anvi'o. Nat. Microbiol. 6, 3–6 (2021).

Frankel, R. B., Bazylinski, D. A. & Johnson, M. S. Magneto-aerotaxis in marine coccoid bacteria. Biophys. J. 73, 994–1000 (1997).

Gilchrist, C. L. M. & Chooi, Y.-H. clinker & clustermap.js: Automatic generation of gene cluster comparison figures. Bioinformatics 37, 2473–2475 (2021).

Goswami, P. et al. Magnetotactic bacteria and magnetofossils: Ecology, evolution and environmental implications. npj Biofilms Microbiomes 8, 43 (2022).

Graham, E. D., Heidelberg, J. F. & Tully, B. J. Potential for primary productivity in a globally-distributed bacterial phototroph. ISME J. 12, 1861–1866 (2018).

Grant, C. R., Wan, J. & Komeili, A. Organelle formation in bacteria and archaea. Annu. Rev. Cell Dev. Biol. 34, 217–238 (2018).

Greenberg, M. et al. Observation of magnetoreceptive behavior in a multicellular magnetotactic prokaryote in higher than geomagnetic fields. Biophys. J. 88, 1496–1499 (2005).

Hedlund, B. P. et al. SeqCode: A nomenclatural code for prokaryotes described from sequence data. Nat. Microbiol. (2022).

Jain, C. et al. High throughput ANI analysis of 90K prokaryotic genomes reveals clear species boundaries. Nat. Commun. 9, 5114 (2018).

Ji, R. et al. Linking morphology, genome, and metabolic activity of uncultured magnetotactic Nitrospirota at the single-cell level. Microbiome 12, 158 (2024).

Ji, R. et al. MagCluster: a tool for identification, annotation, and visualisation of magnetosome gene clusters. Microbiol. Resour. Announc. 11, e01031-21 (2022).

Jogler, C. et al. Cultivation-independent characterisation of 'Candidatus Magnetobacterium bavaricum' via ultrastructural, geochemical, ecological and metagenomic methods. Environ. Microbiol. 12, 2466–2478 (2010).

Jørgensen, B. B., Findlay, A. J. & Pellerin, A. The biogeochemical sulphur cycle of marine sediments. Front. Microbiol. 10, 849 (2019).

Kang, D. D. et al. MetaBAT 2: An adaptive binning algorithm for robust and efficient genome reconstruction from metagenome assemblies. PeerJ 7, e7359 (2019).

Kolinko, S. et al. Single-cell genomics of uncultivated deep-branching magnetotactic bacteria reveals a conserved set of magnetosome genes. Environ. Microbiol. 18, 21–37 (2016).

Langmead, B. & Salzberg, S. L. Fast gapped-read alignment with Bowtie 2. Nat. Methods 9, 357–359 (2012).

Lefèvre, C. T. et al. Moderately thermophilic magnetotactic bacteria from hot springs in Nevada. Appl. Environ. Microbiol. 76, 3740–3743 (2010).

Lefèvre, C. T. & Bazylinski, D. A. Ecology, diversity, and evolution of magnetotactic bacteria. Microbiol. Mol. Biol. Rev. 77, 497–526 (2013).

Lefèvre, C. T. et al. Culture-independent characterisation of a novel, uncultivated magnetotactic member of the Nitrospirae phylum. Environ. Microbiol. 13, 538–549 (2011).

Letunic, I. & Bork, P. Interactive Tree of Life (iTOL) v6: Recent updates to the phylogenetic tree display and annotation tool. Nucleic Acids Res. 52, W78–W82 (2024).

Li, H. et al. The sequence alignment/map format and SAMtools. Bioinformatics 25, 2078–2079 (2009).

Li, J. H. et al. Magnetotaxis as an adaptation to enable bacterial shuttling of microbial sulphur and sulphur cycling across aquatic oxic-anoxic interfaces. J. Geophys. Res.-Biogeo. 125, e2020JG006012 (2020).

Lin, W. et al. Genomic insights into the uncultured genus 'Candidatus Magnetobacterium' in the phylum Nitrospirae. ISME J. 8, 2463–2477 (2014).

Lin, W. et al. On the origin of microbial magnetoreception. Natl. Sci. Rev. 7, 472–479 (2020).

Lin, W. & Pan, Y. Temporal variation of magnetotactic bacterial communities in two freshwater sediment microcosms. FEMS Microbiol. Lett. 302, 85–92 (2010).

Lin, W., Pan, Y. & Bazylinski, D. A. Diversity and ecology of and biomineralisation by magnetotactic bacteria. Environ. Microbiol. Rep. 9, 345–356 (2017).

Lin, W. et al. Origin of microbial biomineralisation and magnetotaxis during the Archean. Proc. Natl. Acad. Sci. U.S.A. 114, 2171–2176 (2017).

Lin, W. et al. Expanding magnetic organelle biogenesis in the domain Bacteria. Microbiome 8, 152 (2020).

Lin, W. et al. Genomic expansion of magnetotactic bacteria reveals an early common origin of magnetotaxis with lineage-specific evolution. ISME J. 12, 1508–1519 (2018).

Liu, J. et al. Magnetotactic bacteria in Tengchong hot springs, China. EGU General Assembly 2020 Online, 4–8 (2020).

McGinnis, S. & Madden, T. L. BLAST: At the core of a powerful and diverse set of sequence analysis tools. Nucleic Acids Res. 32, W20–W25 (2004).

Müller, F. D., Schüler, D. & Pfeiffer, D. A compass to boost navigation: Cell biology of bacterial magnetotaxis. J. Bacteriol. 202, e0039820 (2020).

Nash, C. Mechanisms and Evolution of Magnetotactic Bacteria. California Institute of Technology, Pasadena, CA (2008).

Nguyen, L.-T. et al. IQ-TREE: A fast and effective stochastic algorithm for estimating maximum-likelihood phylogenies. Mol. Biol. Evol. 32, 268–274 (2015).

Nurk, S. et al. metaSPAdes: A new versatile metagenomic assembler. Genome Res. 27, 824–834 (2017).

Olm, M. R. et al. dRep: A tool for fast and accurate genomic comparisons that enables improved genome recovery from metagenomes through de-replication. ISME J. 11, 2864–2868 (2017).

Parks, D. H. et al. CheckM: Assessing the quality of microbial genomes recovered from isolates, single cells, and metagenomes. Genome Res. 25, 1043–1055 (2015).

Pernthaler, J. et al. Fluorescence in situ hybridization (FISH) with rRNA-targeted oligonucleotide probes. In: Methods in Microbiology. Elsevier, 207–226 (2001).

Qian, X. et al. Identification of novel species of marine magnetotactic bacteria affiliated with Nitrospirae phylum. Environ. Microbiol. Rep. 11, 330–337 (2019).

Quast, C. et al. The SILVA ribosomal RNA gene database project: improved data processing and web-based tools. Nucleic Acids Res. 41, D590–D596 (2012).

Sanger, F., Nicklen, S. & Coulson, A. R. DNA sequencing with chain-terminating inhibitors. Proc. Natl. Acad. Sci. U.S.A. 74, 5463–5467 (1977).

Seemann, T. Prokka: Rapid prokaryotic genome annotation. Bioinformatics 30, 2068–2069 (2014).

Shen, J. et al. Renaissance for magnetotactic bacteria in astrobiology. ISME J. 17, 1526–1534 (2023).

Shen, J. et al. Identifying sulphate-reducing and magnetotactic bacteria in a hyperalkaline cave system. Cave Karst Sci. 50(1), 16–20 (2023).

Spring, S. et al. Dominating role of an unusual magnetotactic bacterium in the microaerobic zone of a freshwater sediment. Appl. Environ. Microbiol. 59, 2397–2403 (1993).

Spring, S. & Bazylinski, D. A. Magnetotactic Bacteria. In: Dworkin, M. et al. (eds), The Prokaryotes. Springer Verlag, New York, 842–862 (2006).

Tamura, K., Stecher, G. & Kumar, S. MEGA11: molecular evolutionary genetics analysis version 11. Mol. Biol. Evol. 38, 3022–3027 (2021).

Tanaka, K. J. et al. Selective substrate uptake: The role of ATP-binding cassette (ABC) importers in pathogenesis. Biochim. Biophys. Acta 1860, 868–877 (2018).

Thompson, J. D., Higgins, D. G. & Gibson, T. J. CLUSTAL W: Improving the sensitivity of progressive multiple sequence alignment through sequence weighting, position-specific gap penalties and weight matrix choice. Nucleic Acids Res. 22, 4673–4680 (1994).

Trifinopoulos, J. et al. W-IQ-TREE: A fast online phylogenetic tool for maximum likelihood analysis. Nucleic Acids Res. 44, W232–W235 (2016).

Tseng, T.-T., Tyler, B. M. & Setubal, J. C. Protein secretion systems in bacterial-host associations, and their description in the Gene Ontology. BMC Microbiol. 9, S2 (2009).

Uebe, R. & Schüler, D. Magnetosome biogenesis in magnetotactic bacteria. Nat. Rev. Microbiol. 14, 621–637 (2016).

Uritskiy, G. V., DiRuggiero, J. & Taylor, J. MetaWRAP—a flexible pipeline for genome-resolved metagenomic data analysis. Microbiome 6, 158 (2018).

Uzun, M. et al. Unravelling the diversity of magnetotactic bacteria through analysis of open genomic databases. Sci. Data 7, 252 (2020).

Whitman, W. B. et al. Development of the SeqCode: A proposed nomenclatural code for uncultivated prokaryotes with DNA sequences as type. Syst. Appl. Microbiol. 45, 126305 (2022).

Whitman, W. B. et al. Why and how to use the SeqCode. mLife 3, 1–13 (2024).

Wolfe, R. S., Thauer, R. K. & Pfennig, N. A 'capillary racetrack' method for isolation of magnetotactic bacteria. FEMS Microbiol. Lett. 45, 31–35 (1987).

Wu, Y.-W., Simmons, B. A. & Singer, S. W. MaxBin 2.0: An automated binning algorithm to recover genomes from multiple metagenomic datasets. Bioinformatics 32, 605–607 (2016).

Xiang, X., Wang, H., Gong, L. & Liu, Q. Vertical variations and associated ecological function of bacterial communities from Sphagnum to underlying sediments in Dajiuhu Peatland. Sci. China Earth Sci. 57, 1013–1020 (2014).

Zhang, W. et al. Identification and genomic characterisation of two previously unknown magnetotactic Nitrospirae. Front. Microbiol. 12, 690052 (2021).

Zhao, Y. et al. Insight into the metabolic potential and ecological function of a novel magnetotactic Nitrospirota in coral reef habitat. Front. Microbiol. 14, 1182330 (2023).

Chapter 5: Magnetosome Gene Cluster-Containing Bacteria in Oxygen Minimum Zones: Genomic Insights from Metagenome-Assembled Genomes

SUMMARY OF CHAPTER

Oxygen Minimum Zones

OMZs are regions located between depths of 100 and 1,000 metres in the global oceans (Stramma et al., 2008). OMZs have extremely low oxygen concentrations, typically less than 20 μmol kg^{-1}. In certain regions, such as the eastern tropical Pacific Ocean, concentrations can fall below 4.5 μmol kg^{-1}, and within its core zones, even reach below 1 μmol kg^{-1}. OMZs provide a niche for a wide range of microorganisms that are crucial to global biogeochemical cycles and marine ecosystems, making them a focal point of oceanographic and marine biology research (Wright et al., 2012; Bertagnolli and Stewart, 2018). Their importance extends far beyond their immediate ecological role, with implications for predicting ocean ecosystem changes in response to climate-related phenomena such as ocean acidification and warming (Breitburg et al., 2018; Levin, 2018). Expanding OMZs create cascading feedback loops by altering microbial processes that enhance greenhouse gas emissions, aggravating climate change and affecting ecosystems both within and beyond these zones (Keeling et al., 2010; Long et al., 2021; Schmidtko et al., 2017). The formation and persistence of OMZs represent an intricate confluence of biological, chemical and physical forces within the oceanic depths (Karstensen et al., 2008; Ulloa et al., 2012; Stramma et al., 2008). At the core of OMZ development is the biological consumption of oxygen. Organic matter, which is rich in organic carbon and nutrients, cascades down from the productive sunlit layers to deeper waters, fuelling microbial respiration that consumes oxygen in mid-water depths (Bianchi et al., 2012; Thamdrup et al., 2012; Ulloa et al., 2012). This biological oxygen demand, compounded by poor ventilation driven by sluggish

ocean circulation and thermal stratification, effectively locks oxygen-depleted waters in place (Wright et al., 2012; Karstensen et al., 2008). These regions are often associated with the intense productivity of eastern boundary upwelling systems, where nutrient-rich waters rise to the surface, stimulating large phytoplankton blooms (Chavez and Messié, 2009). The aftermath of these blooms is an avalanche of organic material sinking to depth and further exacerbating oxygen depletion (Paulmier and Ruiz-Pino, 2009; Busecke et al., 2019). These conditions gives rise to OMZs, which are not uniformly distributed but rather cluster in the Eastern Tropical North Pacific Ocean, the Eastern Tropical South Pacific Ocean, the Arabian Sea and the Bay of Bengal (Karstensen et al., 2008; Stramma et al., 2008; Paulmier and Ruiz-Pino, 2009). In these regions, upwelling, high surface productivity, and limited horizontal ventilation combine to form and sustain OMZs (Chavez and Messié, 2009; Resplandy et al., 2012; Schmidt and Eggert, 2016). The spatial and temporal variability of these zones is of significant interest, particularly given the potential for these regions to expand and intensify with climate change. As the oceans warm and stratification increases, OMZs may proliferate, with serious consequences for marine life, nutrient cycling, and broader global ocean health (Rabalais et al., 2010; Levin, 2018).

Microbial Ecology in OMZs

Despite their extremely low-oxygen conditions, OMZs are home to diverse microbial life that has adapted to thrive in environments that would be inhospitable to most other life forms. These microbes, from diverse bacterial and archaeal lineages, have developed remarkable metabolic strategies that allow them to drive critical biogeochemical processes (Ulloa et al., 2012; Wright et al., 2012). In particular, members of the *Planctomycetes*, *Proteobacteria* (currently *Pseudomonadota*), and *Actinobacteria* have become adept at exploiting anaerobic environments, using alternative electron acceptors such as nitrate, sulphate or metal oxides for respiration (Bertagnolli and Stewart, 2018; Stewart et al., 2012; Wright et al., 2012).

Denitrification and anaerobic ammonium oxidation (anammox) are of particular importance, together accounting for a substantial portion of nitrogen loss from the ocean (Thamdrup et al., 2012). By converting bioavailable nitrogen to inert nitrogen gas (N_2), these processes regulate the ocean nitrogen balance, positioning OMZs as crucial sinks in the global nitrogen cycle (Devol, 2015; Kalvelage et al., 2015). The role of OMZ microbial communities extends beyond nitrogen cycling; they are also central to oceanic carbon dynamics. Microbial organic matter degradation within OMZs is largely anaerobic, leading to carbon dioxide (CO_2) production while also contributing to organic carbon sequestration in the deep ocean (Engel et al., 2022; Hansell, 2013; Maßmig et al., 2020). Some microbes within these zones have the ability to fix inorganic carbon, using electron acceptors other than oxygen to sustain primary production in these otherwise energy-limited environments (Wright et al., 2012; Bianchi et al., 2012). Incomplete organic material breakdown can also result in formation of refractory dissolved organic carbon, a carbon pool that is resistant to further degradation and, thus, represents a significant long-term carbon sink (Hansell et al., 2009; Jiao et al., 2010; Wakeham, 2020). Sulphur cycling, too, plays a prominent role in OMZs, where sulphate-reducing bacteria facilitate the reduction of sulphate to sulphide (Callbeck et al., 2021; Canfield et al., 2010; Lavik et al., 2009). This process, in turn, can fuel growth of sulphur-oxidising bacteria, which thrive in regions where sulphide-rich sediments meet oxygen-depleted waters. These sulphur-based metabolisms not only contribute to the ocean sulphur cycle but also provide critical support for chemosynthetic production, further enhancing overall OMZ microbial community productivity (Canfield et al., 2010; Callbeck et al., 2018; Long et al., 2021).

Potential Presence of Magnetotactic Bacteria in OMZs

MTB appear to have found a place amidst the mosaic of microbial life thriving in OMZs. Magnetotaxis equips MTB with the distinctive ability to sense the geomagnetic field and migrate along it across redox

gradients (Bazylinski et al., 2013; Lin et al., 2020), an ecological trait that may be especially advantageous within the sharp chemical stratifications of OMZs (Levin, 2018; Wright et al., 2012). While extensively studied in freshwater sediments and estuarine interfaces, early evidence for MTB in marine environments was provided by Stolz et al. (1986) and Petermann and Bleil (1993), who detected magnetite-producing bacteria in hemipelagic and deep-sea sediments. More recent studies using molecular and metagenomic techniques have expanded our understanding of their diversity and distribution in marine settings, including tropical coasts and deep volcanic arcs (Tan et al., 2021; Liu et al., 2017; Xu et al., 2018). Their contributions extend well beyond iron metabolism. MTB are now known to be involved in the cycling of carbon, nitrogen, sulphur, phosphorus, etc., particularly at redox interfaces where metabolic flexibility becomes an ecological currency (Bazylinski & Blakemore, 1983; Bazylinski et al., 2004; Goswami et al., 2025; Isambert et al., 2007; Jiang et al., 2002; Jogler et al., 2010; Kolinko et al., 2012; Lefèvre et al., 2011; Li et al., 2020; Monteil et al., 2020; Qian et al., 2020; Rivas-Lamelo et al., 2017; Schultheiss et al., 2005; Schulz-Vogt et al., 2019). Notably, MTB appear to co-localise with gradients of electron acceptors — a spatial preference that aligns well with OMZ conditions (Frankel et al., 1997; Flies et al., 2004).

In this study, MGC are used as key genomic markers to identify potential MTB within recovered MAGs from OMZ metagenomic sequences available from genomic databases. Detection of non-redundant, functionally relevant MGCs led to identification of 30 candidate MAGs, including 6 high-confidence MAGs (putative MTB) from global OMZs. These results highlight the potential wide distribution of MGC-containing bacteria and their likely role in elemental cycling within marine redox gradients. Given their functional versatility and use as paleoenvironmental proxies, MTB may serve as key players in sustaining oceanic redox balance under future stratification trends.

Magnetosome Gene Cluster-Containing Bacteria in Oxygen Minimum Zones: Genomic Insights from Metagenome-Assembled Genomes

Pranami Goswami[1,2,3,4], Runjia Ji[1,2,3], Andrew P. Roberts[4*] and Wei Lin[1,2,3*]

[1]Key Laboratory of Planetary Science and Frontier Technology, Institute of Geology and Geophysics, Chinese Academy of Sciences, Beijing 100029, China.

[2]France-China Joint Laboratory for Evolution and Development of Magnetotactic Multicellular Organisms, Chinese Academy of Sciences, Beijing 100029, China.

[3]College of Earth and Planetary Sciences, University of Chinese Academy of Sciences, Beijing 100049, China.

[4]Research School of Earth Sciences, Australian National University, ACT, Canberra 2601, Australia.

[*]Corresponding authors: weilin@mail.iggcas.ac.cn (Wei Lin), andrew.roberts@anu.edu.au (Andrew P. Roberts)

ABSTRACT

OMZs are expanding low-oxygen regions in the ocean where specialised microbial communities drive critical biogeochemical processes. Among these, magnetotactic bacteria (MTB) have been largely overlooked, despite their potential roles in elemental cycling. Here, we used genome-resolved metagenomics to investigate the presence and ecological functions of MTB across global OMZ metagenomes. In this study, we identify six high-confidence MGC-containing metagenome assembled genomes (MAGs)— putative

MTB— across four phyla (three known phyla harbouring MTB lineages and one novel phylum) using metagenomic analyses of global OMZ datasets. These MTB have functional potential in key nitrogen, sulphur, and carbon cycling pathways. Gene-based predictions suggest that they may contribute to major redox processes, including denitrification and sulphate reduction, all of which have significant implications for nitrogen and sulphur fluxes in marine systems. Taxonomic and metabolic characterisation of the six MAGs shed light on the biogeochemical potential of putative MTB identified from OMZs. Our findings expand the ecological and phylogenetic scope of MTB, positioning them as versatile contributors to redox-driven OMZ processes. Identification of MTB within OMZs suggests that they are important contributors to ocean biogeochemistry, pointing to the necessity of integrating them into elemental cycling models to help account for marine oxygen conditions caused by climate change.

Keywords: magnetotactic bacteria; oxygen minimum zones; magnetosome gene cluster; metagenomics; metabolic function

INTRODUCTION

The upper layers of the productive ocean twilight zones can form OMZs, between depths of 100 and 1,000 meters (Stramma et al., 2008). These persistent layers in the water column contain extremely low oxygen concentrations and are most prominently found in the eastern tropical Pacific Ocean, northern Indian Ocean and parts of the Atlantic Ocean (Karstensen et al., 2008; Paulmier and Ruiz-Pino, 2009). OMZs have garnered attention in recent years in oceanography due to their chemical stratification and microbial ecology (Bertagnolli and Stewart, 2018; Wright et al., 2012). Their expansion is closely associated with anthropogenic climate change and is expected to grow in future (Breitburg et al., 2018; Levin, 2018). OMZs support diverse microbial assemblages that are adapted to low-oxygen conditions, yet there is a lack of quantitative data on their metabolic activities, growth rates and

interactions with organic matter cycling (Engel et al., 2022). This hinders prediction of how expanding OMZs will affect oceanic nutrient cycles and global biogeochemical feedbacks under future climate scenarios.

Among such microbial communities, MTB represent an understudied group in marine OMZs. These microorganisms biomineralise intracellular nanocrystals of magnetite (Fe_3O_4) or greigite (Fe_3S_4), forming highly ordered organelles called magnetosomes that enable orientation and migration along Earth's magnetic field. This behaviour, termed magnetotaxis, allows MTB to navigate within redox gradients, making them particularly well-suited to navigating the steep oxygen and nutrient transitions characteristic of OMZs (Bazylinski et al., 2013; Levin, 2018; Lin et al., 2020; Wright et al., 2012). Despite this ecological fit, MTB have received limited attention in marine OMZ contexts. Their metabolic capabilities suggest that they may play critical roles in coupling iron cycling with other elemental transformations, yet their diversity, distribution and functional relevance across OMZ systems remain poorly understood.

MTB have been studied extensively in freshwater and estuarine environments, where their contributions extend well beyond iron metabolism. MTB are now known to be involved in the cycling of carbon, nitrogen, sulphur, phosphorus, etc., particularly at redox interfaces where metabolic flexibility becomes an ecological currency (Bazylinski & Blakemore, 1983; Bazylinski et al., 2004; Goswami et al., 2025; Isambert et al., 2007; Jiang et al., 2002; Jogler et al., 2010; Kolinko et al., 2012; Lefèvre et al., 2011; Li et al., 2020; Lin et al., 2014, 2017, 2018; Monteil et al., 2020; Qian et al., 2020; Rivas-Lamelo et al., 2017; Schultheiss et al., 2005; Schulz-Vogt et al., 2019). Early evidence of MTB in marine systems came from studies that detected magnetite-producing bacteria in hemipelagic and deep-sea sediments (Petermann and Bleil, 1993; Stolz et al., 1986). More recently, metagenomic approaches have expanded our view of MTB presence in diverse marine niches, including tropical coastal regions and deep volcanic arcs (Liu et

al., 2017; Tan et al., 2021; Xu et al., 2018). Notably, many MTB appear to co-localise with redox gradients, a spatial preference that overlaps with OMZ physicochemical conditions. However, their taxonomic scope, ecological roles and contributions to OMZ-specific biogeochemistry remain under-characterised.

In this study, we use genome-resolved metagenomics to explore systematically the presence, diversity and metabolic potential of MTB within global OMZ metagenomes. We use metagenomic analyses of global OMZ datasets to identify MTB MAGs and ascertain their functional capabilities for biogeochemical cycling, in order to assess the role of MTB in OMZs. This extensive characterisation of putative MTB from OMZs seeks to expand the ecological and phylogenetic boundaries of magnetotaxis in understanding MTB as contributors to marine biogeochemistry in low-oxygen environments.

MATERIALS AND METHODS

Data Acquisition, Quality Control, Preliminary Assembly and Annotation

In this study, 101 Sequence Read Archives (SRA) associated with OMZs were downloaded from the European Nucleotide Archive (ENA). The search was conducted using the keyword “oxygen minimum zone” to target bacterial datasets from global low-oxygen environments (Supplementary table S1). After downloading the raw sequencing data, quality control was conducted using metaWRAP v1.1.5 (Uritskiy et al., 2018). The read_qc module was employed with the ‘--skip-bmtagger’ flag to remove low-quality reads and to trim adapter sequences, ensuring high-quality data for subsequent analyses. The high-quality reads were then assembled into contigs using the MEGAHIT v1.0 assembler (Li et al., 2015), integrated within the metaWRAP pipeline. A minimum contig length of 2000 bp (‘-l 2000’) was set to avoid smaller, potentially less reliable contigs and focus on more substantial sequences.

Magnetosome Gene Cluster (MGC) Screening and Annotation

Following assembly, the data pool was reduced by filtering contigs that did not align with known MTB proteins. This was enabled by MagCluster v0.2.11 (Ji et al., 2022), which identifies and annotates MGCs. These consist of genes responsible for the synthesis and organisation of magnetosomes, the key organelles that enable magnetotactic bacteria to align with the Earth's magnetic field. MagCluster is a three-step process, the first step being genome annotation using Prokka v1.13.4 (Seemann, 2014), which assigns functional annotations to predicted genes based on homology. An e-value threshold of 1e-05 was used to ensure the accuracy of the gene predictions. The mgc_screen module of MagCluster is the second step to identify putative MGCs. The presence of magnetosome genes such as *mam, man*, and *mad*, which are key to magnetosome formation, are manually verified by comparison with known MTB genomes. The MGCs can be visualised and compared across different genomes using clinker v0.0.21 (Gilchrist and Chooi, 2021), which is the third and final step, and this allows for the graphical representation of synteny and gene cluster organisation.

Reassembly of the Reduced Data Pool, Genome Binning and Bin Refinement

To improve genome resolution, the reduced pool, which contained contigs associated with magnetotactic bacteria, was reassembled using metaSPAdes (Nurk et al., 2017), to improve the contiguity and quality of the genomes associated with magnetosome gene clusters. After reassembly, the resulting contigs were subjected to genome binning to group the contigs into distinct microbial genomes. Genome binning was carried out using the metaWRAP Binning module, which integrates three binning algorithms: MaxBin2 (Wu et al., 2016), MetaBAT2 (Kang et al., 2019), and CONCOCT (Alneberg et al., 2014). Each of these tools utilizes different approaches, such as sequence composition (GC

content) and coverage depth across samples, to cluster contigs into coherent bins representing individual microbial genomes. After binning, the resulting bins were refined using Bin_refinement, a module in metaWRAP. Bins with ≥ 50% completeness and ≤ 10% contamination ('-c 50 -x 10') were retained, ensuring that only high- and medium-quality MAGs were included in subsequent analyses.

MGC Screening and Annotation, Genome Quality Assessment and Dereplication

MGC screening and annotation were carried out again as described above with an additional check. Putative magnetosome protein sequences are compared against the NCBI non-redundant (nr) protein sequence database. This is achieved by using the NCBI Blast+ suite v2.12.0 Position-Specific Iterated (PSI-BLAST) algorithm, where the number of iterations was set to 1 (-num_iterations 1). All results obtained after PSI-BLAST for all putative magnetosome proteins were checked manually, with visualisation carried out using clinker.

Putative MGC-containing assembled genomes were then evaluated for quality using CheckM v1.0.12 (Parks et al., 2015), which estimates genome completeness and contamination by identifying single-copy marker genes. Genomes that met the ≥ 70% completeness and ≤ 10% contamination thresholds were included for further analysis. To reduce redundancy and to ensure that unique genomes were analysed, dereplication was performed using dRep v3.4.0 (Olm et al., 2017). dRep clusters genomes based on ANI, which measures the genetic similarity between genomes. A 90% ANI threshold is used for clustering, ensuring that closely related genomes are grouped, and only a non-redundant representative was selected for further analysis.

Taxonomic Classification and Relative Abundance Estimation

The non-redundant genomes identified through dereplication were taxonomically classified using GTDB-Tk v2.1.0 (Chaumeil et al., 2020),

which references the Genome Taxonomy Database (GTDB) for classification. The taxonomic placement of each genome provided insights into their evolutionary relationships with other known magnetotactic bacterial MAGs.

To estimate the relative abundance of MGC-containing MAGs across OMZ samples, high-quality paired-end sequencing reads from all 101 OMZ-associated metagenomes were mapped to the 30 MGC-containing bacterial MAGs using Bowtie2 v2.4.4 (Langmead and Salzberg, 2012). An index was constructed from the combined contig file using the bowtie2-build function. Each sample's reads were aligned to this indexed reference using the bowtie2 command in paired-end mode with default parameters. SAM output files from Bowtie2 were subsequently converted to BAM format, sorted, and indexed using SAMtools v1.15.1 (Li et al., 2009). These BAM files were then used as input for Anvi'o v7.1 (Eren et al., 2021) profiling. The anvi-profile command was executed for each sample with the corresponding BAM file and contigs.db, generating individual profile databases for downstream abundance analysis. Relative abundance values were calculated by Anvi'o as the proportion of reads mapped to each contig normalized by contig length and sequencing depth. For genome-level abundance estimation, contig-level abundances were aggregated by MAG using the anvi-merge and anvi-summarize modules. Final relative abundance values were tabulated and visualised at the phylum level using Python (matplotlib v3.5.2 (https://matplotlib.org/), seaborn v0.11.2 (https://seaborn.pydata.org/)) to show taxonomic distribution across various depth intervals (100–600 m).

ANI Estimation and Phylogenomic Analysis of Six High-confidence MGC-containing Bacterial MAGs

To assess the genomic similarity among the six high-confidence MGC-containing bacterial genomes in the dataset, Average Nucleotide Identity (ANI) was performed using FastANI (Jain et al., 2018). ANI is

a widely accepted metric for species delineation in prokaryotic taxonomy, with a threshold of 95-96% ANI typically used to classify genomes as belonging to the same species (Chun et al., 2018). A diverse set of bacterial genomes were analysed, including 23 references identified from "Taxonomy Tree" of GTDBtk's website (https://gtdb.ecogenomic.org/tree) and the six high-confidence MGC-containing bacterial MAGs identified after MagCluster. The ANI heatmap was visualised using PairwiseANIviz (Ji et al., 2024), where hierarchical clustering was applied to group highly similar genomes. The colour gradient in the heatmap was adjusted to highlight high-identity clusters, particularly those with ANI ≥ 98%, to identify potential closely related strains.

To investigate the evolutionary placement of the six high-confidence MGC-containing MAGs, a phylogenomic tree was generated using the anvi'o platform (Eren et al., 2021). Twenty-four reference genomes were considered for this analysis based on close proximity from the GTDB website's "Taxonomy Tree" (https://gtdb.ecogenomic.org/tree). Genome FASTA files (both for MAGs and reference genomes) were first converted into anvi'o-compatible contigs databases. A genomes storage database was then created from these using anvi-gen-genomes-storage. To identify conserved phylogenetic markers, HMM searches were run for bacterial single-copy core genes using anvi'o's default bacterial HMM profile. Protein sequences of these markers were extracted and concatenated across all genomes. This concatenated alignment was used to construct a maximum likelihood tree using FastTree2 (Price et al., 2010), implemented through anvi-gen-phylogenomic-tree. The resulting tree was visualised using iTOL (Letunic and Bork, 2021).

Metabolic Pathway Prediction of Potential MGC-containing Bacterial MAGs

The metabolic capacity of the six high-confidence MGC-containing bacterial genomes were assessed using KofamScan v1.3.0 (Aramaki et al., 2020), that assigned KEGG Orthology (KO) terms to protein-coding genes. Key metabolic pathways of interest, such as carbon fixation, nitrogen metabolism, and sulphur cycling, were focused on. The completeness of these pathways was evaluated using KEGG-Decoder (Graham et al., 2018), which allows for a detailed analysis of the functional capabilities of these genomes. For visualisation, the matrix was processed using Python (matplotlib v3.5.2 (https://matplotlib.org/), seaborn v0.11.2 (https://seaborn.pydata.org/) and pandas) to plot a bubble heatmap, where bubble size and colour indicate the presence and completeness of specific metabolic pathways across bins.

RESULTS

Global Distribution of OMZ Accession Numbers and Identification of Potential MGC-Containing Bacteria

To understand the spatial distribution of potential MGC-containing bacteria across marine OMZs, a global map was generated (Figure 1a) using the NOAA World Ocean Atlas 2023 (https://www.ncei.noaa.gov). The background heatmap depicts mean dissolved oxygen concentration (μmol/kg) at 300 m, illustrating the geographic distribution of accession numbers from OMZs analyzed in this study. The sizes of the bubbles correspond to the frequency of accessions at specific locations, while the colour gradient represents the mean sample depth, which spans from 100 m to 600 m. The highest concentration of accessions is observed in the Indian Ocean, particularly in the Arabian Sea region, where depths predominantly range between 300 m and 600 m. Additional regions with notable accession frequencies

include the Eastern Pacific and the Atlantic Ocean, though these are less densely represented.

The relationships between key environmental parameters and depth in OMZ regions are shown in Figure 1b, with bubble sizes reflecting the frequency of accessions at each depth. Salinity remains stable across depths, clustering between 35 and 36 PSU, particularly at 600 m. Oxygen levels are consistently low (<2 μmol/L) at all depths, highlighting the oxygen-depleted OMZs conditions. Nitrate concentrations peak at 600 m, supporting its role as an alternative electron acceptor in anaerobic microbial processes. Chlorophyll-a concentrations are higher at shallower depths (100-200 m), indicating active primary productivity near the surface, while temperature reveals a pronounced thermocline which stabilises around 12-15°C at 600 m. These gradients reflect the distinct environmental conditions under which microbial communities metabolise within OMZs.

Genome quality comparisons (Figure 2) reveal clear differences between high- and medium-quality bins. High-quality MAGs consistently have higher completeness scores and lower contamination, along with significantly larger genome sizes and higher N50 values, which indicate improved assembly continuity. These quality metrics are crucial in supporting the integrity of downstream analyses, including functional prediction and phylogenomic classification.

To reconstruct potential MGC-containing genomes from this dataset, a multi-step computational pipeline was implemented (Figure 3). Raw reads were first quality-checked and assembled, followed by genome binning using MetaBAT2 and MaxBin2, which generated 8,716 initial bins. Refinement using metaWRAP yielded 2,604 high- and medium-quality bins with ≥50% completeness and ≤10% contamination. These bins were screened for MGCs using MagCluster and PSI-BLAST against known magnetosome-associated genes (*mam*, *man*, *mad*, *mms*). This step identified 358 MGC-positive bins, which were further filtered using a manual keyword search (“mam”, “mad”, “man”, and

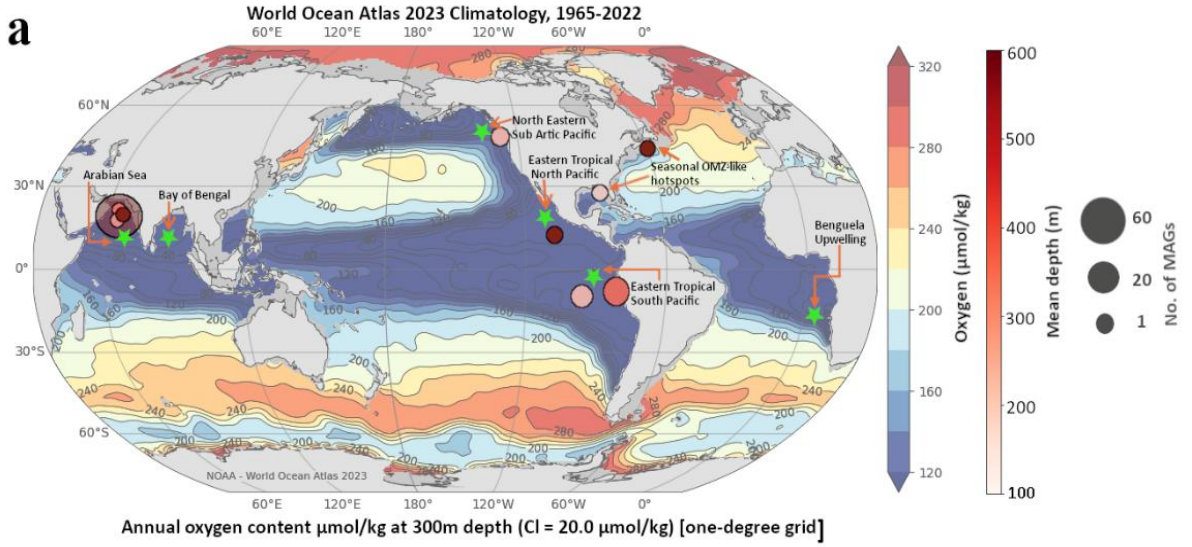

Figure 1: Global distribution and environmental parameters of the 101 SRA datasets. (a) Global distribution of the 101 SRA datasets from various OMZs used in this study. Circle size reflects the number of MAGs per site, and colour indicates average sampling depth. The background heatmap represents annual mean dissolved oxygen concentrations (µmol/kg) at 300 m water depth from the World Ocean Atlas 2023. Stars indicate key OMZ regions.

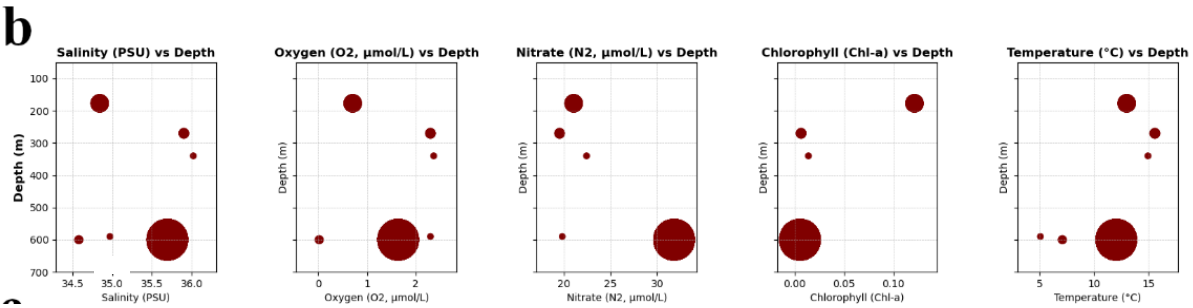

Figure 1: Global distribution and environmental parameters of the 101 SRA datasets. (b) Environmental parameters plotted by sampling depth. Salinity (PSU) remained stable (~35–36), oxygen was consistently low (<2 µmol/L), nitrate increased with depth, chlorophyll-a was enriched in surface waters, and temperature declined with increasing depth—typical characteristics of OMZ water.

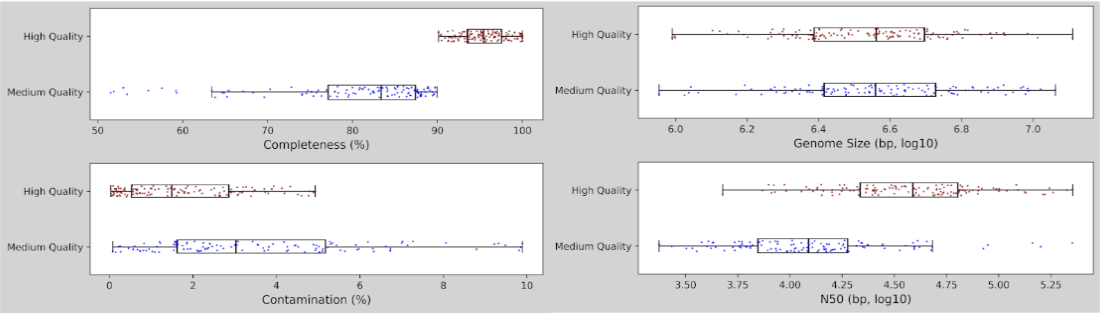

Figure 2: Box plots comparing genome quality metrics between high- and medium-quality MAGs from OMZ metagenomes. A total of 243 MAGs were evaluated using CheckM for completeness and contamination, and subsequently compared for genome size and N50 values. High-quality MAGs (≥90% completeness, ≤5% contamination) and medium-quality MAGs (≥50% completeness, ≤10% contamination) are visualised by completeness, contamination, estimated genome size, and N50 metrics. All values are plotted on a per-genome basis, with genome size and N50 shown in log10 scale.

"magnetosome"), resulting in 243 bins with putative magnetosome potential. To remove redundancy and improve taxonomic resolution, bins were dereplicated using dRep, ultimately yielding 97 non-redundant bins. These were then subjected to manual curation via clinker, where genomes were retained only if they contained at least three core non-redundant magnetosome genes with conserved synteny. After this final filtering round, 30 MAGs with putative magnetotactic genomes were recovered. This was filtered further to obtain a more stringent set of six high-confidence putative MTB MAGs.

Depth-Stratified Microbial Diversity and Taxonomic Classification of Potential MGC-containing Bacterial MAGs

The phylum-level distribution of 30 potential MGC-containing bacterial MAGs across depth gradients in OMZs was assessed to

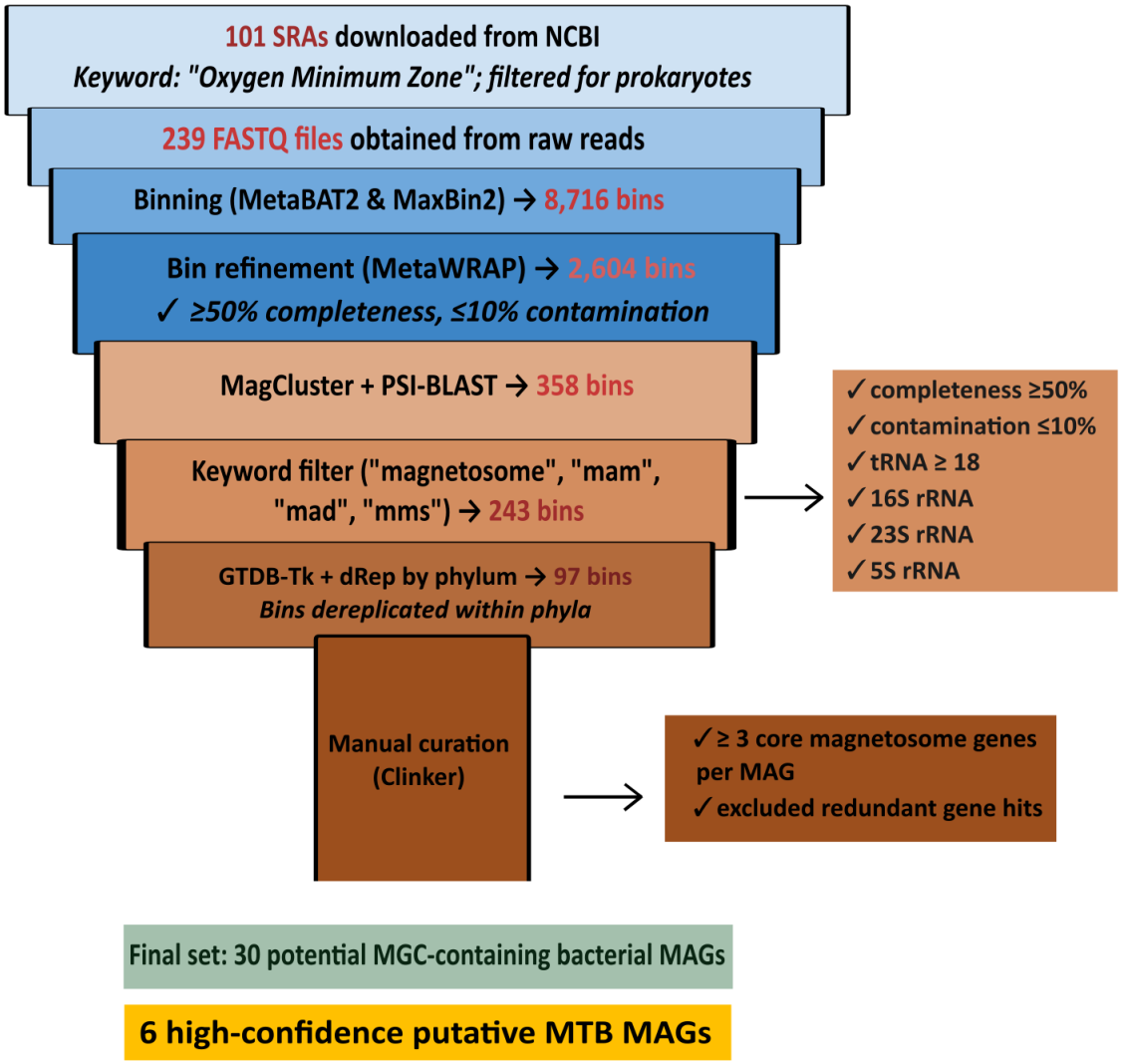

Figure 3: Overview of the bioinformatics pipeline used to recover and refine MGC-containing bacterial MAGs.

evaluate vertical ecological structuring (Figure 4). Distinct stratification patterns were observed, with marked shifts in community composition corresponding to specific depth intervals. At 130 m, the community is dominated overwhelmingly by *Nitrospinota*, whose prevalence sharply declines at greater depths, which suggests that this lineage may be confined to the upper OMZ redox gradient. In contrast, the relative abundance of *Pseudomonadota* increases steadily with depth, peaking at 340 m. This trend implies a broader ecological range for this phylum,

potentially facilitated by its metabolic versatility and capacity to thrive under oxygen-depleted, nitrate-enriched conditions. The mid-depth range (242–301 m) contains the highest taxonomic diversity, with phyla such as *Planctomycetota*, *Nitrospinota*, *Desulfobacterota* and *Actinomycetota*, as well as candidate lineages including *SM23-31*, *Zixibacteria* and *Krumholzibacteriota* also detected. By water depths of 590 m, a pronounced community structure shift was observed, with appearance of *Myxococcota* and a presence of *Bacteroidota*.

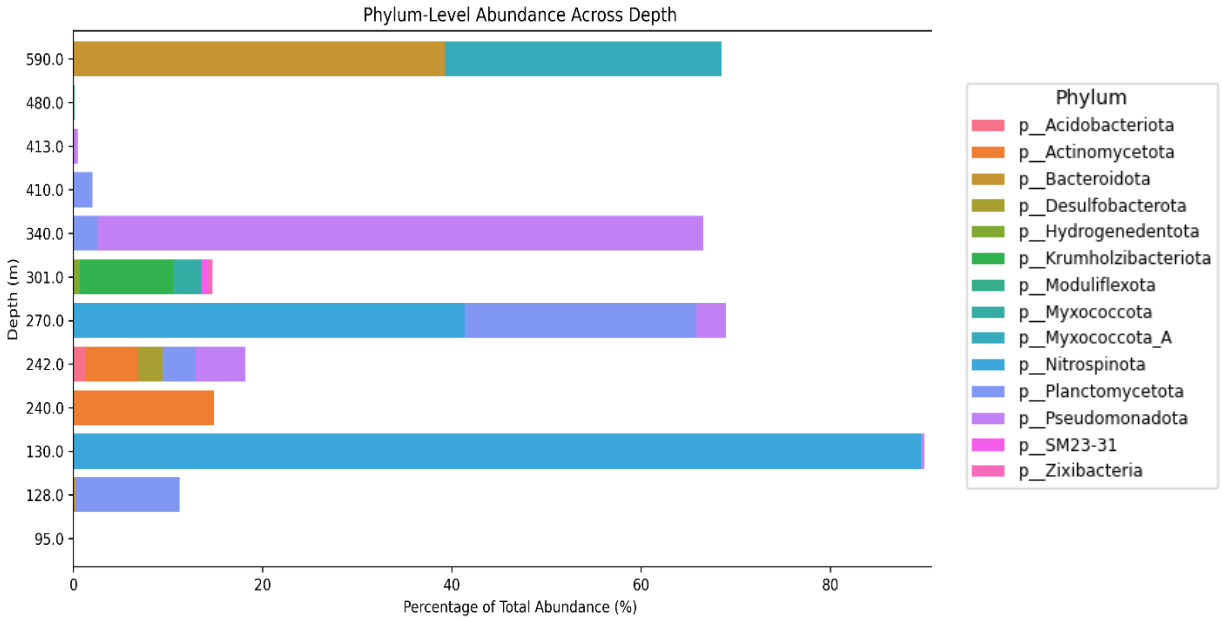

Figure 4: Phylum-level relative abundance and taxonomic classification of the 30 identified potential MGC-containing bacterial MAGs (a) Phylum-level relative abundance of the 30 potential MGC-containing bacterial MAGs at different depth intervals, highlighting variations in taxonomic composition with depth. Each phylum is represented by a distinct colour. Dominant taxa shift across depth gradients.

Taxonomic classification of 30 potential MGC-containing bacterial MAGs reveals broad phylogenetic diversity across 14 bacterial phyla (Table 1). In a Sankey diagram, the hierarchical taxonomic

classification of the six high-confidence MGC-containing bacterial MAGs is shown from phylum to genus level based on classifications assigned using GTDB-Tk v2.1.0 (Figure 5). Dominant contributions are observed from well-established MTB-hosting phyla, including *Planctomycetota* and *Pseudomonadota*. Within *Pseudomonadota*, members of both *Alphaproteobacteria* and *Gammaproteobacteria* classes are identified. Notably, MGC-containing representatives are also identified in a less-characterised phylum, *SM23-31*, previously not been recognised as hosts for magnetotactic lineages.

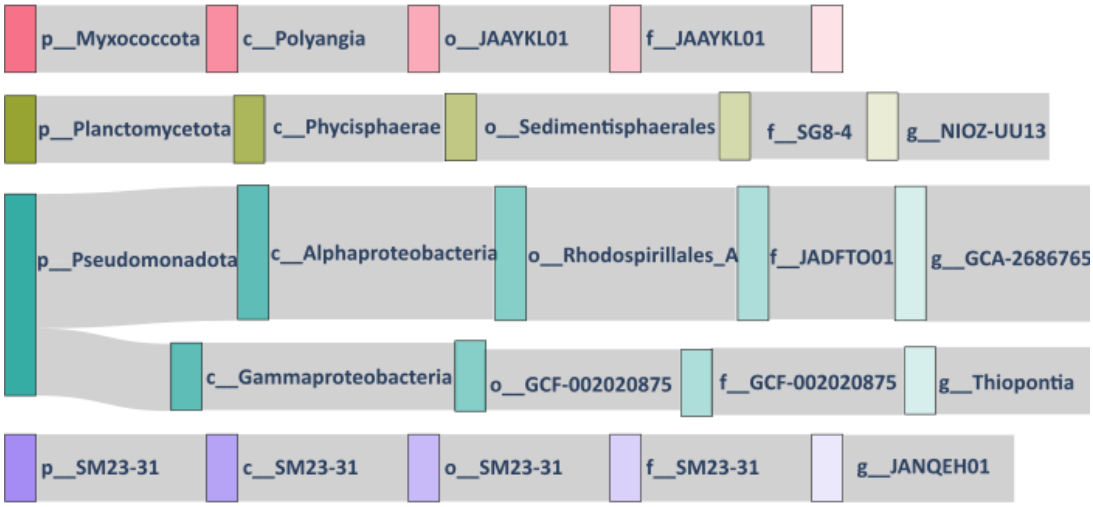

Figure 5: Taxonomic classification of the 6 high-confidence MGC-containing bacterial MAGs. Sankey diagram representing the hierarchical taxonomic classification of the 6 high-confidence MGC-containing bacterial MAGs, which illustrate relationships from phylum to genus level based on classifications assigned using GTDB-Tk v2.1.0.

Genera such as *JANQEH01*, *GCA-2686765* and *NIOZ-UU13* are detected as potentially novel. Recovery of potential MGC-containing MAGs from these phylogenetically distant and ecologically distinct lineages may underscore the evolutionary versatility of magnetotaxis in

OMZs and reveal OMZ environments as untapped reservoirs for discovering novel magnetotactic taxa.

Magnetosome Gene Cluster Architecture in Six High-Confidence MGC-containing MAGs

The structure and composition of the six high-confidence MGC-containing MAGs recovered from OMZ metagenomes were further examined. Candidate magnetosome genes, including *mam*, *mad*, *mms* and accessory elements, were identified using MagCluster, and verified using PSI-BLAST. Gene cluster organisation was visualised using clinker (Figure 6), enabling comparison of synteny and gene content across lineages. Bins classified under *Pseudomonadota* (*Proteobacteria*) are seen to include core magnetosome genes, such as *mamABEKMQOP*, with *mms6* and *mmsF* only seen in this taxonomic group. Certain bins, specifically ERR868468_bin.6 and SRR5271171_bin.39, contain nearly complete MGCs encompassing all core mam genes (*mamABEKMQOP*) alongside additional accessory components, offering high-confidence indicators of MTB functionality. Another complete MGC structure is observed in the *Myxococcota* bin SRR8144078_bin.14, which implies an almost certain MTB genome. MGCs are also identified in one phylum not previously known to harbour MTB, viz., *SM23-31*, which has unique and non-canonical MGC structures with partial or rearranged *mam* and *mad* gene components. These six MAGs, based on their confirmed MGC architecture, were subsequently subjected to phylogenomic analysis and metabolic reconstruction.

Species-Level Relatedness and Genome Novelty Revealed by ANI Clustering and Phylogenomic Tree

Pairwise ANI comparisons among the 29 selected genomes, including six high-confidence MGC-containing MAGs and 23 reference genomes, reveal species-level associations in some cases and significant genomic divergence in others, indicating the presence of potentially

novel lineages (Figure 7). Among the six MAGs, ERR868455_bin.1 and ERR868468_bin.6 have 98.6% ANI, which suggests that they represent closely related strains within the same species.

These two genomes also cluster with reference genomes assigned to *Pseudomonadota*, which is consistent with their GTDB-Tk taxonomic placement. Another high-confidence MAG, SRR5271171_bin.39, has a 99.7% ANI with GCA_018695175.1, which indicates that they likely belong to the same species. This close identity confirms that SRR5271171_bin.39 corresponds to a known isolate-level genome belonging to the genus *Thiopontia,* this genome may be classified as having an MTB lineage. In contrast, the remaining three genomes, viz., SRR8144078_bin.14, SRR8144078_bin.74 and SRR8144084_bin.89, lack ANI ≥95% with any reference genome in the dataset, which suggests that they may represent novel taxa.

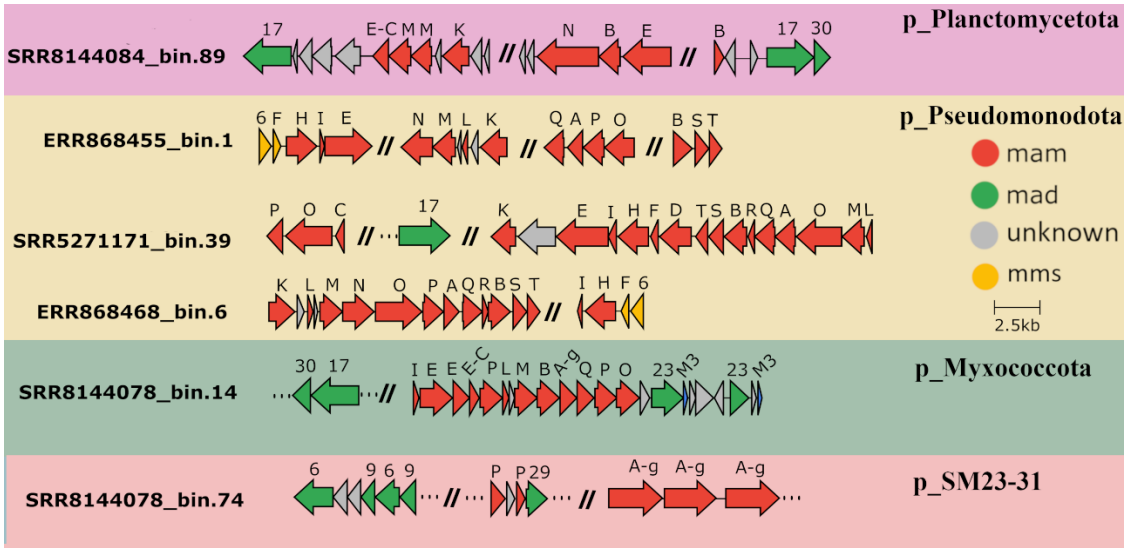

Figure 6: Clinker-based visualisation of magnetosome gene clusters in the six high-confidence MGC-containing bacterial MAGs. Red arrows represent *mam* genes, green arrows represent *mad* genes, yellow arrows indicate *mms* genes, and grey arrows denote unknown genes.

Specifically, SRR8144078_bin.74 has its highest ANI value (77.8%) with GCA_028278455.1, which falls well below the genus-level threshold. This points to the possibility that it represents a divergent lineage within the candidate phylum *SM23-31*. SRR8144078_bin.14 and SRR8144084_bin.89 do not exceed 80% ANI with any other genome, which further supports their status as genomically distinct and uncultured lineages within phyla *Myxococcota* and *Planctomycetota*, respectively.

To validate the species- and genus-level relationships inferred from ANI analysis, a maximum likelihood phylogenomic tree based on 71 bacterial single-copy marker genes was constructed to examine the evolutionary placement of the six high-confidence MGC-containing MAGs. The resulting phylogenomic tree (Figure 8) depicts the placement of the six high-confidence MAGs (shown in red) alongside known MTB reference genomes (magenta) and non-MTB genomes (black). Coloured boxes (top to bottom) indicate clades corresponding to different phyla: *SM23-31* lineage (pink), *Myxococcota* (yellow), *Planctomycetota* (green), and *Pseudomonadota* (blue). Notably, the six putative MTB MAGs cluster within these four phyla. The tree was rooted at Deltaproteobacterium nDJH15bin4.

Metabolic Capacity of the Six High-confidence MGC-containing MAGs

KEGG functional annotation of the six high-confidence MGC-containing MAGs reveals distinct patterns of carbon, energy, nitrogen and sulphur metabolism (Figure 9). Carbon metabolism was moderately represented across all six MAGs. Glycolysis metabolism is partially present in all genomes, which indicates a shared capacity for sugar catabolism. The TCA cycle is strongly represented only in SRR5271171_bin.39 (*g_Thiopontia*), while it is partially present in ERR868455_bin.1 (*p_Pseudomonadota*), ERR868468_bin.6 (*p_Pseudomonadota*), SRR8144078_bin.14 (*p_Myxococcota*) and SRR8144078_bin.74 (*p_SM23-31*). Notably, SRR8144078_bin.74 is the

only MAG with strong potential for gluconeogenesis, which suggests a unique ability to generate glucose from non-carbohydrate sources. Also, three MAGs, ERR868455_bin.1, ERR868468_bin.6 and SRR5271171_bin.39, harbour both RuBisCO and genes encoding the Calvin–Benson–Bassham (CBB) cycle, which indicate a genomic potential for autotrophic carbon fixation via the CBB pathway.

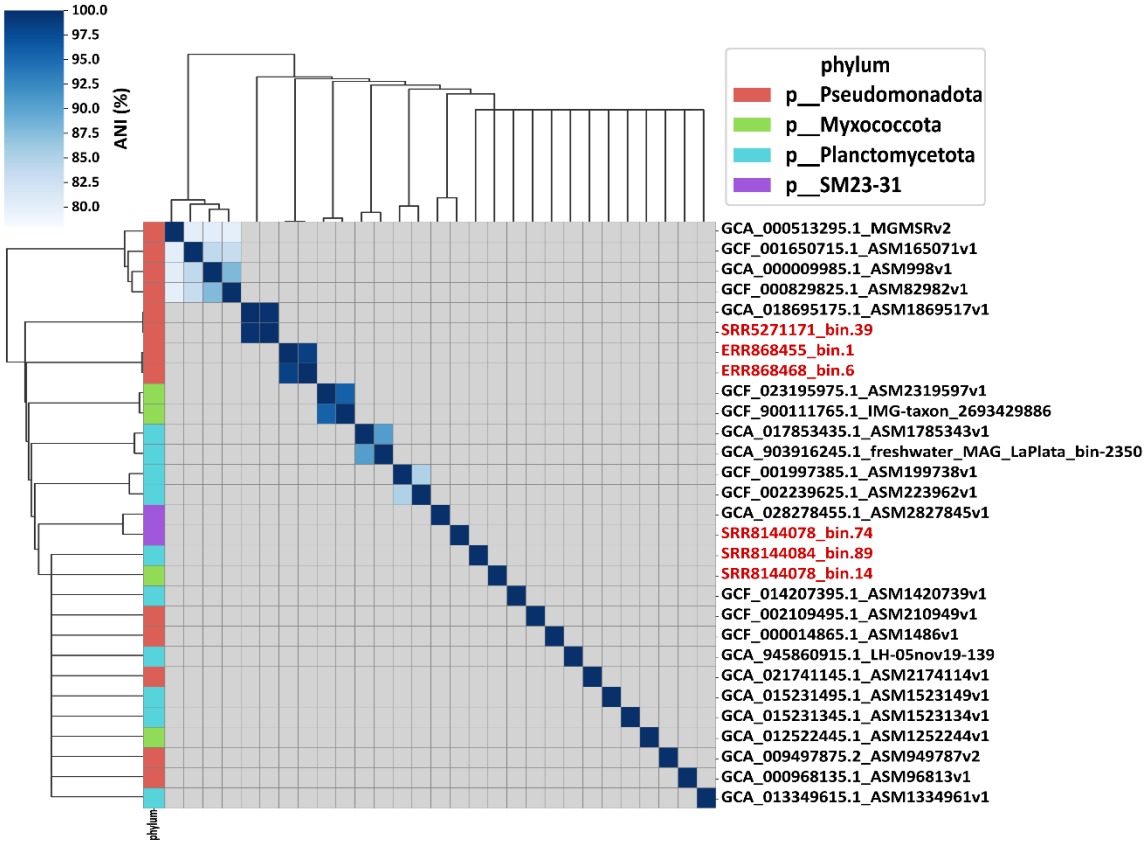

Figure 7: ANI heatmap with pairwise genomic similarity across bacterial genomes. The hierarchical clustering dendrogram groups genomes based on ANI values, with the colour gradient indicating sequence similarity, ranging from low (light blue) to high (deep blue). Genomes are annotated with their respective genus classifications, which are represented by coloured labels. High ANI values along the diagonal indicate intra-genus similarity, while off-diagonal patterns reveal inter-genus relationships.

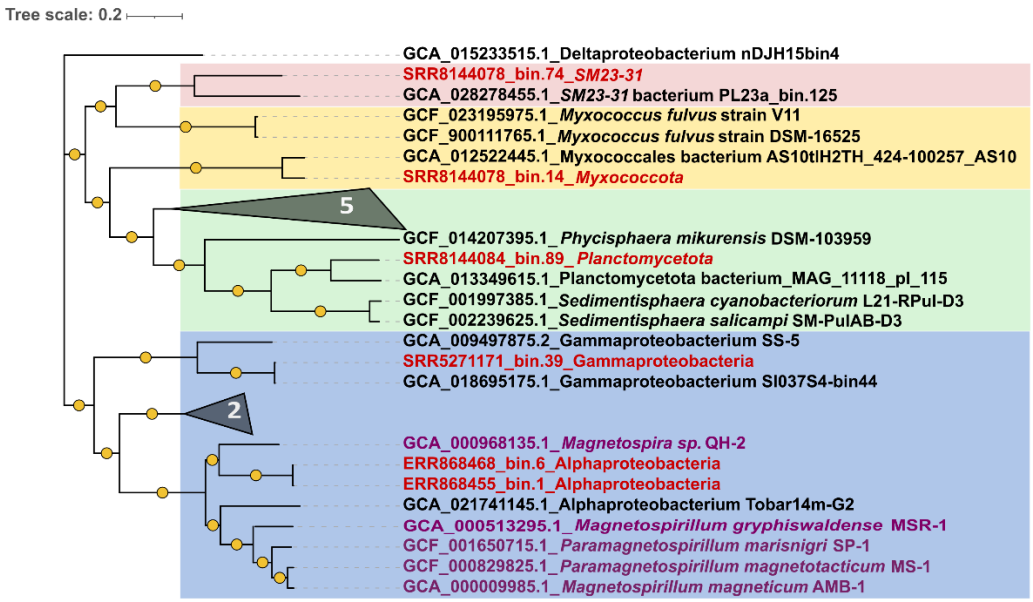

Figure 8: Maximum likelihood phylogenomic tree constructed from concatenated single-copy core genes with evolutionary placement of six high-confidence MGC-containing MAGs alongside reference MTB and non-MTB genomes. Coloured boxes indicate phylogenetic clusters at the phylum level: from top to bottom—*SM23-31* lineage, *Myxococcota*, *Planctomycetota* and *Pseudomonadota*. The six high-confidence MGC-containing MAGs recovered from OMZs are shown in red, known reference MTB genomes in magenta and non-MTB genomes in black. The tree is rooted at Deltaproteobacterium nDJH15bin4.

Energy metabolism pathways vary significantly. NADH-quinone oxidoreductase and F-type ATPase are strongly present in four genomes, ERR868455_bin.1, ERR868468_bin.6, SRR5271171_bin.39 and SRR8144078_bin.74, which indicates efficient electron transport and ATP synthesis capabilities. Cytochrome c oxidase, a terminal oxidase typically associated with aerobic respiration, is strongly present only in SRR5271171_bin.39. Given the oxygen-limited nature of OMZs, this suggests a potential for microaerophilic respiration, distinguishing this genome from its more anaerobically adapted counterparts. Interestingly, SRR8144084_bin.89 (p_Planctomycetota) also has strong potential for

hydroxylamine oxidation and Na-NADH-ubiquinone oxidoreductase, hinting at specialised or alternative energy pathways in this genome.

Nitrogen metabolism is most comprehensive in SRR5271171_bin.39, which has strong potential for dissimilatory nitrate-, nitrite- and nitrous-oxide-reduction, which suggests complete denitrification capacity. Partial denitrification is observed in ERR868455_bin.1 and ERR868468_bin.6, which are capable of strong nitrite reduction only. SRR8144078_bin.14 also has strong dissimilatory nitrate reduction capability, although without downstream denitrification steps. Notably, SRR8144084_bin.89 has strong potential for hydroxylamine oxidation, a key intermediate step in nitrification. Although canonical ammonia monooxygenase genes are absent, this suggests a possible role in nitrogen turnover through hydroxylamine scavenging or incomplete nitrification in redox-stratified OMZ environments. None of the genomes possessed genes indicative of nitrogen fixation.

Sulphur metabolism capability reveals functional divergence among the MAGs. SRR5271171_bin.39 has the most comprehensive sulphur profile, with strong presence of sulphide oxidation, dissimilatory sulphate reduction and thiosulphate oxidation. Both ERR868455_bin.1 and ERR868468_bin.6 also have strong potential for sulphide oxidation, with partial thiosulphate oxidation. In contrast, SRR8144078_bin.14 and SRR8144078_bin.74 harbour strong signatures of dissimilatory sulphate reduction but lack other sulphur oxidation genes, which suggests narrower sulphur metabolic capabilities.

CONCLUSIONS

OMZs are crucial oceanic regions for nutrient cycling and climate regulation. Microbial communities, including MTB, are vital for biogeochemical transformations of iron, nitrogen, sulphur and carbon. However, climate change is expanding OMZs, disrupting these

microbial processes with significant effects on marine ecosystems and global cycles. Rising ocean temperatures, increased stratification, and human nutrient inputs are depleting oxygen in midwater zones, leading to predicted growth of OMZs in the coming decades (Stramma et al., 2008). These changes will alter microbial communities and reshape nutrient flow and greenhouse gas emissions.

In this study, we provide a taxonomic and metabolic characterisation of putative MTB in OMZs. Using metagenomic analyses, 30 MGC-containing bacterial MAGs spanning 14 phyla (Table 1; asterisked bins are the high-confidence putative MTB MAGs) were identified, with a refined, more stringent set of six high-confidence MGC-containing MAGs (putative MTB) spanning four phyla, *Pseudomonadota*, *Planctomycetota*, *Myxococcota* and *SM23-31*. Functional predictions suggest that these organisms contribute to critical processes that influence oceanic carbon, nitrogen and sulphur fluxes. The presence of magnetosome-associated genes, although varying in completeness, suggests that magnetotaxis-driven niche specialisation plays a role in microbial adaptations to low-oxygen environments. In conclusion, this study provides a novel perspective on the taxonomic and functional diversity of putative MTB in OMZs. With magnetotaxis emerging as a widespread and ecologically significant trait, we are only beginning to unravel its implications in nutrient cycling, microbial biogeography and ecosystem dynamics. With accelerating ocean oxygenation changes, further research into these microbial processes is important, not only for understanding their role in marine biogeochemistry but also for predicting their responses to a rapid planetary change.

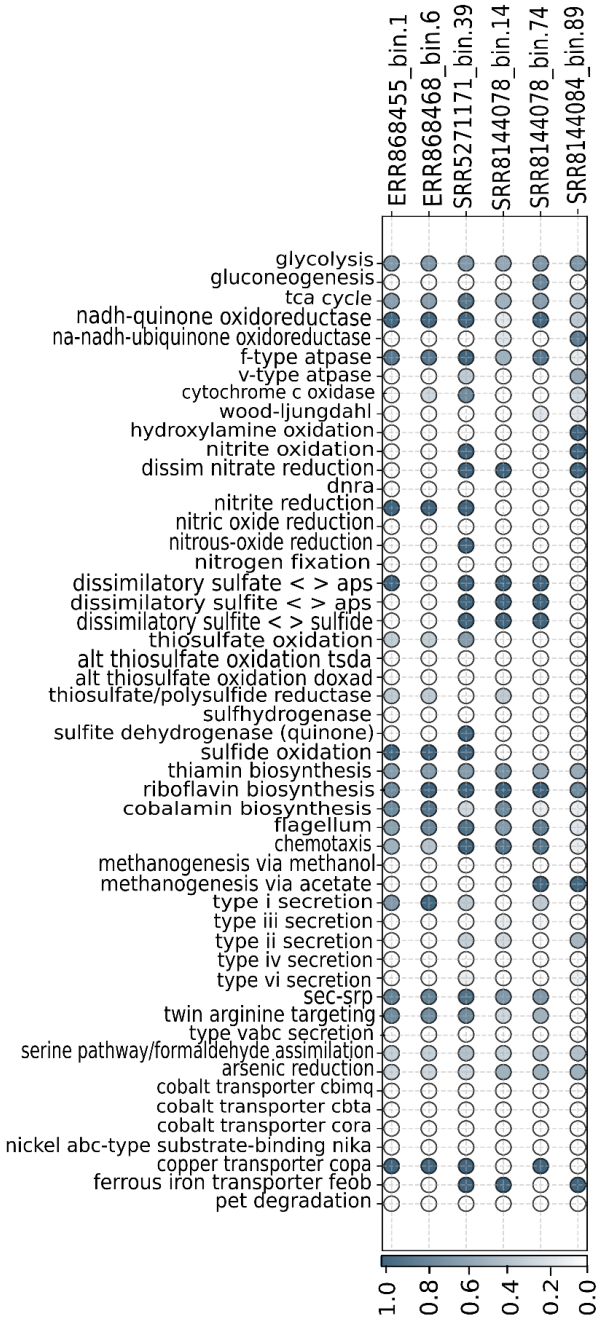

Figure 9: Functional capacity of the six high-confidence MGC-containing MAGs based on the presence of key metabolic pathways, electron transport systems and transporters. The intensity of filled circles represents the relative completeness of each function across genomes, from absent (white) to fully present (dark blue). Pathways such as glycolysis, the TCA cycle, nitrogen metabolism, sulphur oxidation and secretion systems have varying distributions, highlighting metabolic diversity across bacterial lineages.

Table 1: Genomic, taxonomic, and environmental metadata for thirty potential MGC-containing bacterial MAGs recovered from OMZ metagenomes.

MAG ID	Taxonomy	Completeness	Contamination	Biosample	Latitude (°)	Longitude (°)	Depth (m)
ERR868495_bin.9	d__Bacteria;p__Myxococcota_A;c__UBA9160;o__UBA9160;f__UBA4427;g__JAZXM01;s__	92.74	1.39	SAMEA2623667	39.0869	-70.0111	590
ERR599037_bin.10	d__Bacteria;p__Nitrospinota;c__Nitrospinia;o__Nitrospinales;f__VA-1;g__Nitromaritima;s__Nitromaritima sp003451695	96.43	0.72	SAMEA2620097	18.7341	66.3896	270
ERR868353_bin.40	d__Bacteria;p__Pseudomonadota;c__Gammaproteobacteria;o__GCA-2729495;f__GCA-2729495;g__GCA-002729875;s__GCA-002729875 sp002688175	94.98	0.21	SAMEA2620043	18.9918	64.5757	340
ERR868353_bin.6	d__Bacteria;p__Planctomycetota;c__Phycisphaerae;o__Phycisphaerales;f__Phycisphaeraceae;g__;s__	93.5	1.8	SAMEA2620043	18.9918	64.5757	340
*ERR868455_bin.1	d__Bacteria;p__Pseudomonadota;c__Alphaproteobacteria;o__Rhodospirillales_A;f__JADFTO01;g__GCA-2686765;s__GCA-2686765 sp013349695	92.67	1.55	SAMEA2620113	18.735	66.3895	270

Table 1: Genomic, taxonomic, and environmental metadata for thirty potential MGC-containing bacterial MAGs recovered from OMZ metagenomes (continued).

MAG ID	Taxonomy	Completeness	Contamination	Biosample	Latitude (°)	Longitude (°)	Depth (m)
*SRR5271171_bin.39	d__Bacteria;p__Pseudomonadota;c__Gammaproteobacteria;o__GCF-002020875;f__GCF-002020875;g__Thiopontia;s__Thiopontia sp013349825	95.74	0.27	SAMN06267773	48.6	-123.5	130
SRR8144075_bin.61	d__Bacteria;p__Actinomycetota;c__Acidimicrobiia;o__Acidimicrobiales;f__Microtrichaceae;g__JAAEPF01;s__JAAEPF01 sp024222295	97.22	0.97	SAMN10181161	-12	-77.5	240
*ERR868468_bin.6	d__Bacteria;p__Pseudomonadota;c__Alphaproteobacteria;o__Rhodospirillales_A;f__JADFTO01;g__GCA-2686765;s__GCA-2686765 sp013349695	91.34	0.23	SAMEA2620113	18.735	66.3895	270
SRR8144077_bin.147	d__Bacteria;p__Krumholzibacteriota;c__Krumholzibacteria;o__LZORAL124-64-63;f__LZORAL124-64-63;g__JAAEQC01;s__JAAEQC01 sp024231905	96.03	0.77	SAMN10181162	-12	-77.5	301
*SRR8144078_bin.14	d__Bacteria;p__Myxococcota;c__Polyangia;o__JAAYKL01;f__JAAYKL01;g__;s__	92.22	3.94	SAMN10181162	-12	-77.5	301

Table 1: Genomic, taxonomic, and environmental metadata for thirty potential MGC-containing bacterial MAGs recovered from OMZ metagenomes (continued).

MAG ID	Taxonomy	Completeness	Contamination	Biosample	Latitude (°)	Longitude (°)	Depth (m)
SRR8144085_bin.3	d__Bacteria;p__Planctomycetota;c__Planctomycetia;o__Pirellulales;f__Pirellulaceae;g__;s__	91.66	4.77	SAMN10181158	-12	-77.5	128
*SRR8144085_bin.39	d__Bacteria;p__Bacteroidota;c__Bacteroidia;o__Bacteroidales;f__SMBSF77;g__SMBSF77;s__	91.22	0.84	SAMN10181158	-12	-77.5	128
SRR8144087_bin.56	d__Bacteria;p__Acidobacteriota;c__Polarisedimenticolia;o__Polarisedimenticolales;f__Polarisedimenticolaceae;g__JAAELQ01;s__JAAELQ01 sp024226515	99.39	3.2	SAMN10181157	-12	-77.5	242
SRR8144087_bin.7	d__Bacteria;p__Planctomycetota;c__Phycisphaerae;o__Phycisphaerales;f__SM1A02;g__JAAELP01;s__JAAELP01 sp024226535	93.94	1.47	SAMN10181157	-12	-77.5	242
SRR8144088_bin.56	d__Bacteria;p__Actinomycetota;c__Acidimicrobiia;o__Acidimicrobiales;f__Poriferisodaliceae;g__JAAETH01;s__JAAETH01 sp024228575	97.18	4.89	SAMN10181157	-12	-77.5	242

Table 1: Genomic, taxonomic, and environmental metadata for thirty potential MGC-containing bacterial MAGs recovered from OMZ metagenomes (continued).

MAG ID	Taxonomy	Completeness	Contamination	Biosample	Latitude (°)	Longitude (°)	Depth (m)
ERR868468_bin.17	d__Bacteria;p__Planctomycetota;c__Planctomycetia;o__Pirellulales;f__Pirellulaceae;g__ARS98;s__ARS98 sp030744095	91.96	4.13	SAMEA2620113	18.735	66.3895	270
SRR10556723_bin.69	d__Bacteria;p__Acidobacteriota;c__UBA890;o__UBA890;f__UBA890;g__UBA890;s__UBA890 sp002722645	95.17	1.79	SAMN09202732	20.3333	107	
*SRR8144078_bin.74	d__Bacteria;p__SM23-31;c__SM23-31;o__SM23-31;f__SM23-31;g__JANQEH01;s__	94.41	1.64	SAMN10181162	-12	-77.5	301
*SRR8144084_bin.89	d__Bacteria;p__Planctomycetota;c__Phycisphaerae;o__Sedimentisphaerales;f__SG8-4;g__NIOZ-UU13;s__	90.9	2.22	SAMN10181159	-12	-77.5	410
SRR5271171_bin.17	d__Bacteria;p__Nitrospinota;c__Nitrospinia;o__Nitrospinales;f__VA-1;g__LS-NOB;s__LS-NOB sp018653085	95.16	0.16	SAMN06267773	48.6	-123.5	130

Table 1: Genomic, taxonomic, and environmental metadata for thirty potential MGC-containing bacterial MAGs recovered from OMZ metagenomes (continued).

MAG ID	Taxonomy	Completeness	Contamination	Biosample	Latitude (°)	Longitude (°)	Depth (m)
SRR8144084_bin.77	d__Bacteria;p__Planctomycetota;c__Brocadia;o__Brocadiales;f__Bathyanammoxibiaceae;g__Bathyanammoxibius;s__	94.05	0.99	SAMN10181159	-12	-77.5	410
SRR8144080_bin.55	d__Bacteria;p__Pseudomonadota;c__Gammaproteobacteria;o__GCA-001735895;f__GCA-001735895;g__GCA-001735895;s__GCA-001735895 sp024222685	91.23	1.39	SAMN10181165	-12	-77.5	413
ERR868495_bin.10	d__Bacteria;p__Bacteroidota;c__Bacteroidia;o__Flavobacteriales;f__Flavobacteriaceae;g__Zunongwangia;s__Zunongwangia profunda	93.76	1.09	SAMEA2623667	39.0869	-70.0111	590
SRR8144087_bin.122	d__Bacteria;p__Pseudomonadota;c__Gammaproteobacteria;o__GCA-001735895;f__GCA-001735895;g__GCA-001735895;s__GCA-001735895 sp024224415	98.03	1.7	SAMN10181157	-12	-77.5	242

Table 1: Genomic, taxonomic, and environmental metadata for thirty potential MGC-containing bacterial MAGs recovered from OMZ metagenomes (continued).

MAG ID	Taxonomy	Completeness	Contamination	Biosample	Latitude (°)	Longitude (°)	Depth (m)
SRR12431144_bin.40	d__Bacteria;p__Nitrospinota;c__Nitrospinia;o__Nitrospinales;f__VA-1;g__Nitromaritima;s__Nitromaritima sp003451695	93.55	1.05	SAMN15793615	18.9	-104.9	
SRR13374099_bin.18	d__Bacteria;p__Desulfobacterota;c__DSM-4660;o__Desulfatiglandales;f__Desulfatiglandaceae;g__NaphS2;s__NaphS2 sp016844935	93.11	3.27	SAMN17197931	27.28748	-83.1613	95
SRR8144088_bin.62	d__Bacteria;p__Desulfobacterota;c__Desulfobacteria;o__Desulfobacterales;f__JAAELO01;g__JAAELO01;s__JAAELO01 sp024226555	96.74	2.07	SAMN10181157	-12	-77.5	242
SRR10556723_bin.26	d__Bacteria;p__Pseudomonadota;c__Alphaproteobacteria;o__Rhodospirillales_A;f__JADFTO01;g__GCA-2686765;s__GCA-2686765 sp013349695	92.84	1.61	SAMN09202732	20.3333	107	
SRR3718413_bin.11	d__Bacteria;p__Actinomycetota;c__Acidimicrobiia;o__Acidimicrobiales;f__Poriferisodaliceae;g__UBA2110;s__UBA2110 sp002388005	95.46	2.44	SAMN05192635	15	-95	

REFERENCES

Alneberg, J. et al. Binning metagenomic contigs by coverage and composition. Nat. Methods 11, 1144–1146 (2014).

Bazylinski, D. A. & Blakemore, R. P. Iron biomineralisation in prokaryotes: Magnetotactic bacteria. Met. Ions Biol. Syst. 21, 485–507 (1983).

Bazylinski, D. A. et al. Controlled biomineralisation of magnetite by magnetotactic bacteria. Adv. Biochem. Eng. Biotechnol. 96, 219–255 (2004).

Bazylinski, D. A. et al. Magnetosome formation and function in bacteria. Nat. Rev. Microbiol. 11, 623–636 (2013).

Bertagnolli, A. D. & Stewart, F. J. Microbial niches in marine oxygen minimum zones. Nat. Rev. Microbiol. 16, 723–729 (2018).

Bianchi, D., Babbin, A. R. & Galbraith, E. D. Enhancement of anammox by the excretion of diel vertical migrators. Nat. Geosci. 7, 167–173 (2012).

Breitburg, D. et al. Declining oxygen in the global ocean and coastal waters. Science 359, eaam7240 (2018).

Busecke, J. J. M., Abernathey, R., Levy, M. & Jullion, L. The structure of water mass transformation in the Southern Ocean. J. Phys. Oceanogr. 49, 113–134 (2019).

Callbeck, C. M. et al. Biogeochemical insights from metagenomics. Nat. Microbiol. 3, 1280–1290 (2018).

Callbeck, C. M. et al. Oxygen minimum zone microbial communities. ISME J. 15, 2514–2527 (2021).

Canfield, D. E., Glazer, B. T. & Falkowski, P. G. The evolution and future of Earth's nitrogen cycle. Science 330, 192–196 (2010).

Chaumeil, P. A., Mussig, A. J., Hugenholtz, P. & Parks, D. H. GTDB-Tk: A toolkit to classify genomes with the Genome Taxonomy Database. Bioinformatics 36, 1925–1927 (2020).

Chavez, F. P. & Messié, M. A comparison of eastern boundary upwelling ecosystems. Progr. Oceanogr. 83, 80–96 (2009).

Chun, J. et al. Proposed minimal standards for the use of genome data for the taxonomy of prokaryotes. Int. J. Syst. Evol. Microbiol. 68, 461–466 (2018).

Devol, A. H. Denitrification, anammox, and N_2 production in marine sediments. Annu. Rev. Mar. Sci. 7, 403–423 (2015).

Engel, A. et al. Preferential export of polysaccharide-rich organic matter from the surface ocean. Sci. Adv. 8, eabm6032 (2022).

Eren, A. M. et al. Community-led, integrated, reproducible multi-omics with anvi'o. Nat. Microbiol. 6, 3–6 (2021).

Flies, C. B., Peplies, J. & Schüler, D. Combined approach for analyzing the biodiversity of magnetotactic bacteria using PCR and FISH techniques. Appl. Environ. Microbiol. 71, 2723–2731 (2004).

Frankel, R. B., Bazylinski, D. A., Johnson, M. S. & Taylor, B. L. Magneto-aerotaxis in marine coccoid bacteria. Biophys. J. 73, 994–1000 (1997).

Gilchrist, C. L. M. & Chooi, Y. H. clinker & clustermap.js: Automatic generation of gene cluster comparison figures. Bioinformatics 37, 2473–2475 (2021).

Goswami, P. et al. Magnetotactic bacteria and magnetofossils: Ecology, evolution and environmental implications. npj Biofilms Microbiomes 11, 43 (2025).

Hansell, D. A. Recalcitrant dissolved organic carbon fractions. Annu. Rev. Mar. Sci. 5, 421–445 (2013).

Hansell, D. A., Carlson, C. A., Repeta, D. J. & Schlitzer, R. Dissolved organic matter in the ocean: A controversy stimulates new insights. Oceanography 22, 202–211 (2009).

Isambert, A. et al. Environmental constraints and genome reduction in symbiotic bacteria. Genome Res. 17, 1149–1154 (2007).

Jain, C. et al. High-throughput ANI analysis of 90K prokaryotic genomes reveals clear species boundaries. Nat. Commun. 9, 5114 (2018).

Ji, X. et al. Efficient metagenome-assembled genome quality assessment and improvement with MAGpurify2. Nat. Biotechnol. 42, 350–358 (2024).

Ji, X. et al. MAGpurify: A pipeline for improving metagenome-assembled genome quality using machine learning. Nat. Commun. 13, 7600 (2022).

Jiang, W. et al. Synthesis of nanocrystalline magnetite by magnetotactic bacteria. J. Biol. Chem. 277, 325–328 (2002).

Jiao, N. et al. Mechanisms of microbial carbon sequestration in the ocean—A synthesis of the microbial carbon pump. Nat. Rev. Microbiol. 8, 593–599 (2010).

Jogler, C. et al. Comparative analysis of magnetosome gene clusters in magnetotactic bacteria. Environ. Microbiol. 12, 2469–2477 (2010).

Kalvelage, T. et al. Aerobic microbial respiration in oceanic oxygen minimum zones. PLoS ONE 10, e0133526 (2015).

Kang, D. D. et al. MetaBAT 2: An adaptive binning algorithm for robust and efficient genome reconstruction from metagenome assemblies. PeerJ 7, e7359 (2019).

Karstensen, J., Stramma, L. & Visbeck, M. Oxygen minimum zones in the eastern tropical Atlantic and Pacific oceans. Progr. Oceanogr. 77, 331–350 (2008).

Keeling, R. F., Körtzinger, A. & Gruber, N. Ocean deoxygenation in a warming world. Annu. Rev. Mar. Sci. 2, 199–229 (2010).

Kolinko, S. et al. Genetic basis of iron biomineralisation in magnetotactic bacteria. Proc. Natl Acad. Sci. USA 109, 13536–13541 (2012).

Langmead, B. & Salzberg, S. L. Fast gapped-read alignment with Bowtie 2. Nat. Methods 9, 357–359 (2012).

Lavik, G. et al. Detoxification of sulphidic African shelf waters by blooming chemolithotrophs. Nature 457, 581–584 (2009).

Lefèvre, C. T. et al. Isolation and characterisation of a novel magnetotactic bacterium. Environ. Microbiol. 13, 538–553 (2011).

Letunic, I. & Bork, P. Interactive Tree Of Life (iTOL) v5: An online tool for phylogenetic tree display and annotation. Nucleic Acids Res. 49, W293–W296 (2021).

Levin, L. A. Manifestation, drivers, and emergence of open ocean deoxygenation. Annu. Rev. Mar. Sci. 10, 229–260 (2018).

Li, D., Liu, C. M., Luo, R., Sadakane, K. & Lam, T. W. MEGAHIT: An ultra-fast single-node solution for large and complex metagenomics

assembly via succinct de Bruijn graph. Bioinformatics 31, 1674–1676 (2015).

Li, H. et al. The Sequence Alignment/Map format and SAMtools. Bioinformatics 25, 2078–2079 (2009).

Li, Y. et al. Magnetotactic bacteria from hot springs. ISME J. 14, 2321–2333 (2020).

Lin, W. et al. Genomic expansion of magnetotactic bacteria reveals a higher number of magnetosome genes. Nat. Microbiol. 5, 794–802 (2020).

Lin, W., Jogler, C. & Schüler, D. Towards understanding magnetosome formation in magnetotactic bacteria. Nat. Rev. Microbiol. 16, 546–556 (2018).

Lin, W., Pan, Y., Bazylinski, D. A. & Wu, L. Recent advances in genomics of magnetotactic bacteria. Adv. Microb. Physiol. 71, 1–58 (2017).

Lin, W., Zhang, W., Zhao, X. & Pan, Y. Genomic insights into the uncultivated magnetotactic bacteria. Environ. Microbiol. Rep. 6, 524–531 (2014).

Liu, Y. et al. Comparative genomics of magnetotactic bacteria. Front. Microbiol. 8, 2514 (2017).

Long, A. M. et al. Microbial community dynamics and biogeochemical cycling across a seasonally anoxic fjord. Nat. Commun. 12, 2542 (2021).

Maßmig, M. et al. Community composition and function of microbial mats in cold marine hypersaline environments. Front. Microbiol. 11, 246 (2020).

Monteil, C. L. et al. Novel freshwater MTB and their genomic features. ISME J. 14, 2715–2731 (2020).

Nurk, S., Meleshko, D., Korobeynikov, A. & Pevzner, P. A. metaSPAdes: A new versatile metagenomic assembler. Genome Res. 27, 824–834 (2017).

Olm, M. R. et al. dRep: A tool for fast and accurate genomic comparisons that enables improved genome recovery from metagenomes through de-replication. ISME J. 11, 2864–2868 (2017).

Parks, D. H., Imelfort, M., Skennerton, C. T., Hugenholtz, P. & Tyson, G. W. CheckM: Assessing the quality of microbial genomes recovered from isolates, single cells, and metagenomes. Genome Res. 25, 1043–1055 (2015).

Paulmier, A. & Ruiz-Pino, D. Oxygen minimum zones (OMZs) in the modern ocean. Progr. Oceanogr. 80, 113–128 (2009).

Petermann, H. & Bleil, U. Detection of live magnetotactic bacteria in South Atlantic deep-sea sediments. Earth Planet. Sci. Lett. 117, 223–228 (1993).

Price, M. N., Dehal, P. S. & Arkin, A. P. FastTree 2—approximately maximum-likelihood trees for large alignments. PLoS ONE 5, e9490 (2010).

Qian, X. et al. Magnetosome diversity and environmental adaptations. Front. Microbiol. 11, 619644 (2020).

Rabalais, N. N. et al. Dynamics and distribution of natural and human-caused hypoxia. Biogeosciences 7, 585–619 (2010).

Resplandy, L. et al. Controls on oxygen distribution and net biological production in the North Pacific Ocean. Glob. Biogeochem. Cycles 26, GB2003 (2012).

Rivas-Lamelo, S. et al. Phylogenetic diversity of magnetotactic bacteria. Environ. Microbiol. 19, 449–460 (2017).

Schmidt, H. & Eggert, A. Ecophysiological modeling of the influence of light and nutrients on cyanobacterial blooms in shallow lakes. Ecol. Model. 320, 206–221 (2016).

Schmidtko, S., Stramma, L. & Visbeck, M. Decline in global oceanic oxygen content during the past five decades. Nature 542, 335–339 (2017).

Schultheiss, D. et al. Characterisation of uncultivated MTB from lake sediment. Environ. Microbiol. 7, 373–382 (2005).

Schulz-Vogt, H. N. et al. Magnetotactic bacteria in sulfidic environments. ISME J. 13, 239–252 (2019).

Seemann, T. Prokka: Rapid prokaryotic genome annotation. Bioinformatics 30, 2068–2069 (2014).

Stewart, F. J., Ulloa, O. & DeLong, E. F. Microbial metatranscriptomics in a permanent marine oxygen minimum zone. Environ. Microbiol. 14, 23–40 (2012).

Stolz, J. F., Chang, S. B. & Kirschvink, J. L. Magnetotactic bacteria and single-domain magnetite in hemipelagic sediments. Nature 321, 849–851 (1986).

Stramma, L., Johnson, G. C., Sprintall, J. & Mohrholz, V. Expanding oxygen-minimum zones in the tropical oceans. Science 320, 655–658 (2008).

Tan, T. et al. Genome reduction and environmental adaptation in magnetotactic bacteria. mSystems 6, e00796-21 (2021).

Thamdrup, B., Dalsgaard, T. & Revsbech, N. P. Widespread functional anoxia in the oxygen minimum zone of the Eastern South Pacific. Deep-Sea Res. I 65, 36–45 (2012).

Ulloa, O., Canfield, D. E., DeLong, E. F., Letelier, R. M. & Stewart, F. J. Microbial oceanography of anoxic oxygen minimum zones. Proc. Natl Acad. Sci. USA 109, 15996–16003 (2012).

Uritskiy, G. V., DiRuggiero, J. & Taylor, J. MetaWRAP—A flexible pipeline for genome-resolved metagenomic data analysis. Microbiome 6, 158 (2018).

Wakeham, S. G. Review: The distribution of organic compounds in the ocean. Mar. Chem. 224, 103814 (2020).

Wright, J. J., Konwar, K. M. & Hallam, S. J. Microbial ecology of expanding oxygen minimum zones. Nat. Rev. Microbiol. 10, 381–394 (2012).

Wu, Y. W., Simmons, B. A. & Singer, S. W. MaxBin 2.0: An automated binning algorithm to recover genomes from multiple metagenomic datasets. Bioinformatics 32, 605–607 (2016).

Xu, H. et al. Diversity of magnetotactic bacteria in China. Sci. Rep. 8, 144 (2018).

Chapter 6: Conclusions and Future Perspectives

INTRODUCTION

Ecological and genomic characterisation of MTB has long fascinated researchers due to their distinctive biological features and adaptive strategies. In this doctoral research, MTB from two geochemically contrasting and underexplored extreme aquatic environments have been explored: acidic peatland systems and oceanic OMZs. Although highly divergent in their physicochemical properties, these habitats share a key characteristic: they have steep redox gradients that provide ecological niches in which MTB thrive.

This study was driven by a need to address several knowledge gaps. These include the lack of cultivated or genome-resolved MTB representatives from acidic and redox stratified systems, limited insights into the functional potential of uncultivated MTB in OMZs, and a poor understanding of the ecological consequences of expanding OMZs on microbial biogeochemistry. Using a comprehensive set of methods, ranging from targeted magnetic enrichment and microscopy to metagenomic binning and phylogenomics, the research presented in this thesis makes novel contributions to the understanding of the taxonomy, metabolic function and environmental relevance of MTB.

SYNTHESIS OF MAJOR FINDINGS

Insights from Acidic Peatlands: A Novel MTB Genus and Species

A primary outcome of this thesis is the successful magnetic separation and characterisation of *Magnetominusculus dajiuhuensis* DJH-1^{Ts}, a previously unknown magnetotactic bacterium belonging to the phylum *Nitrospirota*. Isolated from the organic-rich acidic Dajiuhu Peatland in Central China (pH of 4.0 ± 0.2), *M. dajiuhuensis* DJH-1^{Ts} represents the first fully characterised MTB from such an environment. This strain has unique morphological traits, including its coccobacilli shape and distinctive magnetosome chain configuration, which were

revealed via scanning and transmission electron microscopy. Genome-resolved metabolic reconstruction shows that *M. dajiuhuensis* DJH-1^{Ts} possesses a nearly complete MGC, along with genomic potential for anaerobic carbon fixation via the Wood–Ljungdahl pathway, denitrification and dissimilatory sulphate reduction. These pathways suggest high metabolic versatility, enabling survival and activity in dynamic and redox-stratified peatland conditions. Moreover, FISH using a species-specific oligonucleotide probe, alongside 16S rRNA gene phylogeny, places *M. dajiuhuensis* DJH-1^{Ts} as a novel genus and species within the class *Thermodesulfovibrionia*.

This discovery expands the known diversity of magnetotactic *Nitrospirota* and highlights acidic peatlands as underappreciated biotopes for novel MTB. From a broader evolutionary perspective, the adaptive strategies observed in *M. dajiuhuensis* DJH-1^{Ts} underscore how magnetotaxis may have originated or been maintained in early Earth-like conditions characterised by acidity and anoxia.

Global Metagenomic Discovery of MTB in Oxygen Minimum Zones

A second core finding in this thesis arises from a metagenomic exploration of OMZs worldwide. Using 101 publicly available metagenomes from OMZs, a total of 30 potential MGC-containing bacterial MAGs were reconstructed, with a further, more stringent refinement based on MGC architecture, narrowing down the selection to six high-confidence putative MTB MAGs. These MAGs (putative MTB) span four phyla, with one novel lineage, *SM23-31*, previously not seen to harbour MTB. This extensive genome mining effort reveals a range of MGC architectures, differing in gene content, orientation and synteny. Importantly, most of the MAGs observed from OMZs encode functional genes for nitrate reduction, sulphur oxidation and/or reduction and in several cases, CO_2 fixation, which highlights their potential involvement in redox-sensitive biogeochemical cycling.

The presence of putative MTB in OMZs has significant ecological implications. As OMZs expand in both spatial extent and intensity due to climate-driven ocean deoxygenation, the niches available for MTB may likewise grow. MTB involvement in nitrogen and sulphur cycling could influence OMZ nutrient budgets, impact greenhouse gas production (e.g., N_2O), and alter sediment geochemistry through biomineralisation. Moreover, the potential for MTB to survive in anoxic OMZ water columns opens avenues for reevaluating their roles in oceanic element cycling.

SIGNIFICANCE OF THE FINDINGS

Integration of findings from Chapters 4 and 5 of this thesis offers compelling evidence for the remarkable adaptability, functional capacity and taxonomic breadth of MTB in two contrasting redox-stratified ecosystems. On one hand, acidic peatlands represent isolated, terrestrial microoxic/anoxic environments with high organic content and extreme pH, while OMZs typify expansive, marine suboxic zones with vertical stratification and variable salinity and pressure. Despite these differences, MTB in both habitats have convergent traits: tolerance to extreme environmental conditions and performance of biogeochemical roles in these niches.

From a methodological perspective, this work also underscores the value of combining 16S rRNA-based analysis with metagenomic profiling to obtain a fuller picture with which to characterise bacterial novelty. Successful magnetic separation and description of *M. dajiuhuensis* DJH-1^{Ts} validates the role of MTB under acidic, anoxic conditions, while the OMZ genome mining reveals an untapped diversity of uncultured MTB in marine settings. These complementary strategies provide a blueprint for future studies that aim to characterise magnetotactic microorganisms from other extreme or cryptic environments.

RESEARCH GAPS AND FUTURE DIRECTIONS

Despite significant advances in MTB research, major knowledge gaps persist regarding their ecological distribution, metabolic versatility and evolutionary development, particularly in extreme, transitional and underexplored habitats. Much of what we currently understand about MTB stems from studies on a limited number of cultivable strains derived from well-characterised freshwater and shallow marine sediments. In contrast, ecosystems such as acidic peatlands, hypersaline lagoons, hydrothermal vents and especially oceanic OMZs remain vastly undersampled. One prominent research frontier involves clarifying the functional roles of MTB in key biogeochemical processes, especially those involving nitrogen, sulphur and carbon. Emerging genomic and metagenomic evidence points to MTB involvement in denitrification, sulphate reduction, and CO_2 fixation pathways; however, experimental validation of these predictions remains limited. Quantifying the ecological impact of these processes is essential, particularly in redox-sensitive systems like OMZs, where MTB may act as natural agents of nutrient turnover and eutrophication mitigation. Given the increasing extent of OMZs due to global ocean deoxygenation, sampling MTB and understanding MTB-mediated nitrogen removal could inform ecosystem-based management strategies. Moreover, the prospect of MTB in accumulating heavy metals through both intracellular biomineralisation and extracellular sorption put them at the forefront as environmentally friendly bioremediation and pollutant recovery agents, aided by their magnetotactic ability that allows facile separation from aqueous environments.

In tandem with their modern ecological functions, MTB are also important geological agents, producing mineral remains known as magnetofossils. These fossilised magnetosomes serve as biosignatures that can inform paleoenvironmental, paleomagnetic and paleoclimatic reconstructions. However, the formation, preservation and detectability of these magnetofossils are still not fully understood. Factors such as sedimentary conditions, redox fluctuations and diagenesis influence the

integrity of MTB-derived magnetic signals. Therefore, future studies must seek to calibrate magnetofossil-based proxies with experimental and observational data across diverse sedimentary contexts.

Building on the findings of this thesis, several avenues for future research become apparent. Functional validation of MTB metabolic pathways under simulated environmental conditions is imperative. Multi-omics approaches, particularly transcriptomics, proteomics and in situ activity assays, should be deployed to confirm the expression and enzymatic activity of genes involved in nitrogen and sulphur cycling. Sampling and isolation efforts targeting OMZ-specific MTB lineages will help to gain deeper insights into their physiology and biogeochemical roles specific to marine systems. Moreover, time-series and depth-resolved sampling of MTB communities in OMZs and other transitional habitats could uncover temporal and spatial dynamics in their metabolic functions, population structure, and responses to environmental perturbations.

A further promising direction lies in exploring the paleoenvironmental implications of MTB. Unravelling information provided by MTB from non-traditional, extreme settings such as acidic peatlands, hypersaline lagoons and OMZs suggests that their magnetofossils could be preserved in corresponding sedimentary archives. Investigating these biosignatures could enhance reconstructions of historical redox conditions in early-Earth settings and may shed light on the origin and diversification of magnetotaxis in prokaryotes.

To conclude, MTB can provide insights into a unique intersection between microbiology, geochemistry and environmental science. They serve as both modern actors in biogeochemical cycles and ancient recorders of Earth's environmental history. Their ecological roles, especially in extreme and redox-stratified environments, are increasingly recognised as critical for understanding the resilience and adaptability of microbial life. As climate change and anthropogenic pressures continue to reshape aquatic ecosystems, MTB research stands at the frontier of microbial ecology, offering valuable insights into ecosystem functioning, environmental remediation and the evolutionary ingenuity of life.

Supplementary Table S1: Sequencing and biosample metadata for 101 OMZ metagenomes used in this study.

Accession	Study title	Library Layout	Biosample	Bioproject	Instrument	Total Size
ERR10123730	Malaspina Expedition 2010 Microbial Vertical Profiles Metagenomes	PAIRED	SAMEA110646526	PRJEB52452	Illumina HiSeq 2000	3.97E+09
ERR10123731	Malaspina Expedition 2010 Microbial Vertical Profiles Metagenomes	PAIRED	SAMEA110646526	PRJEB52452	Illumina HiSeq 2000	4.18E+09
ERR594345	Shotgun Sequencing of Tara Oceans DNA samples corresponding to size fractions for large DNA viruses	PAIRED	SAMEA2619974	PRJEB1788	Illumina HiSeq 2000	2.64E+10
ERR598946	Shotgun Sequencing of Tara Oceans DNA samples corresponding to size fractions for prokaryotes	PAIRED	SAMEA2622149	PRJEB1787	Illumina HiSeq 2000	1.51E+10
ERR598981	Shotgun Sequencing of Tara Oceans DNA samples corresponding to size fractions for prokaryotes	PAIRED	SAMEA2622149	PRJEB1787	Illumina HiSeq 2000	2.77E+09
ERR599037	Shotgun Sequencing of Tara Oceans DNA samples corresponding to size fractions for prokaryotes	PAIRED	SAMEA2620097	PRJEB1787	Illumina HiSeq 2000	1.33E+10
ERR868353	Shotgun Sequencing of Tara Oceans DNA samples corresponding to size fractions for protists	PAIRED	SAMEA2620043	PRJEB4352	Illumina HiSeq 2000	2.2E+10

Supplementary Table S1: Sequencing and biosample metadata for 101 OMZ metagenomes used in this study (continued).

ERR868453	Shotgun Sequencing of Tara Oceans DNA samples corresponding to size fractions for protists	PAIRED	SAMEA2622158	PRJEB4352	Illumina HiSeq 2000	1.77E+10
ERR868455	Shotgun Sequencing of Tara Oceans DNA samples corresponding to size fractions for protists	PAIRED	SAMEA2620113	PRJEB4352	Illumina HiSeq 2000	1.06E+10
ERR868468	Shotgun Sequencing of Tara Oceans DNA samples corresponding to size fractions for protists	PAIRED	SAMEA2620113	PRJEB4352	Illumina HiSeq 2000	1.69E+10
ERR868495	Shotgun Sequencing of Tara Oceans DNA samples corresponding to size fractions for protists	PAIRED	SAMEA2623667	PRJEB4352	Illumina HiSeq 2000	2.23E+10
SRR10556723	Marine microbial and viral communities from oxygen minimum zone, Eastern Pacific Ocean - ETNP2014_SV_400_PacBio MetaG metagenome	PAIRED	SAMN09202732	PRJNA465919	Illumina HiSeq 2500	2.98E+10
SRR10597568	Metagenome-assembled Genomes (MAGs)	SINGLE	SAMN13193013	PRJNA593905	Illumina HiSeq 2000	397482
SRR10597684	Metagenome-assembled Genomes (MAGs)	SINGLE	SAMN13193049	PRJNA593905	Illumina HiSeq 2000	311557

Supplementary Table S1: Sequencing and biosample metadata for 101 OMZ metagenomes used in this study (continued).

SRR12431144	Marine metagenome raw sequence reads	PAIRED	SAMN15793615	PRJNA632347	Illumina HiSeq 2000	5.47E+09
SRR13374099	Amberjack Blue Hole	PAIRED	SAMN17197931	PRJNA689047	Illumina MiSeq	3.76E+09
SRR3718413	Oceanic oxygen minimum zone microbial communities that regulate carbon cycling - Sample ETNP201406SV203	PAIRED	SAMN05192635	PRJNA323948	Illumina HiSeq 2500	4.54E+09
SRR5204552	Marine microbial communities from expanding oxygen minimum zones in the Saanich Inlet - SI037_S4LV_200m_DNA metagenome	PAIRED	SAMN06267774	PRJNA366996	Illumina HiSeq 2000	8.12E+09
SRR5271171	Marine microbial communities from expanding oxygen minimum zones in the Saanich Inlet - SI037_S2LV_130m_DNA metagenome	PAIRED	SAMN06267773	PRJNA366995	Illumina HiSeq 2500	1.26E+10
SRR5321577	Recovery of nearly 8,000 uncultivated bacterial and archaeal genomes substantially flesh out the tree of life	PAIRED	SAMN06450768	PRJNA348753	Illumina HiSeq 2000	97632465
SRR5321578	Recovery of nearly 8,000 uncultivated bacterial and archaeal genomes substantially flesh out the tree of life	PAIRED	SAMN06452187	PRJNA348753	Illumina HiSeq 2000	29264512

Supplementary Table S1: Sequencing and biosample metadata for 101 OMZ metagenomes used in this study (continued).

SRR5321579	Recovery of nearly 8,000 uncultivated bacterial and archaeal genomes substantially flesh out the tree of life	PAIRED	SAMN06457271	PRJNA348753	Illumina HiSeq 2000	5.72E+08
SRR5321580	Recovery of nearly 8,000 uncultivated bacterial and archaeal genomes substantially flesh out the tree of life	PAIRED	SAMN06452186	PRJNA348753	Illumina HiSeq 2000	32759567
SRR5321581	Recovery of nearly 8,000 uncultivated bacterial and archaeal genomes substantially flesh out the tree of life	PAIRED	SAMN06457264	PRJNA348753	Illumina HiSeq 2000	2.24E+08
SRR5321582	Recovery of nearly 8,000 uncultivated bacterial and archaeal genomes substantially flesh out the tree of life	PAIRED	SAMN06452185	PRJNA348753	Illumina HiSeq 2000	24065203
SRR5321583	Recovery of nearly 8,000 uncultivated bacterial and archaeal genomes substantially flesh out the tree of life	PAIRED	SAMN06452184	PRJNA348753	Illumina HiSeq 2000	33721924
SRR5321584	Recovery of nearly 8,000 uncultivated bacterial and archaeal genomes substantially flesh out the tree of life	PAIRED	SAMN06452183	PRJNA348753	Illumina HiSeq 2000	24422452

Supplementary Table S1: Sequencing and biosample metadata for 101 OMZ metagenomes used in this study (continued).

SRR5321585	Recovery of nearly 8,000 uncultivated bacterial and archaeal genomes substantially flesh out the tree of life	PAIRED	SAMN06457265	PRJNA348753	Illumina HiSeq 2000	2.55E+08
SRR5321586	Recovery of nearly 8,000 uncultivated bacterial and archaeal genomes substantially flesh out the tree of life	PAIRED	SAMN06452182	PRJNA348753	Illumina HiSeq 2000	70870068
SRR5321587	Recovery of nearly 8,000 uncultivated bacterial and archaeal genomes substantially flesh out the tree of life	PAIRED	SAMN06452189	PRJNA348753	Illumina HiSeq 2000	2.32E+08
SRR5321588	Recovery of nearly 8,000 uncultivated bacterial and archaeal genomes substantially flesh out the tree of life	PAIRED	SAMN06452181	PRJNA348753	Illumina HiSeq 2000	24039600
SRR5321589	Recovery of nearly 8,000 uncultivated bacterial and archaeal genomes substantially flesh out the tree of life	PAIRED	SAMN06452180	PRJNA348753	Illumina HiSeq 2000	21819315
SRR5321890	Recovery of nearly 8,000 uncultivated bacterial and archaeal genomes substantially flesh out the tree of life	PAIRED	SAMN06450619	PRJNA348753	Illumina HiSeq 2000	86826947

Supplementary Table S1: Sequencing and biosample metadata for 101 OMZ metagenomes used in this study (continued).

SRR5321891	Recovery of nearly 8,000 uncultivated bacterial and archaeal genomes substantially flesh out the tree of life	PAIRED	SAMN06457363	PRJNA348753	Illumina HiSeq 2000	77826594
SRR5321892	Recovery of nearly 8,000 uncultivated bacterial and archaeal genomes substantially flesh out the tree of life	PAIRED	SAMN06450621	PRJNA348753	Illumina HiSeq 2000	45925105
SRR5321893	Recovery of nearly 8,000 uncultivated bacterial and archaeal genomes substantially flesh out the tree of life	PAIRED	SAMN06450622	PRJNA348753	Illumina HiSeq 2000	50327791
SRR5321894	Recovery of nearly 8,000 uncultivated bacterial and archaeal genomes substantially flesh out the tree of life	PAIRED	SAMN06450623	PRJNA348753	Illumina HiSeq 2000	58378134
SRR5321895	Recovery of nearly 8,000 uncultivated bacterial and archaeal genomes substantially flesh out the tree of life	PAIRED	SAMN06450624	PRJNA348753	Illumina HiSeq 2000	28470334
SRR5321896	Recovery of nearly 8,000 uncultivated bacterial and archaeal genomes substantially flesh out the tree of life	PAIRED	SAMN06457369	PRJNA348753	Illumina HiSeq 2000	37434242

Supplementary Table S1: Sequencing and biosample metadata for 101 OMZ metagenomes used in this study (continued).

SRR5321897	Recovery of nearly 8,000 uncultivated bacterial and archaeal genomes substantially flesh out the tree of life	PAIRED	SAMN06450626	PRJNA348753	Illumina HiSeq 2000	31994697
SRR5321898	Recovery of nearly 8,000 uncultivated bacterial and archaeal genomes substantially flesh out the tree of life	PAIRED	SAMN06450627	PRJNA348753	Illumina HiSeq 2000	32315776
SRR5321899	Recovery of nearly 8,000 uncultivated bacterial and archaeal genomes substantially flesh out the tree of life	PAIRED	SAMN06455358	PRJNA348753	Illumina HiSeq 2000	60952049
SRR5321900	Recovery of nearly 8,000 uncultivated bacterial and archaeal genomes substantially flesh out the tree of life	PAIRED	SAMN06455357	PRJNA348753	Illumina HiSeq 2000	34281061
SRR5321901	Recovery of nearly 8,000 uncultivated bacterial and archaeal genomes substantially flesh out the tree of life	PAIRED	SAMN06454312	PRJNA348753	Illumina HiSeq 2000	39689023
SRR5321902	Recovery of nearly 8,000 uncultivated bacterial and archaeal genomes substantially flesh out the tree of life	PAIRED	SAMN06455355	PRJNA348753	Illumina HiSeq 2000	47825922

Supplementary Table S1: Sequencing and biosample metadata for 101 OMZ metagenomes used in this study (continued).

SRR5321903	Recovery of nearly 8,000 uncultivated bacterial and archaeal genomes substantially flesh out the tree of life	PAIRED	SAMN06455362	PRJNA348753	Illumina HiSeq 2000	25078331
SRR5321904	Recovery of nearly 8,000 uncultivated bacterial and archaeal genomes substantially flesh out the tree of life	PAIRED	SAMN06457361	PRJNA348753	Illumina HiSeq 2000	94413605
SRR5321905	Recovery of nearly 8,000 uncultivated bacterial and archaeal genomes substantially flesh out the tree of life	PAIRED	SAMN06455361	PRJNA348753	Illumina HiSeq 2000	1.4E+08
SRR5322040	Recovery of nearly 8,000 uncultivated bacterial and archaeal genomes substantially flesh out the tree of life	PAIRED	SAMN06455087	PRJNA348753	Illumina HiSeq 2000	2.27E+08
SRR5322041	Recovery of nearly 8,000 uncultivated bacterial and archaeal genomes substantially flesh out the tree of life	PAIRED	SAMN06455086	PRJNA348753	Illumina HiSeq 2000	2.12E+08
SRR5322042	Recovery of nearly 8,000 uncultivated bacterial and archaeal genomes substantially flesh out the tree of life	PAIRED	SAMN06455085	PRJNA348753	Illumina HiSeq 2000	1.35E+08

Supplementary Table S1: Sequencing and biosample metadata for 101 OMZ metagenomes used in this study (continued).

SRR5322043	Recovery of nearly 8,000 uncultivated bacterial and archaeal genomes substantially flesh out the tree of life	PAIRED	SAMN06455084	PRJNA348753	Illumina HiSeq 2000	1.05E+08
SRR5322044	Recovery of nearly 8,000 uncultivated bacterial and archaeal genomes substantially flesh out the tree of life	PAIRED	SAMN06455083	PRJNA348753	Illumina HiSeq 2000	82758115
SRR5322045	Recovery of nearly 8,000 uncultivated bacterial and archaeal genomes substantially flesh out the tree of life	PAIRED	SAMN06450342	PRJNA348753	Illumina HiSeq 2000	3.44E+08
SRR5322046	Recovery of nearly 8,000 uncultivated bacterial and archaeal genomes substantially flesh out the tree of life	PAIRED	SAMN06455082	PRJNA348753	Illumina HiSeq 2000	27998274
SRR5322047	Recovery of nearly 8,000 uncultivated bacterial and archaeal genomes substantially flesh out the tree of life	PAIRED	SAMN06455081	PRJNA348753	Illumina HiSeq 2000	43373587
SRR5322048	Recovery of nearly 8,000 uncultivated bacterial and archaeal genomes substantially flesh out the tree of life	PAIRED	SAMN06455080	PRJNA348753	Illumina HiSeq 2000	38555924

Supplementary Table S1: Sequencing and biosample metadata for 101 OMZ metagenomes used in this study (continued).

SRR5322049	Recovery of nearly 8,000 uncultivated bacterial and archaeal genomes substantially flesh out the tree of life	PAIRED	SAMN06450343	PRJNA348753	Illumina HiSeq 2000	2.13E+08
SRR5322050	Recovery of nearly 8,000 uncultivated bacterial and archaeal genomes substantially flesh out the tree of life	PAIRED	SAMN06455089	PRJNA348753	Illumina HiSeq 2000	78036361
SRR5322051	Recovery of nearly 8,000 uncultivated bacterial and archaeal genomes substantially flesh out the tree of life	PAIRED	SAMN06455088	PRJNA348753	Illumina HiSeq 2000	46202692
SRR5322052	Recovery of nearly 8,000 uncultivated bacterial and archaeal genomes substantially flesh out the tree of life	PAIRED	SAMN06451723	PRJNA348753	Illumina HiSeq 2000	54982085
SRR5322053	Recovery of nearly 8,000 uncultivated bacterial and archaeal genomes substantially flesh out the tree of life	PAIRED	SAMN06450344	PRJNA348753	Illumina HiSeq 2000	2.77E+08
SRR5322054	Recovery of nearly 8,000 uncultivated bacterial and archaeal genomes substantially flesh out the tree of life	PAIRED	SAMN06451724	PRJNA348753	Illumina HiSeq 2000	48020806

Supplementary Table S1: Sequencing and biosample metadata for 101 OMZ metagenomes used in this study (continued).

SRR5322055	Recovery of nearly 8,000 uncultivated bacterial and archaeal genomes substantially flesh out the tree of life	PAIRED	SAMN06451721	PRJNA348753	Illumina HiSeq 2000	12823896
SRR5322056	Recovery of nearly 8,000 uncultivated bacterial and archaeal genomes substantially flesh out the tree of life	PAIRED	SAMN06451722	PRJNA348753	Illumina HiSeq 2000	12594076
SRR5322057	Recovery of nearly 8,000 uncultivated bacterial and archaeal genomes substantially flesh out the tree of life	PAIRED	SAMN06451095	PRJNA348753	Illumina HiSeq 2000	15533820
SRR5322058	Recovery of nearly 8,000 uncultivated bacterial and archaeal genomes substantially flesh out the tree of life	PAIRED	SAMN06450349	PRJNA348753	Illumina HiSeq 2000	1.77E+08
SRR5322059	Recovery of nearly 8,000 uncultivated bacterial and archaeal genomes substantially flesh out the tree of life	PAIRED	SAMN06451738	PRJNA348753	Illumina HiSeq 2000	16877779
SRR5322060	Recovery of nearly 8,000 uncultivated bacterial and archaeal genomes substantially flesh out the tree of life	PAIRED	SAMN06450350	PRJNA348753	Illumina HiSeq 2000	1.83E+08

Supplementary Table S1: Sequencing and biosample metadata for 101 OMZ metagenomes used in this study (continued).

SRR5322061	Recovery of nearly 8,000 uncultivated bacterial and archaeal genomes substantially flesh out the tree of life	PAIRED	SAMN06451093	PRJNA348753	Illumina HiSeq 2000	1.89E+08
SRR5504447	Marine microbial and viral communities from oxygen minimum zone, Eastern Pacific Ocean - ETNP201306SV43 metagenome	PAIRED	SAMN06344130	PRJNA375524	Illumina HiSeq 2500	4.41E+09
SRR5504492	Marine microbial and viral communities from oxygen minimum zone, Eastern Pacific Ocean - ETNP201306PF43B metagenome	PAIRED	SAMN06344134	PRJNA375528	Illumina HiSeq 2500	5.23E+09
SRR5504493	Marine microbial and viral communities from oxygen minimum zone, Eastern Pacific Ocean - ETNP201302SV91 metagenome	PAIRED	SAMN06344136	PRJNA375530	Illumina HiSeq 2500	1.18E+10
SRR5504594	Marine microbial and viral communities from oxygen minimum zone, Eastern Pacific Ocean - ETNP201302SV89 metagenome	PAIRED	SAMN06344138	PRJNA375532	Illumina HiSeq 2500	4.23E+09

Supplementary Table S1: Sequencing and biosample metadata for 101 OMZ metagenomes used in this study (continued).

SRR5506557	Marine microbial and viral communities from oxygen minimum zone, Eastern Pacific Ocean - ETNP201310SV72 metagenome	PAIRED	SAMN06344148	PRJNA375542	Illumina HiSeq 2500	3.89E+09
SRR6482100	Collection of 3,087 bacterial metagenome-assembled genomes recovered from metagenomes available from the Sequence Read Archive	PAIRED	SAMN08019896	PRJNA417962	Illumina HiSeq 2000	25420945
SRR6482101	Collection of 3,087 bacterial metagenome-assembled genomes recovered from metagenomes available from the Sequence Read Archive	PAIRED	SAMN08019894	PRJNA417962	Illumina HiSeq 2000	11174331
SRR6482102	Collection of 3,087 bacterial metagenome-assembled genomes recovered from metagenomes available from the Sequence Read Archive	PAIRED	SAMN08019796	PRJNA417962	Illumina HiSeq 2000	89843324
SRR6482104	Collection of 3,087 bacterial metagenome-assembled genomes recovered from metagenomes available from the Sequence Read Archive	PAIRED	SAMN08019893	PRJNA417962	Illumina HiSeq 2000	26793032

Supplementary Table S1: Sequencing and biosample metadata for 101 OMZ metagenomes used in this study (continued).

SRR6482106	Collection of 3,087 bacterial metagenome-assembled genomes recovered from metagenomes available from the Sequence Read Archive	PAIRED	SAMN08019895	PRJNA417962	Illumina HiSeq 2000	12332362
SRR6482129	Collection of 3,087 bacterial metagenome-assembled genomes recovered from metagenomes available from the Sequence Read Archive	PAIRED	SAMN08019918	PRJNA417962	Illumina HiSeq 2000	19873381
SRR6487553	Collection of 3,087 bacterial metagenome-assembled genomes recovered from metagenomes available from the Sequence Read Archive	PAIRED	SAMN08019675	PRJNA417962	Illumina HiSeq 2000	19324514
SRR6488084	Collection of 3,087 bacterial metagenome-assembled genomes recovered from metagenomes available from the Sequence Read Archive	PAIRED	SAMN08019970	PRJNA417962	Illumina HiSeq 2000	30515463
SRR6488089	Collection of 3,087 bacterial metagenome-assembled genomes recovered from metagenomes available from the Sequence Read Archive	PAIRED	SAMN08019969	PRJNA417962	Illumina HiSeq 2000	30557549

Supplementary Table S1: Sequencing and biosample metadata for 101 OMZ metagenomes used in this study (continued).

SRR6488112	Collection of 3,087 bacterial metagenome-assembled genomes recovered from metagenomes available from the Sequence Read Archive	PAIRED	SAMN08019971	PRJNA417962	Illumina HiSeq 2000	14221386
SRR6488124	Collection of 3,087 bacterial metagenome-assembled genomes recovered from metagenomes available from the Sequence Read Archive	PAIRED	SAMN08019965	PRJNA417962	Illumina HiSeq 2000	2965564
SRR8144072	Foraminiferal nitrate respiration in oxygen minimum zones - past and present - Metagenomics	PAIRED	SAMN10181163	PRJNA503328	Illumina HiSeq 4000	1.72E+10
SRR8144075	Foraminiferal nitrate respiration in oxygen minimum zones - past and present - Metagenomics	PAIRED	SAMN10181161	PRJNA503328	Illumina HiSeq 4000	2.26E+10
SRR8144076	Foraminiferal nitrate respiration in oxygen minimum zones - past and present - Metagenomics	PAIRED	SAMN10181161	PRJNA503328	Illumina HiSeq 4000	2.68E+10
SRR8144077	Foraminiferal nitrate respiration in oxygen minimum zones - past and present - Metagenomics	PAIRED	SAMN10181162	PRJNA503328	Illumina HiSeq 4000	2.04E+10
SRR8144078	Foraminiferal nitrate respiration in oxygen minimum zones - past and present - Metagenomics	PAIRED	SAMN10181162	PRJNA503328	Illumina HiSeq 4000	1.94E+10

Supplementary Table S1: Sequencing and biosample metadata for 101 OMZ metagenomes used in this study (continued).

SRR8144079	Foraminiferal nitrate respiration in oxygen minimum zones - past and present - Metagenomics	PAIRED	SAMN10181165	PRJNA503328	Illumina HiSeq 4000	2.59E+10
SRR8144080	Foraminiferal nitrate respiration in oxygen minimum zones - past and present - Metagenomics	PAIRED	SAMN10181165	PRJNA503328	Illumina HiSeq 4000	2.16E+10
SRR8144081	Foraminiferal nitrate respiration in oxygen minimum zones - past and present - Metagenomics	PAIRED	SAMN10181160	PRJNA503328	Illumina HiSeq 4000	2.05E+10
SRR8144082	Foraminiferal nitrate respiration in oxygen minimum zones - past and present - Metagenomics	PAIRED	SAMN10181160	PRJNA503328	Illumina HiSeq 4000	2.09E+10
SRR8144083	Foraminiferal nitrate respiration in oxygen minimum zones - past and present - Metagenomics	PAIRED	SAMN10181159	PRJNA503328	Illumina HiSeq 4000	2.16E+10
SRR8144084	Foraminiferal nitrate respiration in oxygen minimum zones - past and present - Metagenomics	PAIRED	SAMN10181159	PRJNA503328	Illumina HiSeq 4000	2.66E+10
SRR8144085	Foraminiferal nitrate respiration in oxygen minimum zones - past and present - Metagenomics	PAIRED	SAMN10181158	PRJNA503328	Illumina HiSeq 4000	2.39E+10
SRR8144086	Foraminiferal nitrate respiration in oxygen minimum zones - past and present - Metagenomics	PAIRED	SAMN10181158	PRJNA503328	Illumina HiSeq 4000	2.28E+10

Supplementary Table S1: Sequencing and biosample metadata for 101 OMZ metagenomes used in this study (continued).

SRR8144087	Foraminiferal nitrate respiration in oxygen minimum zones - past and present - Metagenomics	PAIRED	SAMN10181157	PRJNA503328	Illumina HiSeq 4000	1.87E+10
SRR8144088	Foraminiferal nitrate respiration in oxygen minimum zones - past and present - Metagenomics	PAIRED	SAMN10181157	PRJNA503328	Illumina HiSeq 4000	2.06E+10